Enclosure 2

General Electric Report

NEDO-10527, "
Rod Drop Accident Analysis for Large Boiling Water Reactors,"
Including Supplement 1

NEDO-10527
72NED18
Class I
March 1972

ROD DROP ACCIDENT ANALYSIS

FOR LARGE BOILING WATER REACTORS

C. J. Paone
R. C. Stirn
J. A. Woolley

Technical Contributions by:

S. W. Smith

Approved:

L. K. Holland, Manager
Systems Engineering

Approved:

W. R. Morgan, Manager
Core Performance Systems

ATOMIC POWER EQUIPMENT DEPARTMENT • GENERAL ELECTRIC COMPANY
SAN JOSE, CALIFORNIA 95114

78/500 - Sys Eng.
MKS - 3/72

GENERAL ELECTRIC

DISCLAIMER OF RESPONSIBILITY

This report was prepared as an account of research and development work performed by General Electric Company. It is being made available by General Electric Company without consideration in the interest of promoting the spread of technical knowledge. Neither General Electric Company nor the individual author:

A. Makes any warranty or representation, expressed or implied, with respect to the accuracy, completeness, or usefulness of the information contained in this report, or that the use of any information disclosed in this report may not infringe privately owned rights; or

B. Assumes any responsibility for liability or damage which may result from the use of any information disclosed in this report.

TABLE OF CONTENTS

LIST OF ILLUSTRATIONS

LIST OF ILLUSTRATIONS (Continued)

ABSTRACT

This report describes the current methods used by the Atomic Power Equipment Department of the General Electric Company for the analysis of super-prompt critical nuclear excursions in large water-moderated reactors. The technical analysis tools used in studying hypothetical nuclear transients are described herein, without considering the probability of such an occurrence.

The rod drop accident has been reanalyzed generically using the improved methods, and the results of these analyses are presented. In addition, detailed sensitivity studies have been performed to evaluate the effects of initial reactor conditions, control rod worth, rod drop velocity, and scram insertion rate on the resultant peak fuel enthalpy.

1. INTRODUCTION

Over the past several years the Atomic Power Equipment Department (APED) of the General Electric Company has issued several documents which deal with the subject of the control rod drop accident in large boiling water reactors (BWR)[1,2,3]. It is not the purpose of this report to reiterate all of the technological developments which have been discussed previously with regard to the rod drop accident analysis, but rather to update the methods and results, to extend the results, and in some cases to clarify the accident analysis. Although extensive preventative measures in the form of equipment design and procedural control have been taken to prevent rod drop excursion, APED still evaluates all possible consequences based on experimental and analytical results. A continual effort is maintained in the area of analytical methods development to assure that these evaluations reflect the current state of technology in this field.

Although the accident analysis has undergone major revisions throughout, the three major changes which reflect the largest perturbations to the results previously reported are: (1) the inclusion of the technical specification scram insertion times; (2) the use of a calculated rather than an assumed ramp or linear function for the scram reactivity; and (3) a reduction in the rod drop velocity. To illustrate the sensitivity of the results of rod drop accident analysis to these changes, parametric analyses involving the extremes of these variables were performed and all of the results are reported to reflect these parameterizations. Previous studies[3] demonstrated the sensitivity of the excursion results to other input variables; therefore, these results will not be re-evaluated here.

These analyses were for the current fuel designs (i.e., temporary control curtains) at the beginning of life, and it is anticipated that the accident consequences will become less severe as core exposure increases. The reasons for the reduced accident consequences are the increase in the Doppler feedback due to Pu-240 buildup (approximately 20% increase at end of cycle) and decrease in the total worth of the control rods with exposure since there is less excess reactivity in the core.

The remainder of this report will be divided into five major sections which will be devoted to a description of the rod drop accident, a discussion of the parametric results, a description of the excursion model, verification of the adiabatic model employed by APED, and finally a description of the development of the experimental and analytical input data used in rod drop accident analysis. Throughout this study it has been our objective to prevent both the most realistic and the most pessimistic conditions which could exist during a rod drop accident, and the results presented herein reflect this approach.

2. DESCRIPTION OF ROD DROP ACCIDENT

Design of the GE BWR considers four assumed design basis accidents: (1) loss-of-coolant accident (LOCA); (2) steam-line break accident (SLBA); (3) fuel bundle drop accident; and (4) the one considered here, a reactivity insertion event – a control rod drop from the core. It is considered appropriate, for reasons of consistency, to define* this assumed design basis control rod drop accident in a similar manner to the way other design basis accidents are defined. There are, however, limitations on the similarity of the accident to such other accidents as the LOCA or the SLBA. The limitations arise because, like the assumed refueling accident, operator action is involved unlike the LOCA and SLBA where fully automatic equipment action occurs. In the case of the LOCA or SLBA, it is assumed that a pipe ruptures suddenly and completely and the ensuing events are analyzed to assure that the appropriate criteria are not exceeded. In the course of evaluating the adequacy of protective features designed to prevent or mitigate the consequences of the LOCA or SLBA, it is customary to assume that any single active component failure can occur. This philosophy can be translated to the assumed control rod drop accident to provide a consistent accident definition.

Based on the above ground rules, the assumed control rod drop accident is defined as the complete (but not necessarily sudden) rupture, breakage, or disconnection of a random fully inserted control rod drive from its cruciform control blade at or near the coupling and in such a way that the blade somehow becomes stuck at its location (fully inserted). It is considered that this initiating event is similar to a sudden complete pipe rupture and equally highly unlikely, since:

(a) The design of the drive and its coupling uses high quality materials and it receives stringent quality control and testing procedures appropriate to other equipment typically listed in the critical component list for a plant. Additionally, tests conducted under both simulated reactor conditions and conditions more extreme than those expected in reactor service have shown that the drive (or coupling) retains its integrity even after thousands of scram cycles. Tests also show that the drive and coupling do not fail when subjected to forces 20 times greater than that which can be achieved in a reactor.

(b) Sticking of the control blade in its fully inserted position is highly unlikely because each blade is equipped with rollers that make contact with the nearly flat fuel channel walls, travelling in a gap of approximately 1/2-in. clearance. Since a control blade weighs approximately 186 pounds, even if it separates from its drive, gravity forces would tend to make the blade follow its drive movement as if it were connected. Control blades of the current design are now in use in operating reactors and have exhibited no tendency to stick.

Thus, the assumed control rod drive/control blade separation does not, of itself, produce any unplanned or uncontrolled perturbation on normal plant operation that requires immediate operator action. This event, therefore, is not of immediate reactor safety consequence as is the LOCA or SLBA. In most cases, if such a separation occurred, it is expected that the blade would not stick, but rather follow its drive movement. The separation would be detected at the next fully withdrawn stroke where the ability to withdraw to the overtravel position would signal separation, since the blade bottoms on a seat and prevents withdrawal to the overtravel position if connected. Thus, this drive could be inserted and declared inoperative in accord with the technical specifications until the next refueling outage where it could be repaired. However, for this analysis, it is presumed that the separated blade somehow sticks at the fully inserted position. This assumption sets up a condition whereby, if the drive were withdrawn, the stuck blade could later fall to its drive position and cause a rod drop reactivity insertion accident.

As shown in Figure 3-9 (lowest curve in figure), the series of events described above could lead to a reactivity insertion of such a worth that the peak fuel enthalpy would be less than 100 cal/gm, which would result in no fuel failure.

It is at this point that consideration of possible operator action differentiates the control rod drop accident from the LOCA or SLBA. The provisions made in the plant design to mitigate the consequences of a control rod drop accident include not only equipment design but operator procedures. As discussed previously, such accident prevention or mitigation features should be evaluated considering any single active component failure. In the case of the control rod

*Previously this accident has been somewhat arbitrarily defined for a given rod worth without consideration of the ability to achieve the stated rod worth.

drop accident, however, the evaluation is extended to include possible operator error (i.e., adequate prevention or mitigation must exist subsequent to the assumed control rod drive-blade separation accident to assure limits are not exceeded, even considering that an additional single active component failure or single operator error occurs).

Figure 2-1 shows the various paths or outcomes of the assumed control rod drive-blade separation. Both the carefully chosen rod withdrawal operating procedures (rod patterns) and the rod worth minimizer (RWM) act to prevent or mitigate the consequences of a blade separation. Both of these provisions are intended primarily to limit control rod worths for reasons of optimizing fuel exposure and to control core peaking factors to within technical specification limits. The RWM will be required to be operable from 0 through 10% of full power and will thus provide backup to operating procedure and additional assurance that, if a rod drop accident occurs, it will be for a normal or in-sequence rod worth.

Thus, the course of the assumed design basis rod drop accident is as follows:

(1) the control rod drive and blade separation occurs on a fully inserted rod in such a way that the blade sticks;
(2) the reactor is operating at or above 10% of full power with the RWM not in operation;
(3) the operator makes the worst single selection error in the course of a normal power ascension and selects the highest worth rod which happens to be the one that experienced the separation failure described in 1 above; and
(4) after full withdrawal of this control rod drive, the blade drops from its fully inserted position and falls at a conservatively assumed velocity of 5 ft/sec.

The control rod drop accident thus defined is analyzed in terms of the peak fuel enthalpy, associated fuel failure, and the radiological consequences considering operation of the plant protective and safety features as shown in Figure 2-2 to assure acceptable consequences. These consequences are not discussed here but will be discussed in individual plant applications (PSAR, FSAR) where individual plant design features can be considered.

Below 10% of full power (see Figure 2-1) the RWM is operating. Thus, evaluation of the consequences of the assumed control rod drive and blade separation accident, along with an accompanying single active component failure or single operator error, shows the accident to have lesser consequences than if operation is above 10% power. If it is assumed that, after the random blade separation occurs, the single operator error is the selection of an out-of-sequence rod even if is is selection of the highest worth rod, the RWM will block withdrawal of this out-of-sequence rod, so no rod drop will occur. Alternatively, if it is assumed the single active component failure is the RWM, since the RWM is designed to be FAIL SAFE (i.e., block any further rod withdrawal), again no withdrawal can occur and therefore not rod drop. If it assumed the RWM does not prohibit withdrawal (i.e., the rod selected is an in-sequence rod), then the consequences of this rod being dropped is that peak fuel enthalpy is < 100 cal/gm and no fuel failure occurs.

The design basis of the plant in terms of the potential for a control rod drop accident is as follows. The RWM must be operable up to the power level where if a rod drop accident as defined above occurs (i.e., maximum worth rod for a single operator error), without benefit of the RWM block, then calculated peak fuel enthalpy must not exceed 280 cal/gm. For plants of current design (i.e., temporary control curtain fuel design analyzed here) this power level is about 2% of full power.

The design basis control rod drop defined above is conservative for the following reasons:

(1) The assumed single operator selection error is the worst error (see paragraph 7.6.1.1).

(2) The rod drop velocity is assumed to be 5 ft/sec, although data show that lower velocities are achieved by the design (see Appendix).

(3) Scram time for the control rods is assumed to be no faster than the technical specification limits. As Figure 3-9 shows, if measured rod drop velocity and measured scram time is considered, then even with no RWM operation and assuming the worst single operator selection error, for any reactor power level, peak fuel enthalpy is below 280 cal/gm.

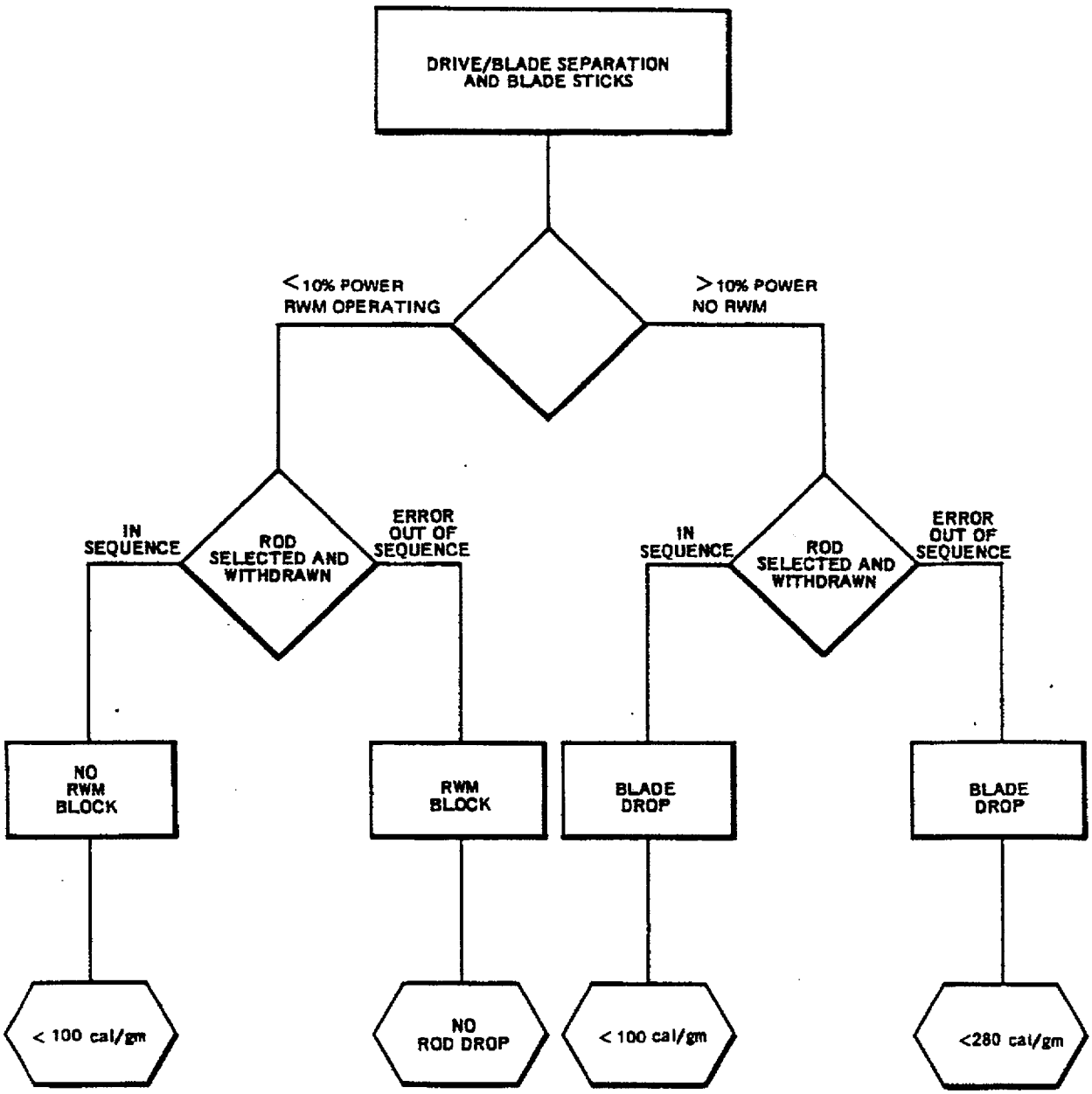

Figure 2-1 Initiation Sequence and Consequences of Control Rod Drop Accident

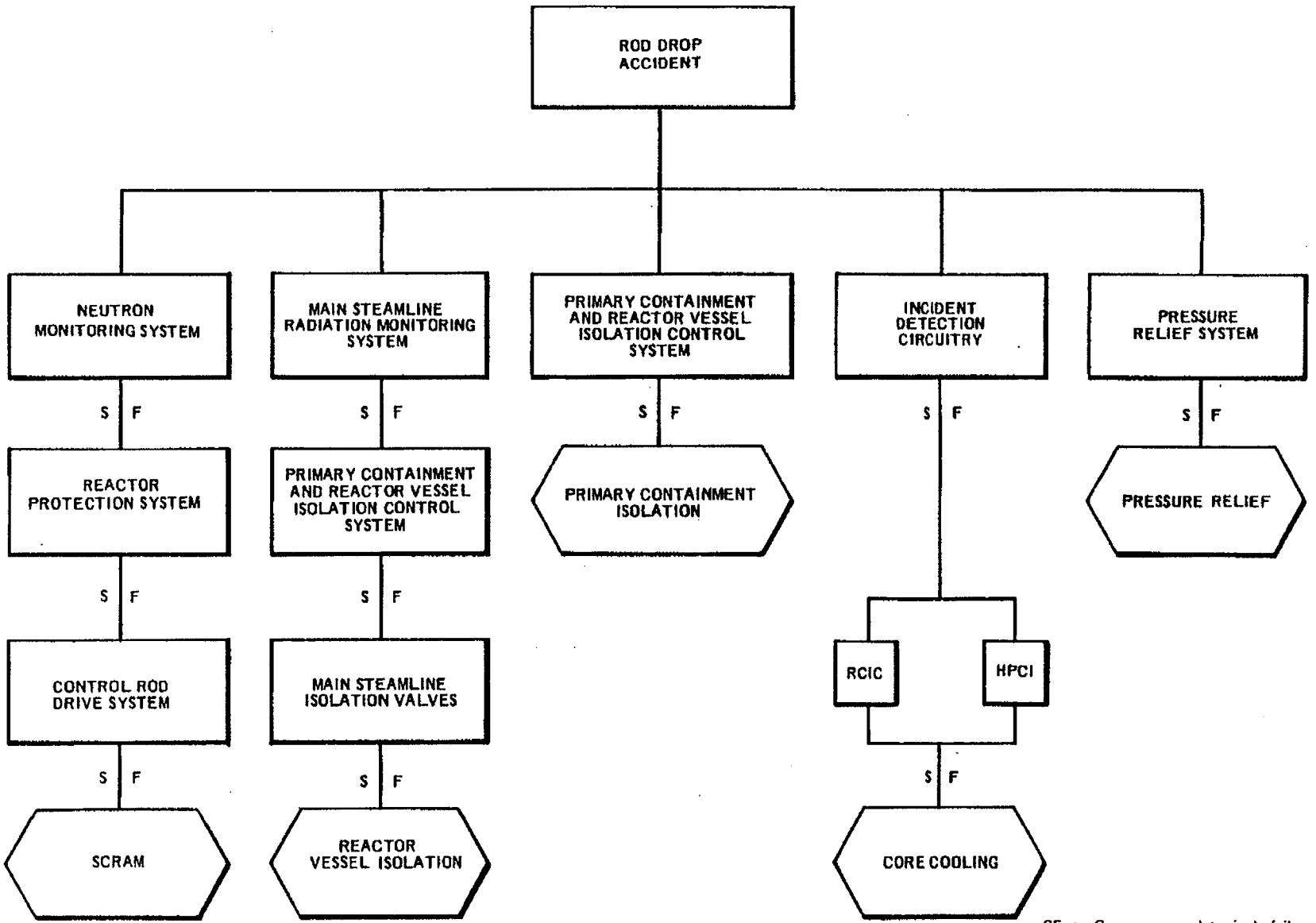

Figure 2-2 Rod Drop Accident Protection Sequence

3. PARAMETRIC RESULTS OF ROD DROP ACCIDENT

3.1 Introduction

The results of the rod drop excursion have been divided into two parts – the startup range and the power range. For reasons of clarification, the following definitions for reactor states will be made and used in this report. The cold startup state will refer to a critical reactor with fuel and moderator temperatures of 20°C, a reactor pressure of one atm, and an initial power fraction of 10^{-8} of rated power level. The hot startup condition will be defined as a critical reactor at operating pressure, saturated temperature, and initial power fraction of 10^{-6} of rated. Hot standby will be used to define a reactor which is producing sufficient power to maintain all electrical systems without the aid of auxiliary power. This is usually in the 5 to 10% power range. From these definitions it is obvious that the cold startup and hot startup states will be in the startup range, and that the hot standby case will be in the power range.

Many of the parameters which are input to the excursion analyses are fixed by the physical design of the reactor. However, other parameters such as scram insertion rates and rod drop velocities may vary. For this reason sensitivity studies based on various input parameters to the excursion analyses were performed to more fully evaluate the effects of these parameters on the results of the accidents. In addition to the initial starting conditions, the parameters which were varied for this study were control rod worth, control rod drop velocity, and scram insertion rate. The sensitivity of the rod drop accident to other variables (e.g., neutron lifetime and delayed neutron fractions) were not evaluated in this study, since previous work involving these parameters has been reported.[3]

The method used in preparing the input data for the rod drop excursion calculations are discussed in detail in Sections 6 and 7. This input, in turn, is used in the excursion model discussed in Section 4, and the results of these analyses are presented below.

Since the peak fuel enthalpy is the most important single parameter for determining the severity of a transient and the onset of fuel pin failure, the results have been presented parametrically as a function of the resultant peak fuel enthalpy. As reference points, the following design and fuel failure criteria have been established by General Electric, based on experimental data generated by the SPERT tests:[4]

Enthalpy = 170 cal/gm, cladding failure threshold
Enthalpy = 280 cal/gm, specific energy design limit
Enthalpy = 425 cal/gm, prompt fuel dispersal threshold

In addition to the design and fuel failure criteria stated above, the points of incipient melting and fully molten UO_2 occur at 269.4 and 336.8 cal/gm, respectively. These values are based on experimental data discussed in subsection 6-1.

3.2 Results of Rod Drop Excursion in Startup Range

The results of the rod accident sensitivity study in the startup range are shown in Figures 3-1 through 3-8. Figures 3-1 through 3-4 give the peak fuel enthalpy for various combinations of rod drop velocities and scram insertion rates. These results are further parameterized as a function of initial starting conditions and control rod worth. Although these figures demonstrate the sensitivity of the rod drop accidents to rod drop velocity and scram insertion rates, these effects are better demonstrated by Figures 3-5 through 3-8.

The sensitivity of the final peak fuel enthalpy to the scram insertion times is shown by Figures 3-5 and 3-6. The important factor to note here is that the sensitivity to scram rates increases with increasing rod worth. By comparing Figures 3-5 and 3-6, it is also seen that, as the rod drop velocity decreases, the sensitivity to the scram insertion rate increases slightly. This can be done by comparing the slopes of the constant rod worth curves.

Figures 3-7 and 3-8 more clearly demonstrate the sensitivity of the resultant peak fuel enthalpy to the rod drop velocity. As expected, the peak enthalpy increases with increasing velocity. In addition, the results are much more sensitive as the control rod worth increases.

3.3 Results of Rod Drop Excursion in Power Range

With the addition of increasing starting power and voids in the power range, the severity of the rod accident rapidly decreases, and the peak enthalpy is much less than the 280 cal/gm design limit at 10% power even when the worst conceivable or maximum worth control rod is dropped from the core. There are four major reasons for this trend. The first two reasons are consequences of the fact that the void distribution results in a much milder accident reactivity insertion rate and also a much more rapid scram reactivity shape function (Figures 7-5 and 7-6, respectively). Both of these effects will work to decrease the severity of the accident.

The third and fourth reasons for the reduction of the peak enthalpy can be attributed to the Doppler reactivity feedback. Since the reactor is initially at 10% of rated power, any increase in power and hence, fuel temperature, will result in a prompt Doppler response, whereas in the startup range the power would have to increase five to seven decades before significant Doppler feedback occurs. The second effect due to Doppler can be assigned to the formation of voids. Because of the decrease in the water-to-fuel ratio, the Doppler reactivity coefficient will become more negative. For the 10% power case, this effect alone can account for an increase of approximately 20% in the Doppler feedback.

Due to the aforementiond effects, the resultant peak enthalpy for a 3.1% control rod dropped from 10% power at 5 ft/sec (using tech spec scram insertion times) is only 172 cal/gm. This is much less than the design limit of 280 cal/gm and just slightly larger than the 170 cal/gm threshold for cladding perforation.

It should also be noted that no credit was taken for the negative void feedback effects for this analysis. From experimental tests conducted at the SPERT-III facility,[22] it was demonstrated that the void reactivity feedback effect generated by prompt moderator heating accounted for approximately 35% of the total prompt reactivity feedback at the time of peak power during the hot standby tests. This would significantly reduce the peak enthalpy below 172 cal/gm.

3.4 Summary of Rod Drop Excursion Results

The best perspective of the rod drop accident can be demonstrated by plotting the results of the rod drop accidents and the control rod worth curves developed in subsection 7.6 together as shown by Figure 3-9. The following conclusions can be made concerning these results assuming tech spec scram rates and a 5 fps rod drop velocity:

(1) rod drop accidents involving in-sequence control rods (no operator errors) will always result in peak fuel enthalpies less than 280 cal/gm;
(2) above 2% power, rod drop accidents involving maximum worth rods developed due to the worst single operator error will always result in peak fuel enthalpies less than 280 cal/gm; and
(3) above 10% power, even multiple operator errors will not produce rod worths large enough to exceed fuel enthalpies of 280 cal/gm.

In addition, Figure 3-9 demonstrates that single operator errors will result in peak fuel enthalpies less than 280 cal/gm if measured scram insertion rates and rod drop velocities are employed when doing the rod drop accident analysis.

These results also indicate that bypassing or shutting down the rod worth minimizer above 10% of rated power is most conservative since, above 2% power, peak fuel enthalpies will always be less than 280 cal/gm (assuming the worst single operator error.)

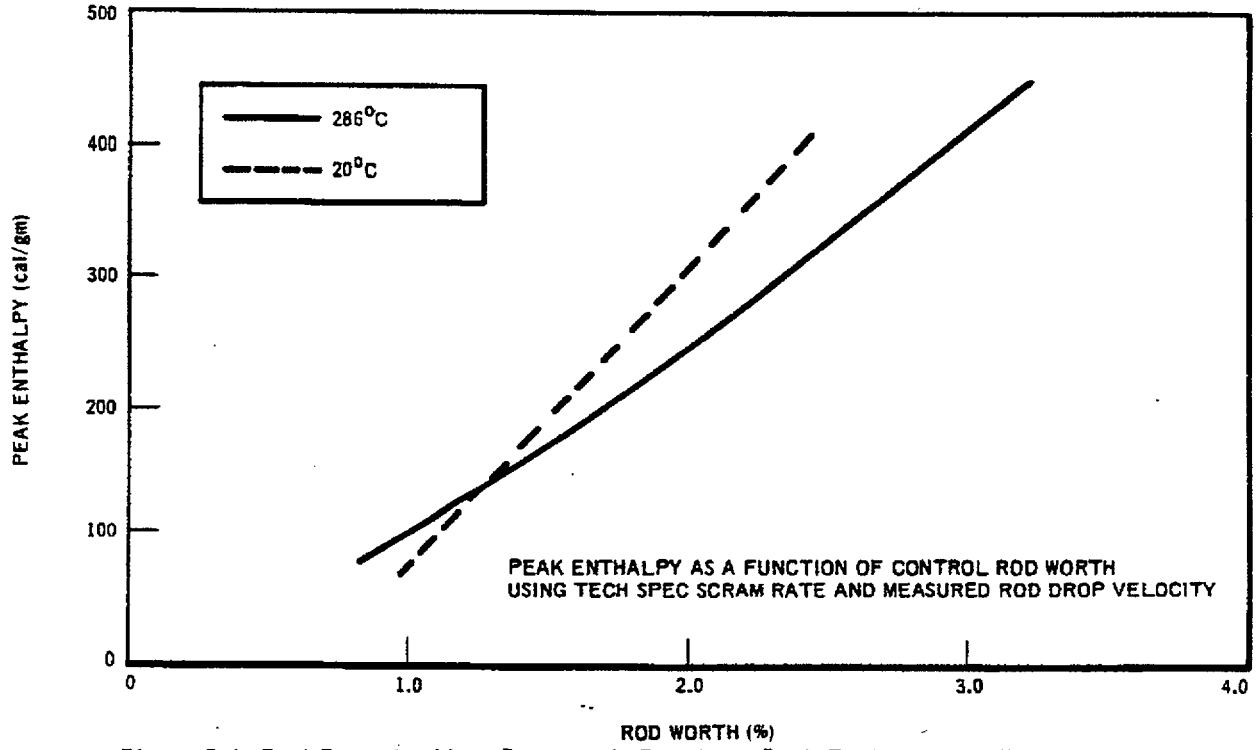

Figure 3-1 Rod Drop Accident Parametric Results – Peak Enthalpy as a Function of Control Rod Worth Using Tech Spec Scram Rate and Measured Rod Drop Velocity

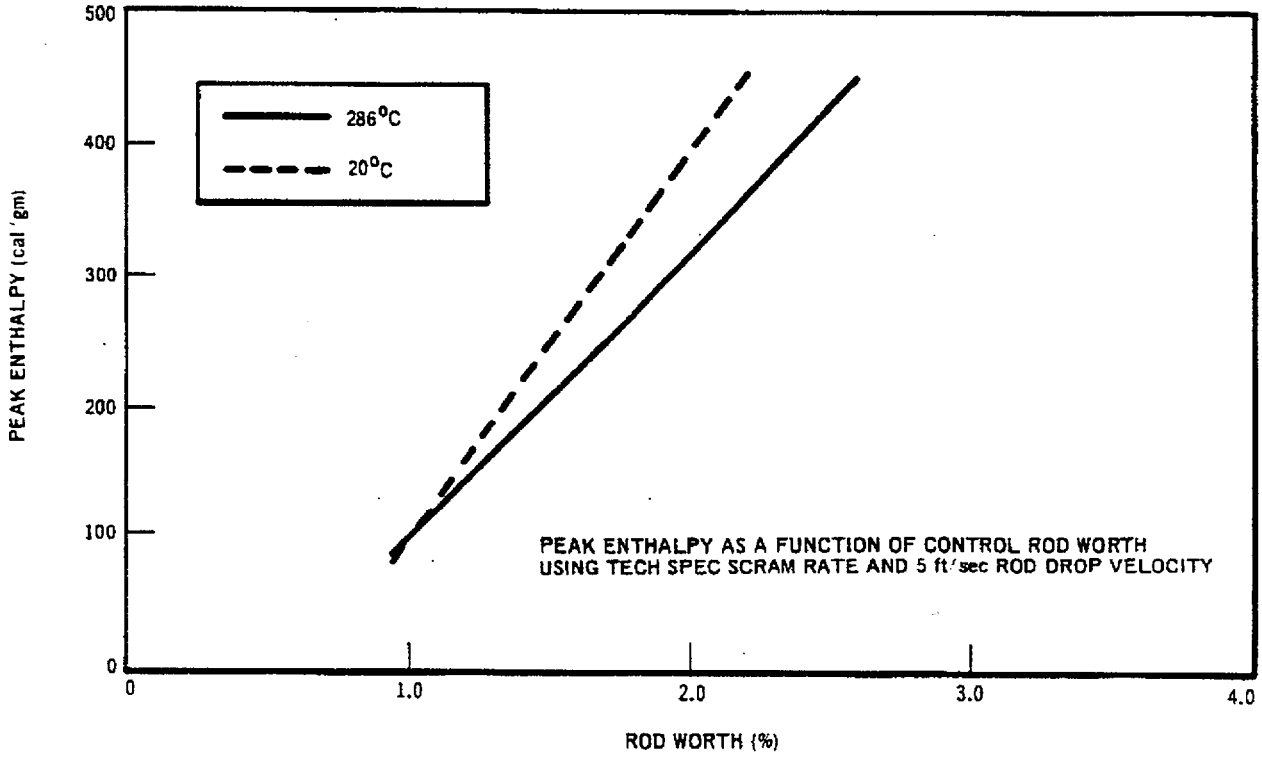

Figure 3-2 Rod Drop Accident Parametric Results – Peak Enthalpy as a Function of Control Rod Worth Using Tech Spec Scram Rate and 5 ft/sec Rod Drop Velocity

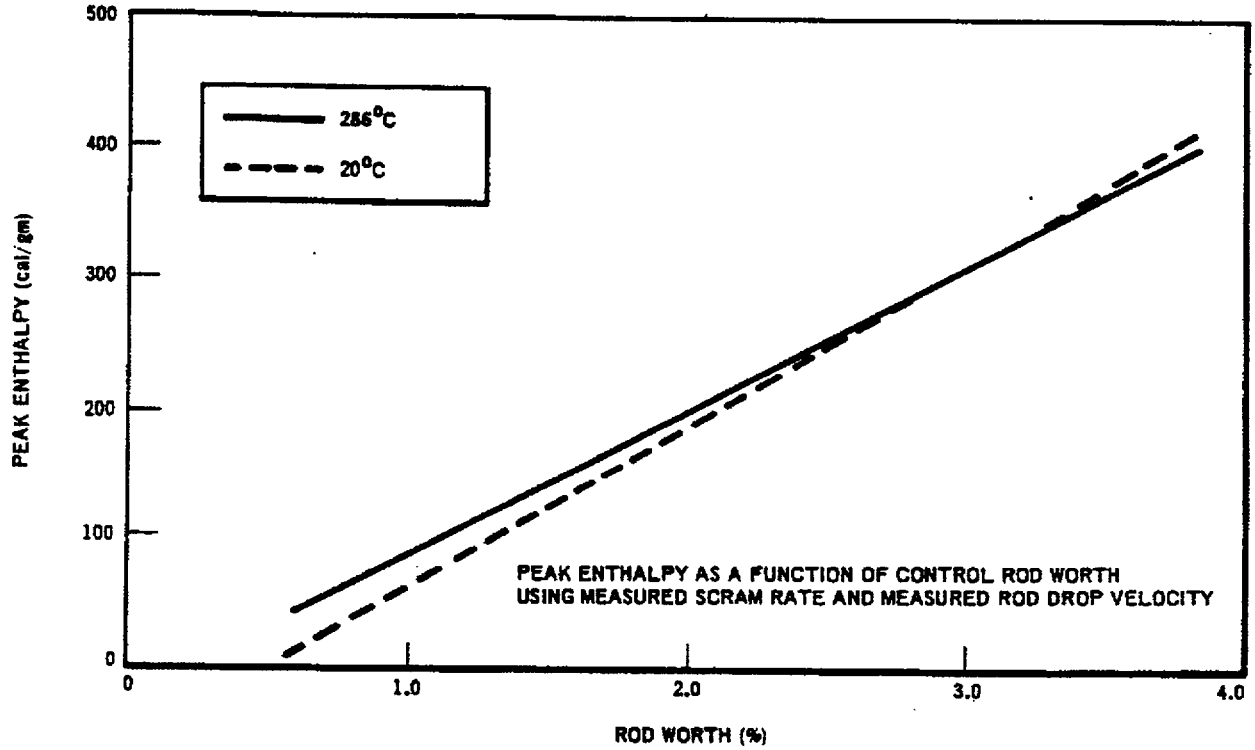

Figure 3-3 Rod Drop Accident Parametric Results — Peak Enthalpy as a Function of Control Rod Worth Using Measured Scram Rate and Measured Rod Drop Velocity

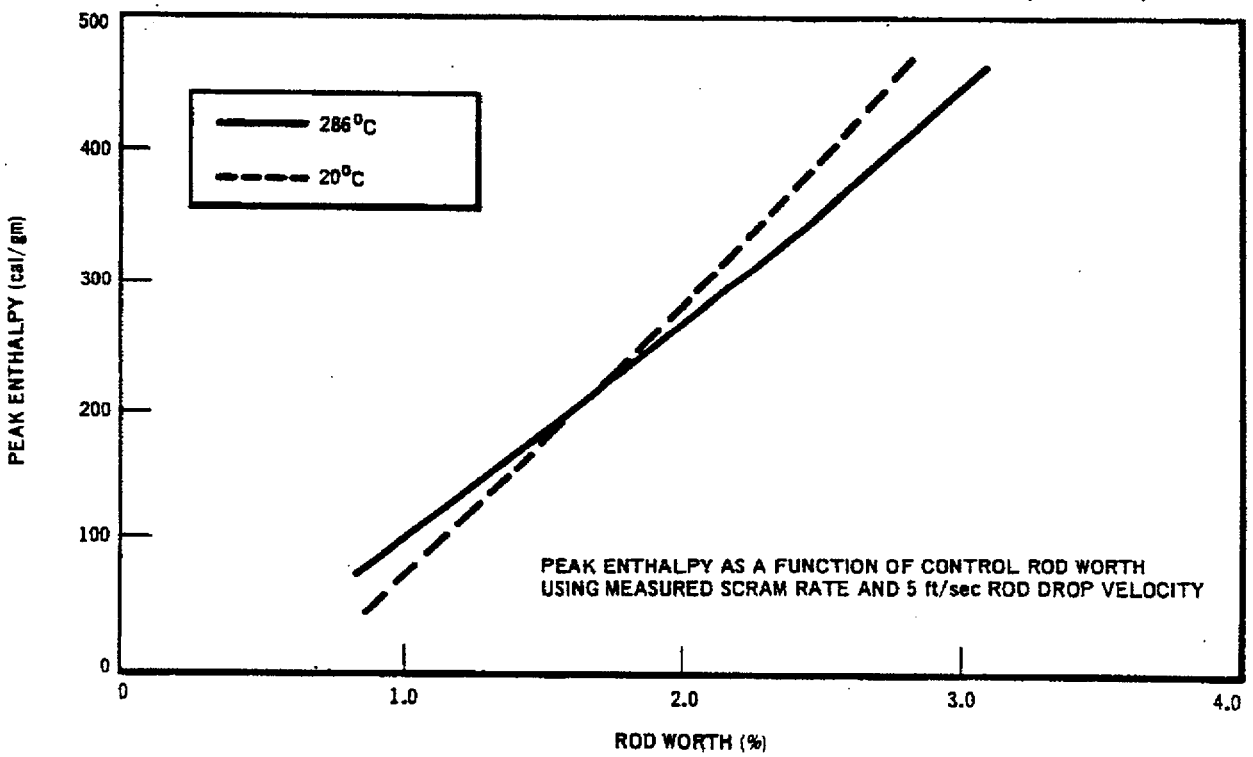

Figure 3-4 Rod Drop Accident Parametric Results — Peak Enthalpy as a Function of Control Rod Worth Using Measured Scram Rate and 5 ft/sec Rod Drop Velocity

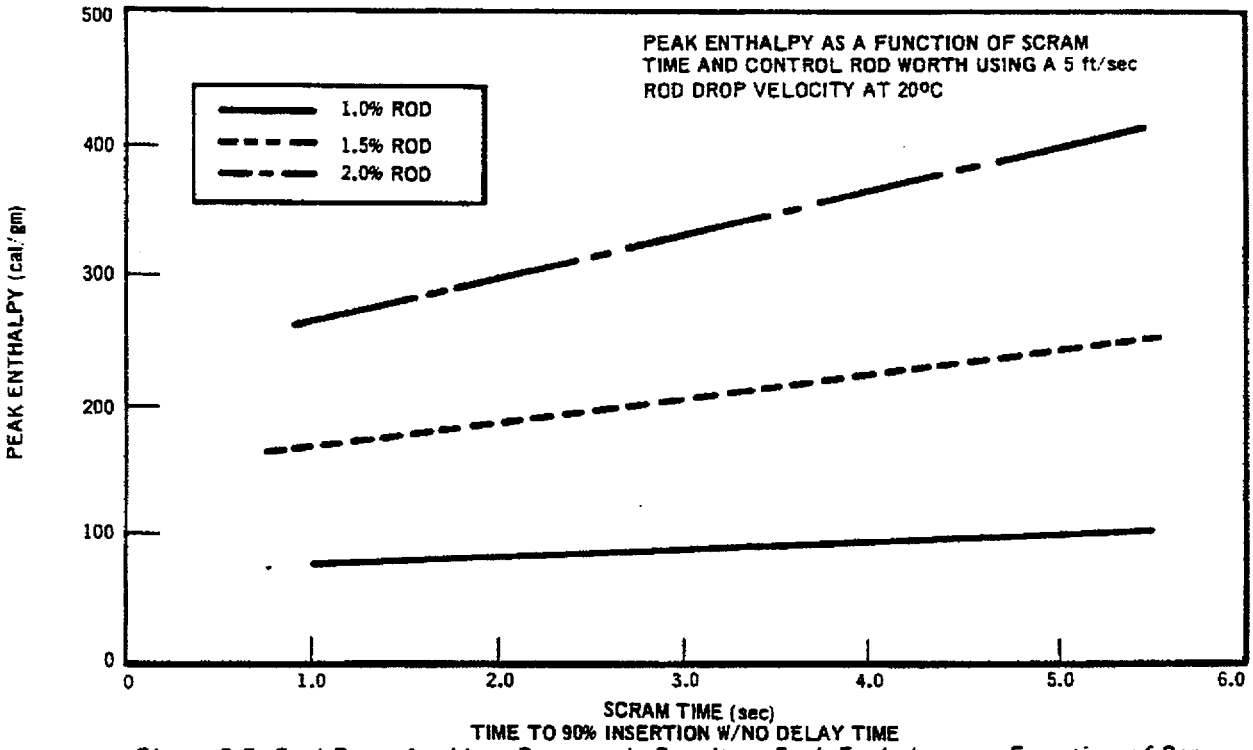

Figure 3-5 Rod Drop Accident Parametric Results – Peak Enthalpy as a Function of Scram Time and Control Rod Worth Using a 5 ft/sec Rod Drop Velocity at 20°C

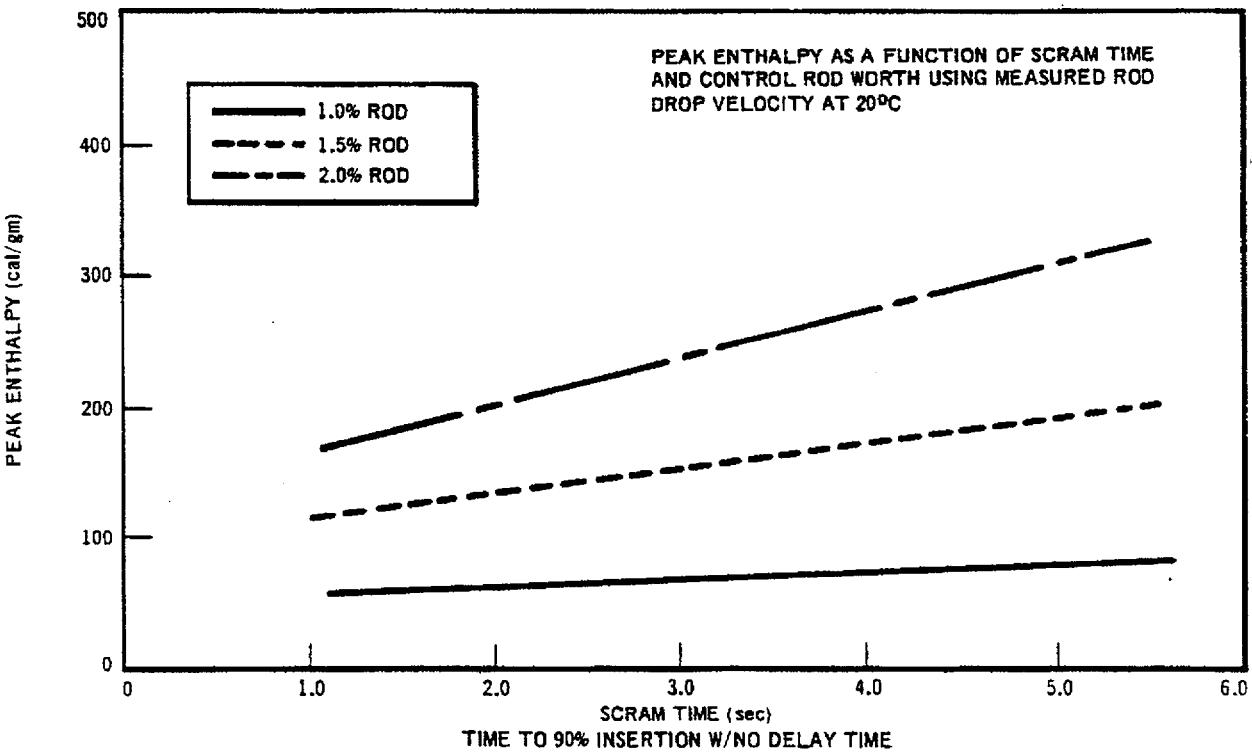

Figure 3-6 Rod Drop Accident Parametric Results – Peak Enthalpy as a Function of Scram Time and Control Rod Worth Using Measured Rod Drop Velocity at 20°C

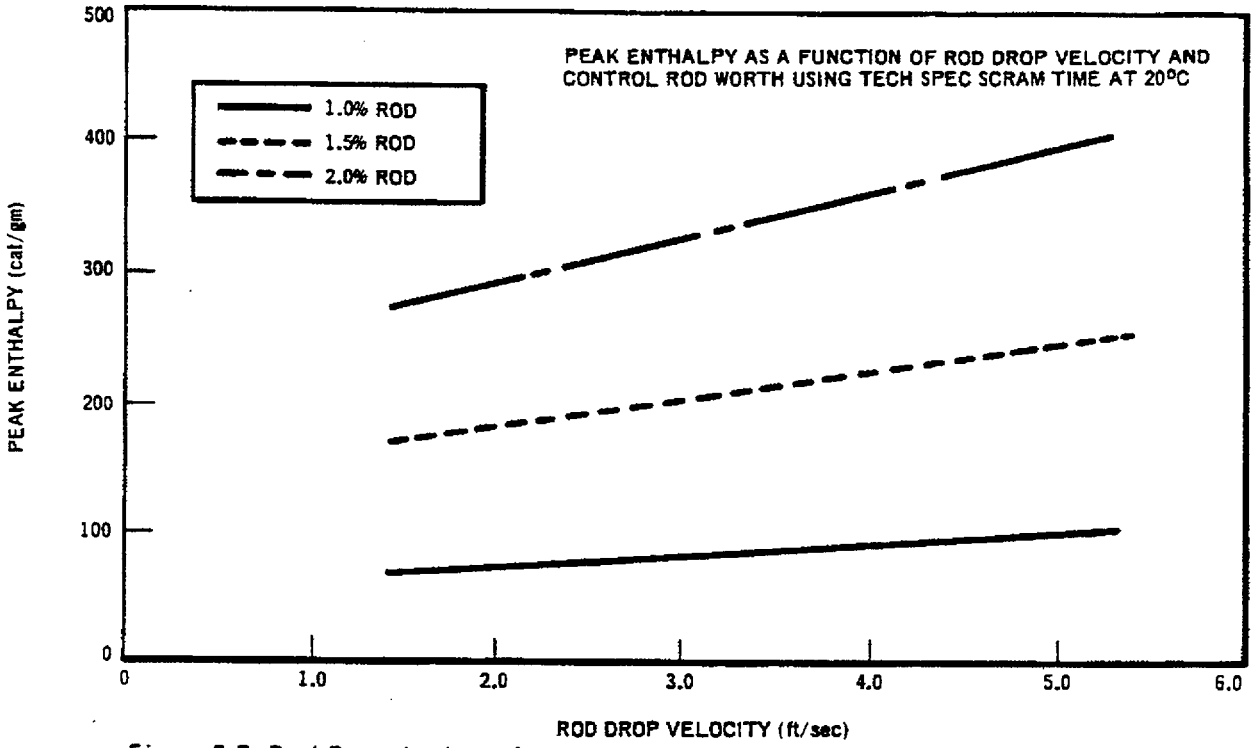

Figure 3-7 Rod Drop Accident Parametric Results — Peak Enthalpy as a Function of Rod Drop Velocity and Control Rod Worth Using Tech Spec Scram Time at 20°C

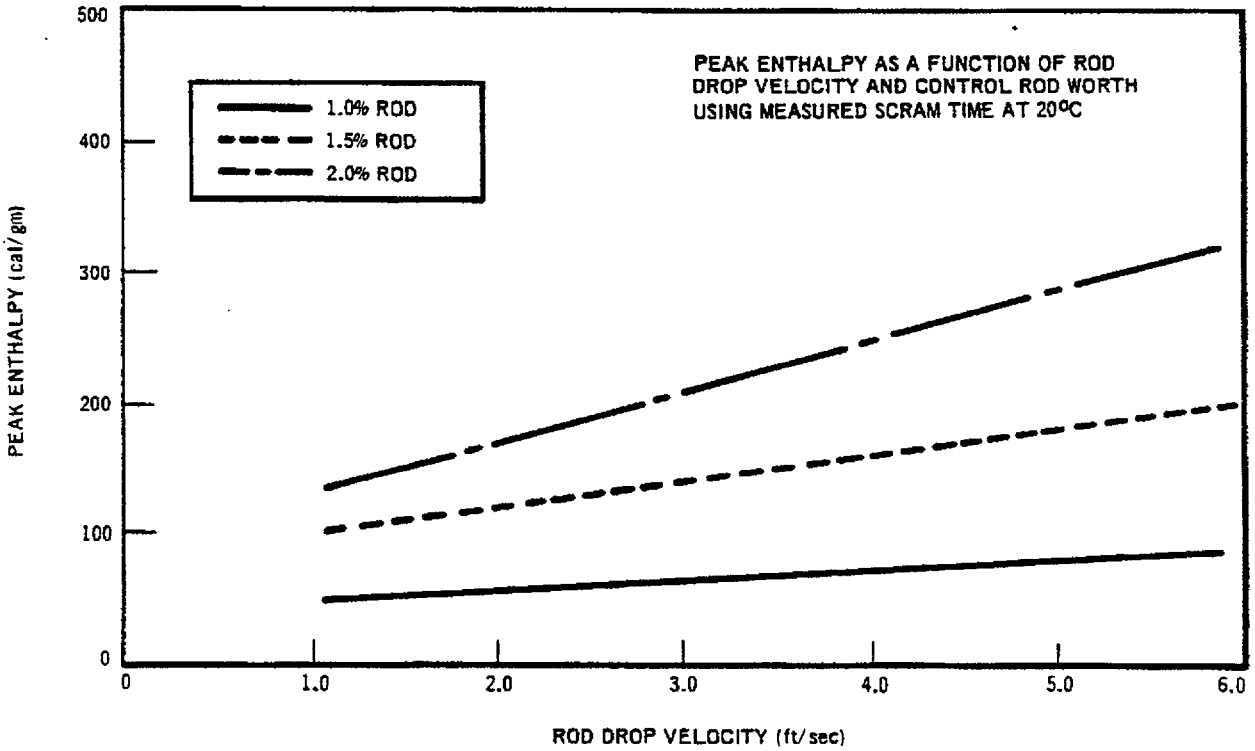

Figure 3-8 Rod Drop Accident Parametric Results — Peak Enthalpy as a Function of Rod Drop Velocity and Control Rod Worth Using Measured Scram Time at 20°C

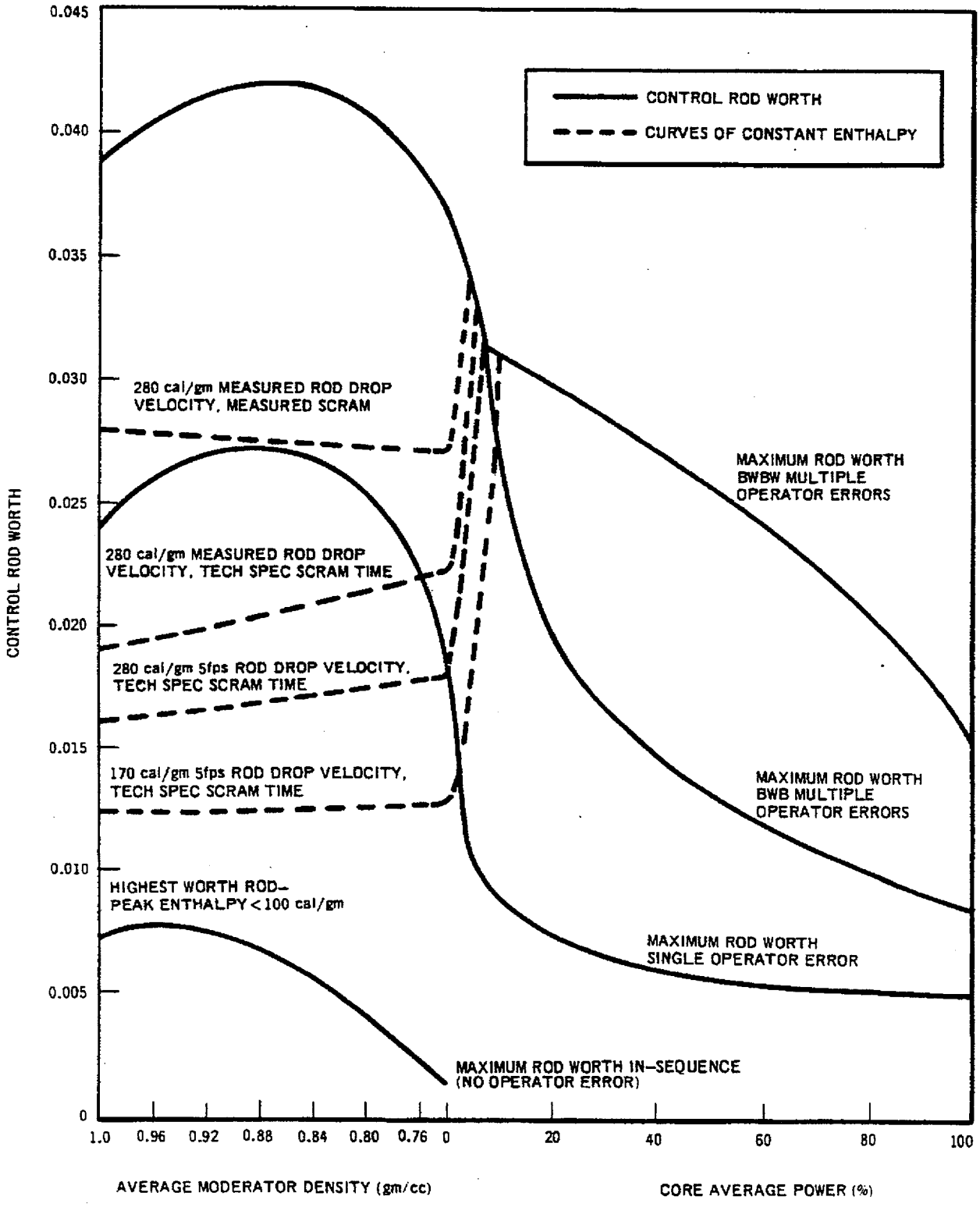

Figure 3-9 Parametric Results of Rod Drop Accident

4. DESCRIPTION OF THE ADIABATIC PROMPT EXCURSION MODEL

4.1 Introduction

Four approaches to large-core excursion analysis have been used at General Electric:

(1) point model with spatial weighting factors;
(2) finite-differenced space-time solution;
(3) time-integrated method[23,24]; and
(4) adiabatic approximation.

Determining accurate spatial weighting factors for the point model is very difficult. Numerical solution of space-time reactor kinetics is more exact but very expensive, especially if more than one space dimension is considered. The time-integrated method yields no time-dependent information, only final results. The primary design method at General Electric for analysis of super-prompt critical large-core nuclear excursions uses the adiabatic approximation with a two-dimensional multi-group flux calculation. This method provides a relatively accurate and inexpensive solution of the problem.

4.2 Adiabatic Approximation

In the adiabatic approximation it is assumed that the space-time flux is given by the product $\phi(\underline{r}, t) = \phi^t(\underline{r})F(t)$, where $F(t)$ is a function dependent upon time only, and $\phi^t(\underline{r})$ is the fundamental mode spatial flux at selected points in time. The shape function $\phi^t(\underline{r})$ will reflect space-time varying nuclear properties at each time point. The eigenvalue of the fundamental mode solution for $\phi^t(\underline{r})$ provides the reactor averaged effect of these changing properties in time. By relating this change in eigenvalue to the time-dependent reactor multiplication factor $k(t)$, this parameter may be used to drive the reactor averaged kinetics equations

$$\dot{P}(t) = \frac{1}{\Lambda}\left[\frac{k(t) - 1}{k(t)} - \beta\right] P(t) + \sum_{i=1}^{N} \lambda_i C_i(t)$$

$$\dot{C}_i(t) = \frac{1}{\Lambda}\beta_i P(t) - \lambda_i C_i(t)$$

$$\dot{h}(t) = K\left[P(t) - P(o)\right]$$

where

$P(t)$ = average power fraction

$C_i(t)$ = average effective precursor concentration for delay group i

$h(t)$ = average fuel enthalpy

Λ = prompt neutron generation time

β_i = delayed neutron fraction

$\beta = \sum_{i=1}^{N} \beta_i$ = total delayed neutron fraction

λ_i = decay constant for delay group i

N = number of delay groups

K = fractor converting average power fraction to average fuel enthalpy rate.

Integrating the kinetics equations yields fuel enthalpy, which may be related to fuel temperature and ultimately to the important effect of Doppler feedback. Thermal-hydraulic effects are ignored because of the typically short duration (< 3 sec) of a prompt-critical excursion.

4.3 General Electric Adiabatic Prompt Excursion Model

At General Electric, the adiabatic prompt excursion model has gone through several phases of development. The original one-dimensional model[25] computed fundamental mode radial flux and power distributions (shape function) for several average fuel temperature increments. For each increment the power distribution was assumed constant in order to approximate the temperature distribution at the end of the step by

$$T_i^{n+1} = T_i^n + P_i^n \overline{\Delta T}^n$$

where

T_i = fuel temperature distribution

P_i = normalized power distribution

$\overline{\Delta T}$ = increment of average temperature

n = step number.

A region averaged power distribution rather than the detailed nodal power distribution was used in the above equation to reduce computer storage. The approximate T_i^{n+1} was related through Doppler feedback to changes in region averaged nuclear properties. Using these properties, the fundamental mode spatial flux and power were obtained for step n+1. The reactor averaged kinetics equations were then used to fill in the time-dependent results, with a constant specific heat relating average fuel enthalpy to average fuel temperature.

The above one-dimensional model was subsequently extended to a two-dimensional (r-z) solution.

The present method (Figure 4-1) uses two-dimensional calculations of fundamental mode flux and power for several average fuel enthalpy increments. For each increment the enthalpy distribution at the end of the step is estimated by

$$h_i^{n+1} = h_i^n + \tilde{P}_i^{n+1} \overline{\Delta h}^n$$

where

h_i = fuel enthalpy distribution

$\tilde{P}_i$ = estimated (extrapolated) normalized power distribution

$\overline{\Delta h}$ = increment of average enthalpy.

The detailed nodal power distribution is used in the above equation to produce the nodal enthalpy distribution, which is related to temperature by a nonlinear function (i.e., variable specific heat is allowed). A nonlinear Doppler feedback

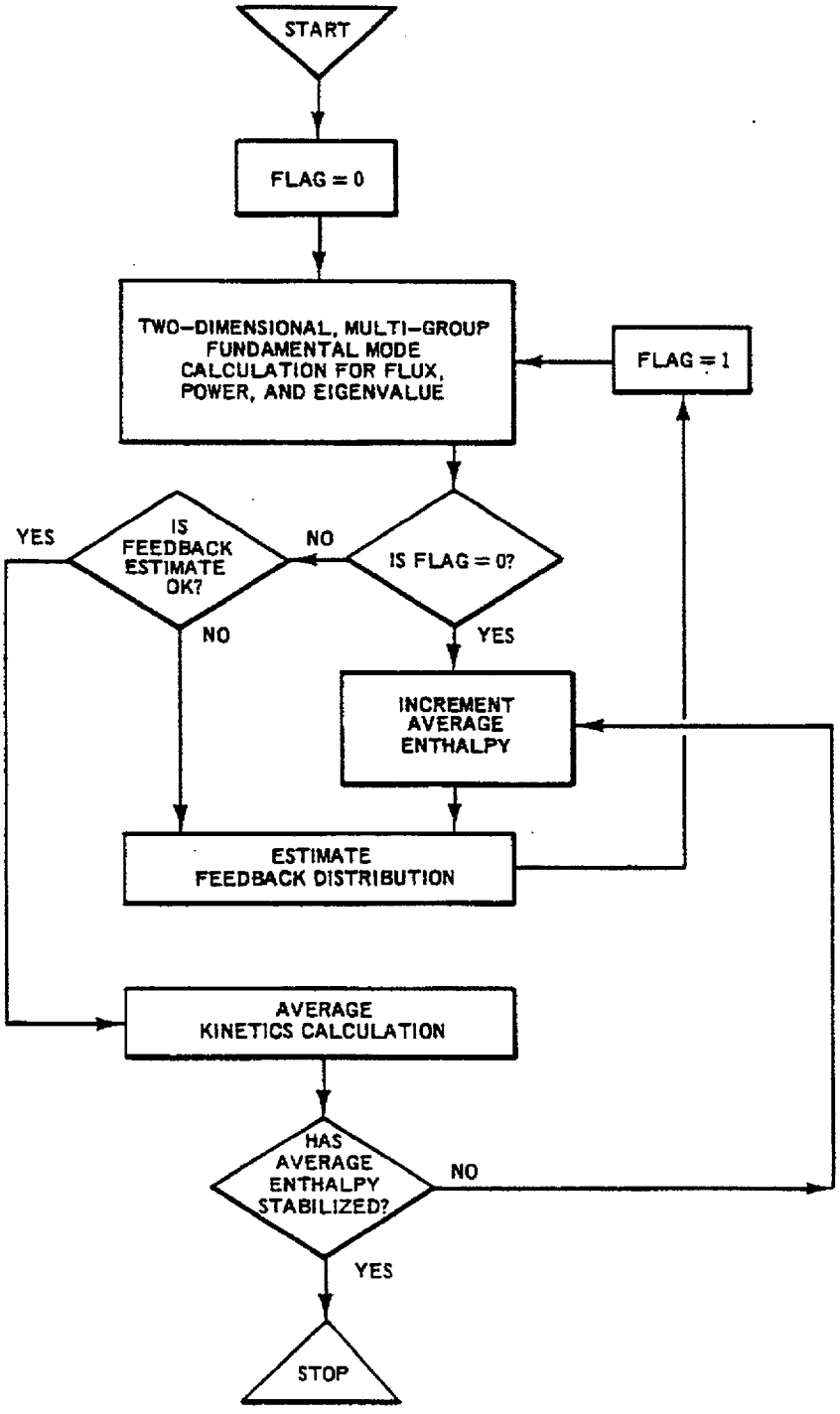

Figure 4-1 Adiabatic Prompt Excursion Model Flow Chart

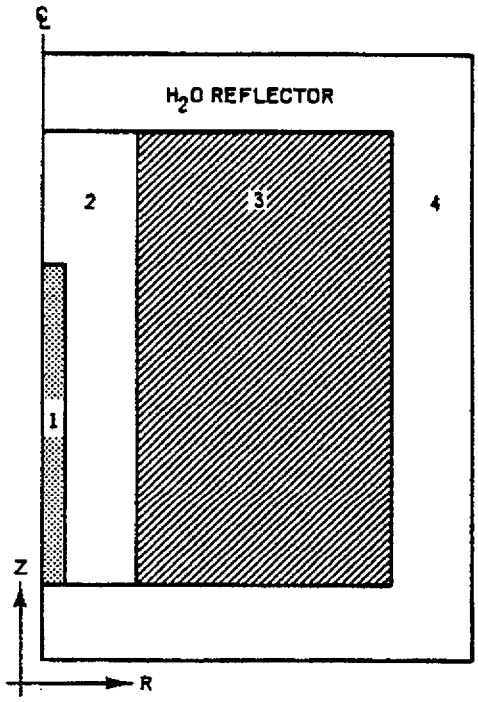

REGION	DESCRIPTION
1	THE RADIUS IS EQUIVALENT TO THAT OF AN EQUIVALENT CRUCIFORM CONTROL ROD.
2	UNCONTROLLED FUEL. THE RADIUS OF THIS REGION IS DETERMINED BY THE ROD WORTH.
3	PARTIALLY CONTROLLED FUEL. THE MATERIAL PROPERTIES IN THIS REGION ARE UNCONTROLLED WITH Σp REPRESENTING EITHER CONTROLLED OR EXPOSED CROSS SECTIONS. Σp IS DEPENDENT ON THE CONTROL ROD WORTH.
4	30 cm H_2O REFLECTOR.

Figure 4-2 Reactor Geometry for Analyzing Rod Drop Accident

relation converts the temperature distribution into changes in nuclear properties on a nodal basis. Using these properties, the fundamental mode spatial flux, power, and associated eigenvalue are obtained for step n+1. Iterative refinement of $\tilde{P}_i$ is then provided to ensure the correct feedback distribution has been used. The reactor averaged kinetics equations provide time dependent results during the step, with

$$k(t) = k(0) + \Delta k_A(t) + \Delta k_S(t-t_S) + \Delta k_F(t)$$

where Δk_A represents the perturbation causing the excursion, Δk_S represents reactor scram, t_S is the time when average power reaches the scram setpoint, and feedback is represented by

$$\Delta k_F(t) = \left\{\lambda^n + \left[\lambda^{n+1} - \lambda^n\right]\left[h(t) - h^n\right] / \overline{\Delta h}^n\right\} / \lambda^\circ - 1.0$$

where

λ^n = fundamental mode eigenvalue at end of step n

h^n = average enthalpy at end of step n.

The excursion calculation is continued until average enthalpy h(t) stabilizes. The final enthalpy distribution is then found by interpolation

$$h_i^f = h_i^n + \left[P_i^n + (P_i^{n+1} - P_i^n)\ \overline{\Delta h}^f / \overline{\Delta h}^n\right] \overline{\Delta h}^f$$

where

f = final result

n = step number of last complete step

$\overline{\Delta h}^f = h^f - h^n$ = partial average enthalpy step.

Finally, local peaking factors and their associated fuel weights are used to generate a fuel weight versus enthalpy histogram.

4.4 Fundamental Mode Flux Solution

The heart of the adiabatic prompt excursion model is its fundamental mode flux solution. The present model uses two-dimensional (r-z or x-y) few-group diffusion theory. Computer storage is allocated at execution time permitting any number of mesh points, prompt flux groups, and materials.

The typical analysis is for full core r-z geometry with 3 prompt groups, 27 radial points, and 51 axial points. The material distribution is usually black-white-gray with the central rod partially withdrawn (Figure 4-2).

The fundamental mode flux and eigenvalue are obtained by fission source iteration with two-parameter Chebyshev acceleration[26]. A direct (noniterative) solution[27] yields the flux for each fission source estimate. A typical problem (as described in the previous paragraph) starting at cold (20°C) reactor conditions initially has a dominance ratio of about 0.98 with nearly 50:1 power peaking. Roughly 55 source iterations are required to converge $(\lambda - \underline{\lambda})/\lambda$ to less than 1×10^{-4}. With each enthalpy step, the source iteration procedure immediately starts Chebyshev acceleration using source and dominance ratio results from the previous step; abour 40 iterations are required for equivalent convergence. From 15 to 25 source iterations are required for refinement of the estimated feedback distribution.

For parametric studies, a scheme has been developed to reduce the few group diffusion equations to one prompt group. The Wielandt method of source iteration[27] is then used. Important results from a one-group analysis are within 1% of those from a three-group solution, with an order of magnitude reduction in computer time and cost. The scheme is based on the use of a buckling which is constant for all groups but varies nodally. Using an estimated k_{eff}, the buckling for each node is found from the roots of a polynominal. This buckling then gives an estimate of the leakage terms in all but one of the few group equations; hence, the reduction to one prompt group. (See reference 28 for more details.)

5. VERIFICATION OF ADIABATIC MODEL

5.1 Comparison of Adiabatic Model With More-Exact Model

5.1.1 Introduction

The adiabatic prompt excursion model previously described has been compared with a more exact space-time diffusion theory model by numerical analysis of a hypothetical problem. The more exact model is a finite-difference representation of one-dimensional (radial or axial) few group time dependent diffusion theory with delayed neutrons and with nonlinear Spatial Doppler and scram feedback. This model has been verified by analysis of published results obtained using the industry standard computer code WIGLE.[29]

5.1.2 Radial Analysis

A hypothetical prompt excursion from hot-startup conditions was analyzed in the radial direction using three prompt groups and six delayed groups. The reactor was initially in a black-white-gray control configuration (Figure 4-2) with 17.2 cm radius for the central controlled region, 25.6 cm radius for the uncontrolled region, 196.8 cm radius for the partially controlled region, and 30 cm of reflector beyond the reactor core.

This pattern produced a center rod worth 1.5% in reactivity. The excursion was initiated by instantaneous removal of this center rod (i.e., approximately a $2.00 step insertion) ($\beta$ = .00724).

The two-dimensional adiabatic model was run with two points and symmetry boundary conditions in the axial direction to produce a one-dimensional radial solution. Both models used the same nonlinear spatial Doppler feedback relation. In both, scram was initiated when average power reached 120% of rated with 0.2 sec delay time. The same radial spatial mesh and boundary conditions were used in both models.

Results from the two models for this hypothetical problem are compared in Figures 5-1, 5-2, and 5-3. The two solutions were found to be in fairly good agreement with the adiabatic model exhibiting a slightly faster rise to peak power and quicker turnaround by Doppler, which translates into 1% higher average fuel enthalpy at termination of the transient. As seen in Figure 5-3, the final enthalpy distribution has very nearly the same shape for both models, but the adiabatic model predicts a peak fuel enthalpy which is about 1% low relative to the finite-differenced space-time model.

5.1.3 Axial Analysis

To determine the effect of moving control rods, the two models were compared for an axial problem simulating a rod dropping out of the core in time with scram rods moving into the core past the dropping rod. The reactor was initialized critical with a uniform control distribution. The uniform control distribution yielding a desired accident rod worth was also determined, representing the accident rod fully withdrawn without scram insertion.

A prompt excursion was simulated in the finite-differenced space-time model by varying the control fraction from rod-in to rod-out values at a constant rate starting at the top of the core and moving downward. Scram was tripped by core average power with 0.2 sec delay time before scram movement, which was simulated by increasing the control fraction to 1.0 at a constant rate from the bottom of the core upward. When the scram rods overlapped with the accident rod, the control fraction was reduced accordingly.

In the adiabatic model the accident rod was placed at the approximate axial position yielding $1.00 positive reactivity and held motionless. Accident reactivity and scram reactivity as functions of time were obtained from steady-state fundamental mode calculations (see Section 7).

This axial comparison was performed for a hypothetical 12 ft core at hot-startup conditions with 30 cm of reflector at each end. Three prompt groups and six delayed groups (β = .00701) were used. Scram setpoints, spatial Doppler feedback relations, axial mesh, and boundary conditions were the same in both models. The two-dimensional adiabatic

model was run with two points and symmetry boundary conditions in the radial direction to produce a one-dimensional axial solution. Rod drop velocity was 2.8 ft/sec with 2.16 ft/sec scram velocity. Comparison calculations were performed for accident rod worth values of 1, 2.5 and 4% relative to the critical $k_{eff} = 1.0$.

Net reactivity vs time results are compared in Figure 5-4, 5-5, and 5-6. The agreement between the two models is very good for the lower rod worth and is fairly good even for 4% rod worth. In all cases, peak enthalpy compared within 3%.

5.2 Comparison of Adiabatic Model to SPERT-I Transients

The final test of any analytical method is to compare the analytical results to actual experimental data. Unfortunately, this is not an easy task for a large light-water reactor due to the extremely high costs of such an experimental test program. However, since 1954, when the Atomic Energy Commission contracted Phillips Petroleum Company to undertake a long-range reactor safety program (SPERT-Special Power Excursion Reactor Tests) which included both nondestructive and integral core destructive tests, experimental data for prompt critical transients in small uranium oxide fueled reactors have been generated.

Although these experiments are of little help in verifying the accuracy of large core kinetics calculations, they are very helpful in verifying both the lattice method, i.e., the analytical methods used to generate nuclear constants and reactivity feedback mechanisms such as Doppler and moderator temperature. For this reason, comparisons have been made using the adiabatic approximation with several of the SPERT-I tests.[30,31] The test most characteristic of BWR excursion analyses was the SPERT-I 3.2 msec period experiment.

Analysis of this experiment using the BWR lattice methods and excursion model has shown very good agreement. The results of this comparison are shown by Figure 5-7. As can be seen, the analytical results are slightly conservative when compared with experiment. As stated previously, the accuracy of these results give credence to the lattice methods and reactivity feedback models.

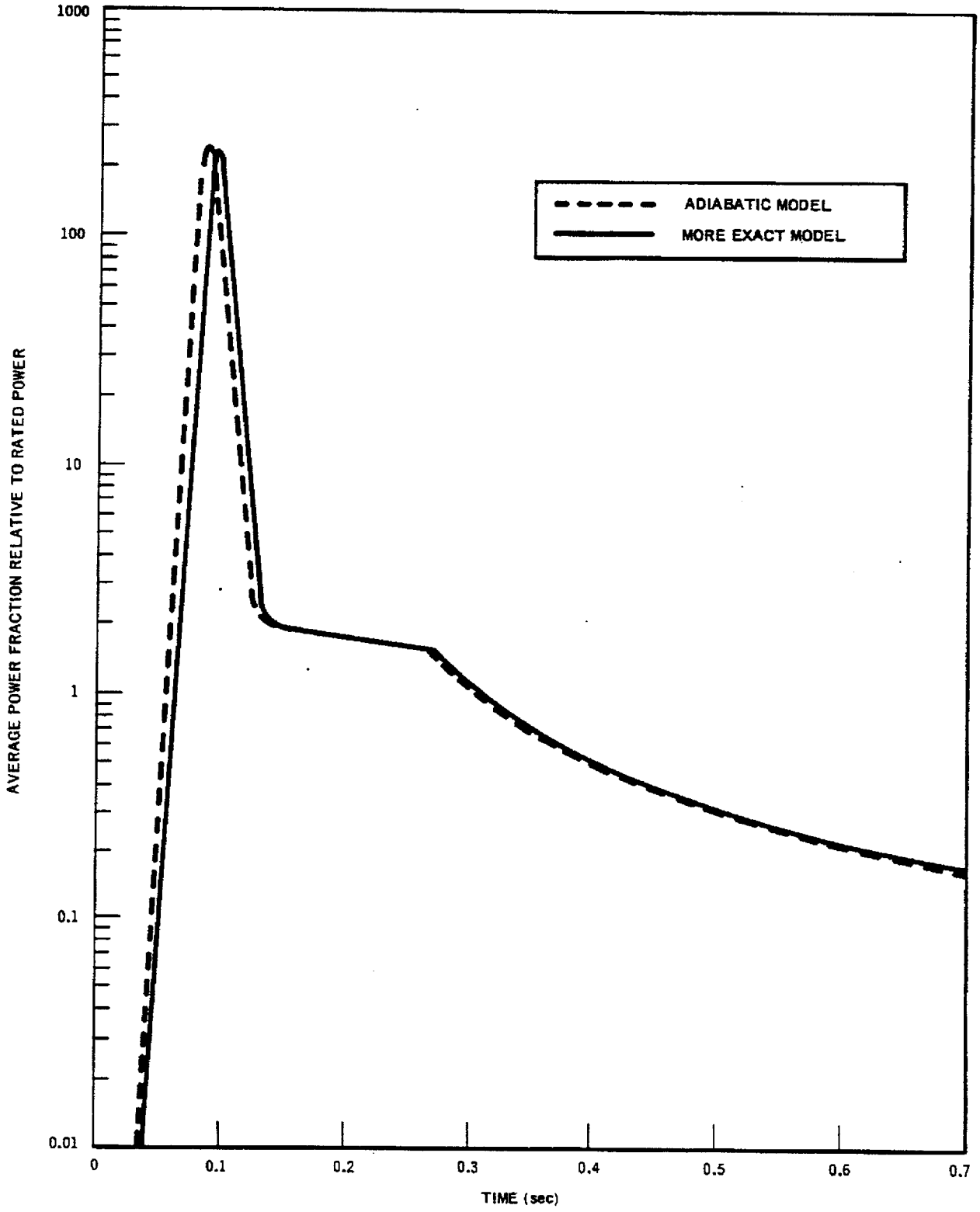

Figure 5-1 Average Power Fraction vs Time — Adiabatic Model Compared with More Exact Model

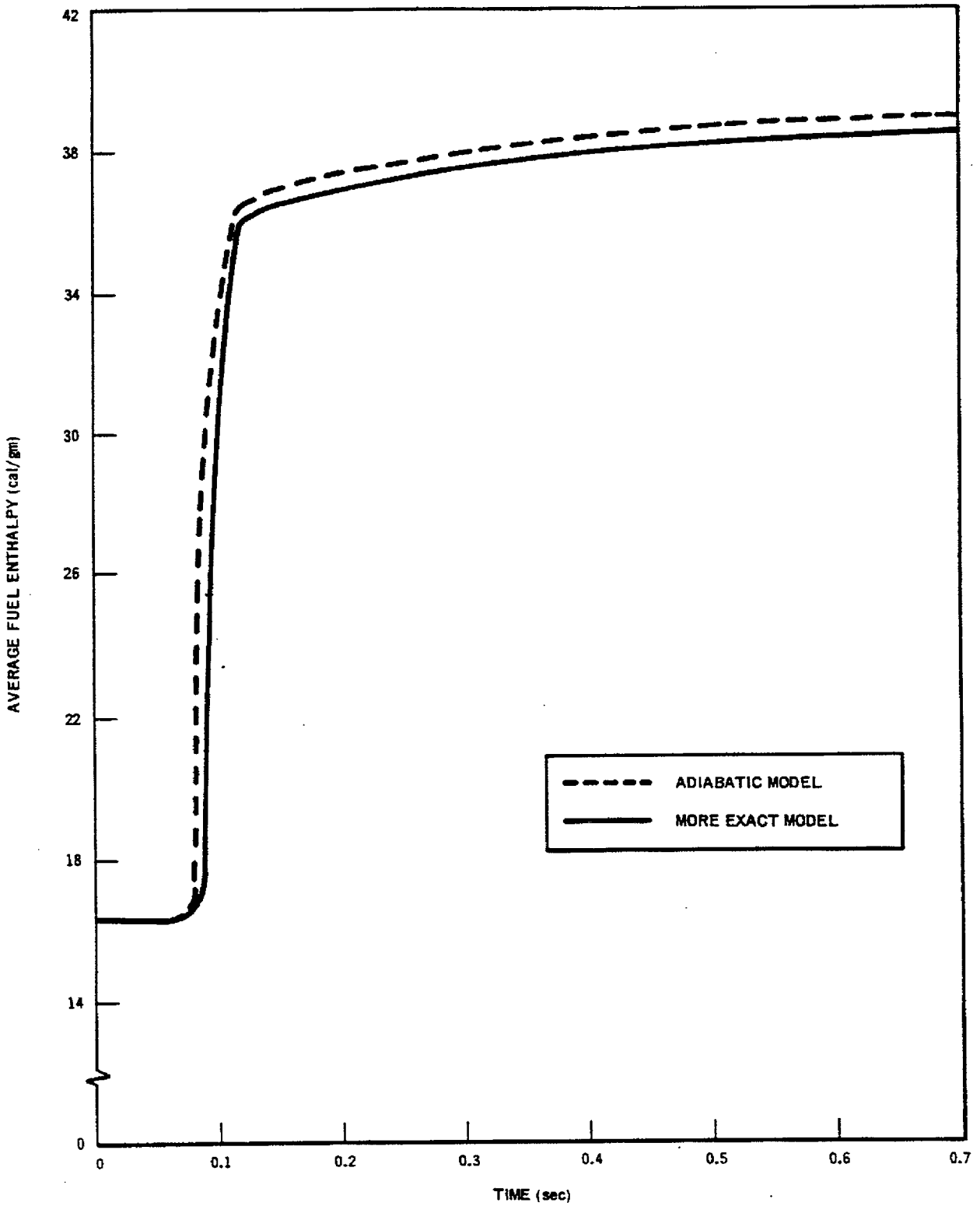

Figure 5-2 Average Fuel Enthalpy vs Time — Adiabatic Model Compared with More Exact Model

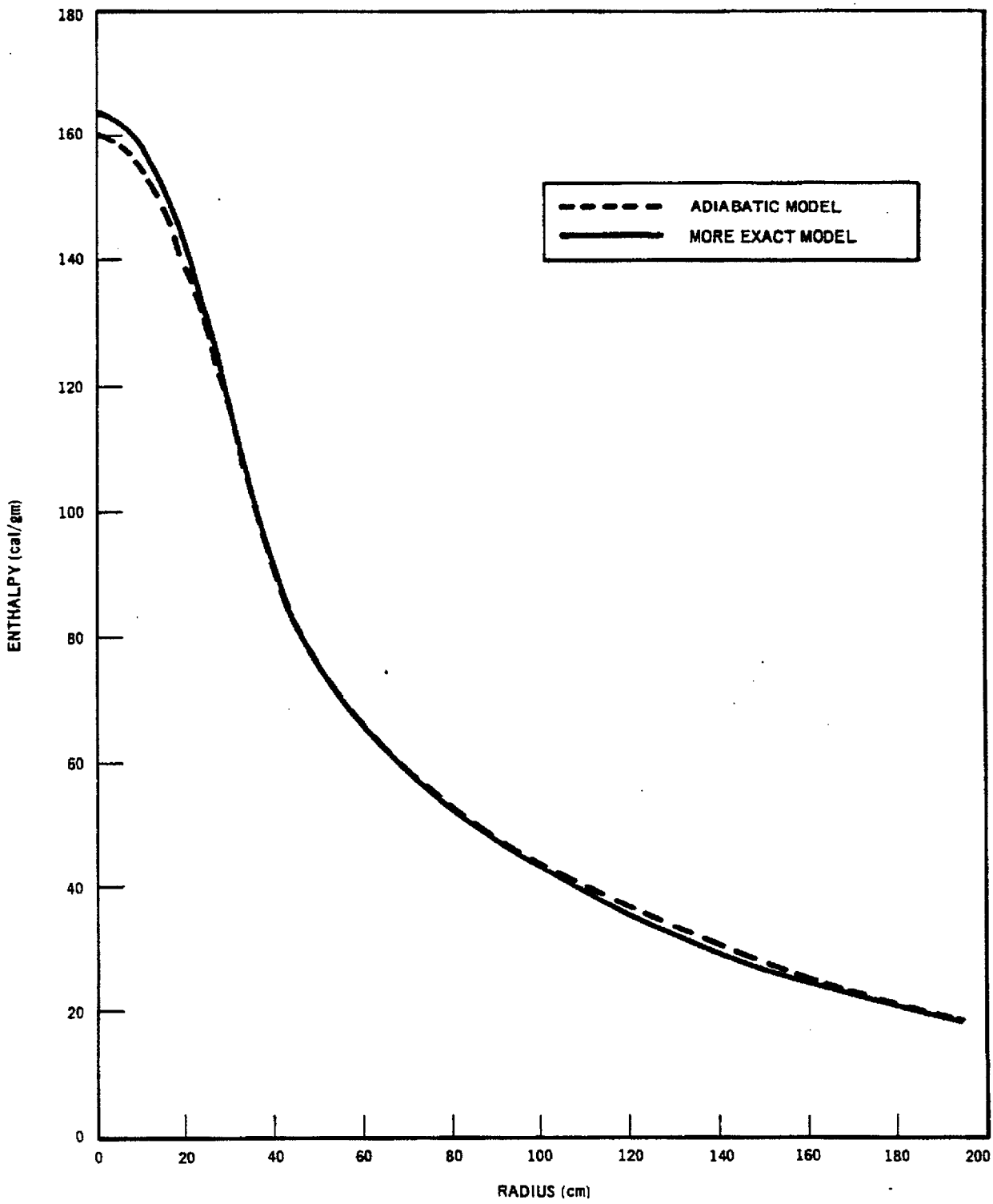

Figure 5-3 Final Enthalpy Distribution – Adiabatic Model Compared with More Exact Model

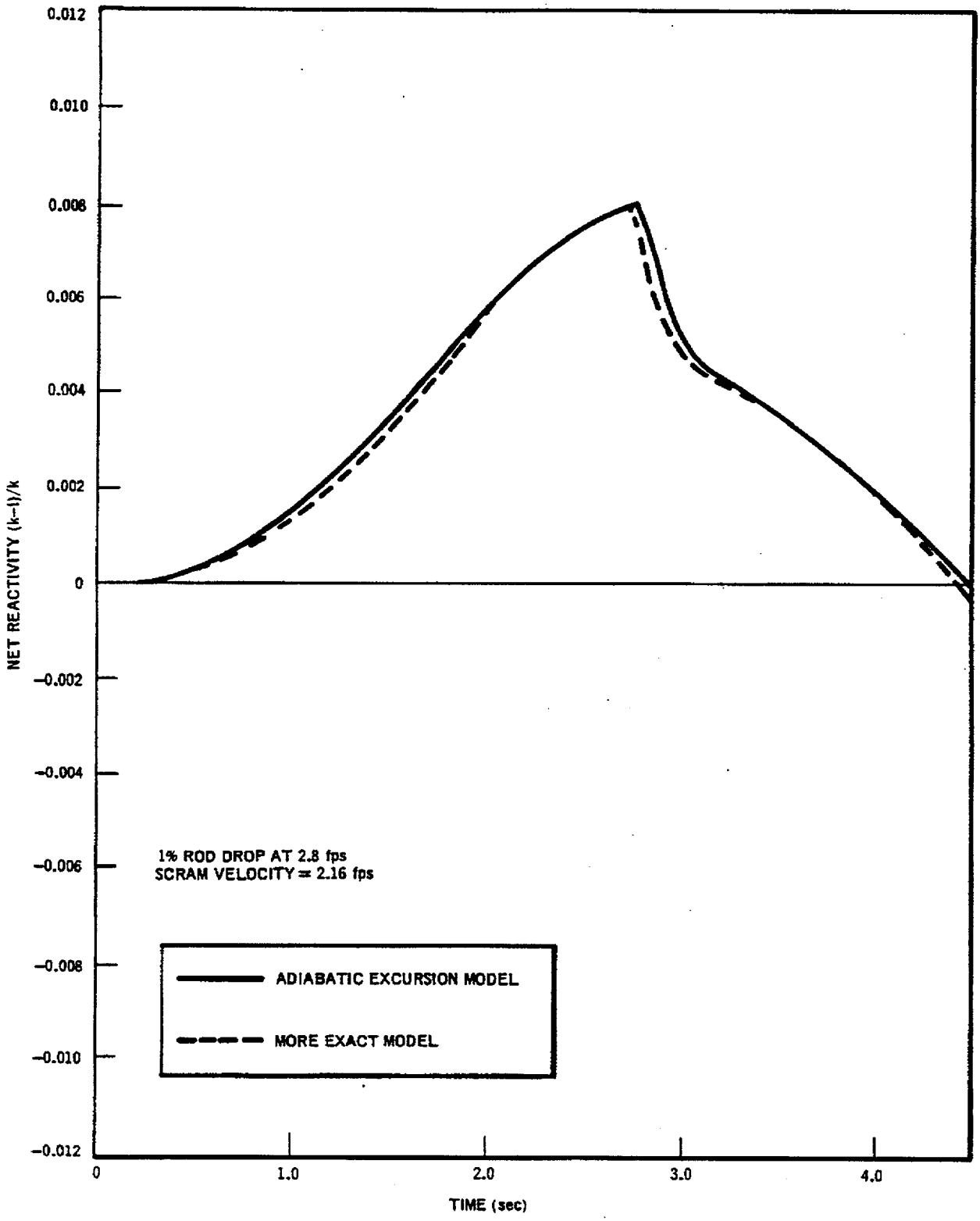

Figure 5-4 Net Reactivity vs Time (1% Rod Drop at 2.8 fps; Scram Velocity at 2.16 fps)

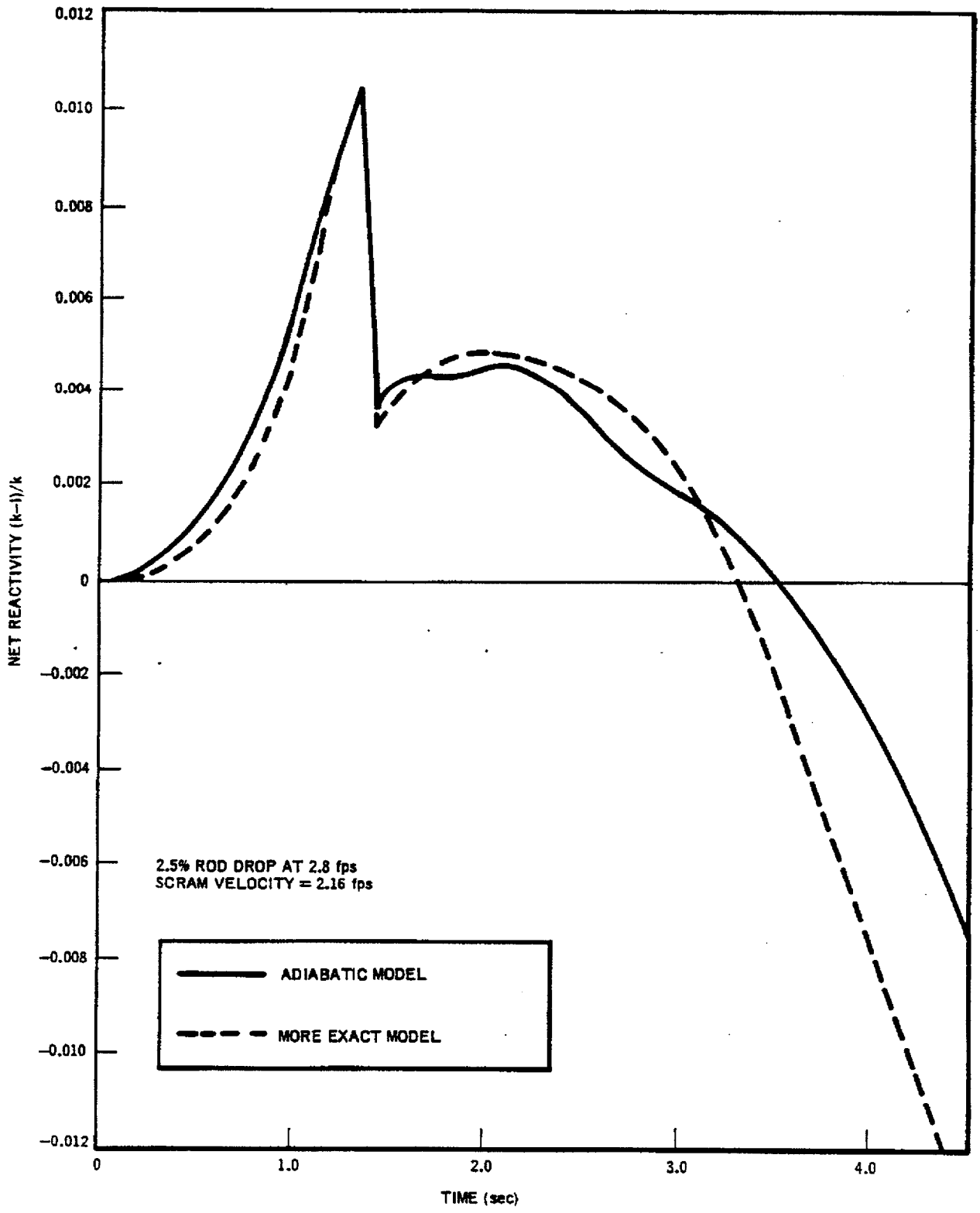

Figure 5-5 Net Reactivity vs Time (2.5% Rod Drop at 2.8 fps; Scram Velocity at 2.16 fps)

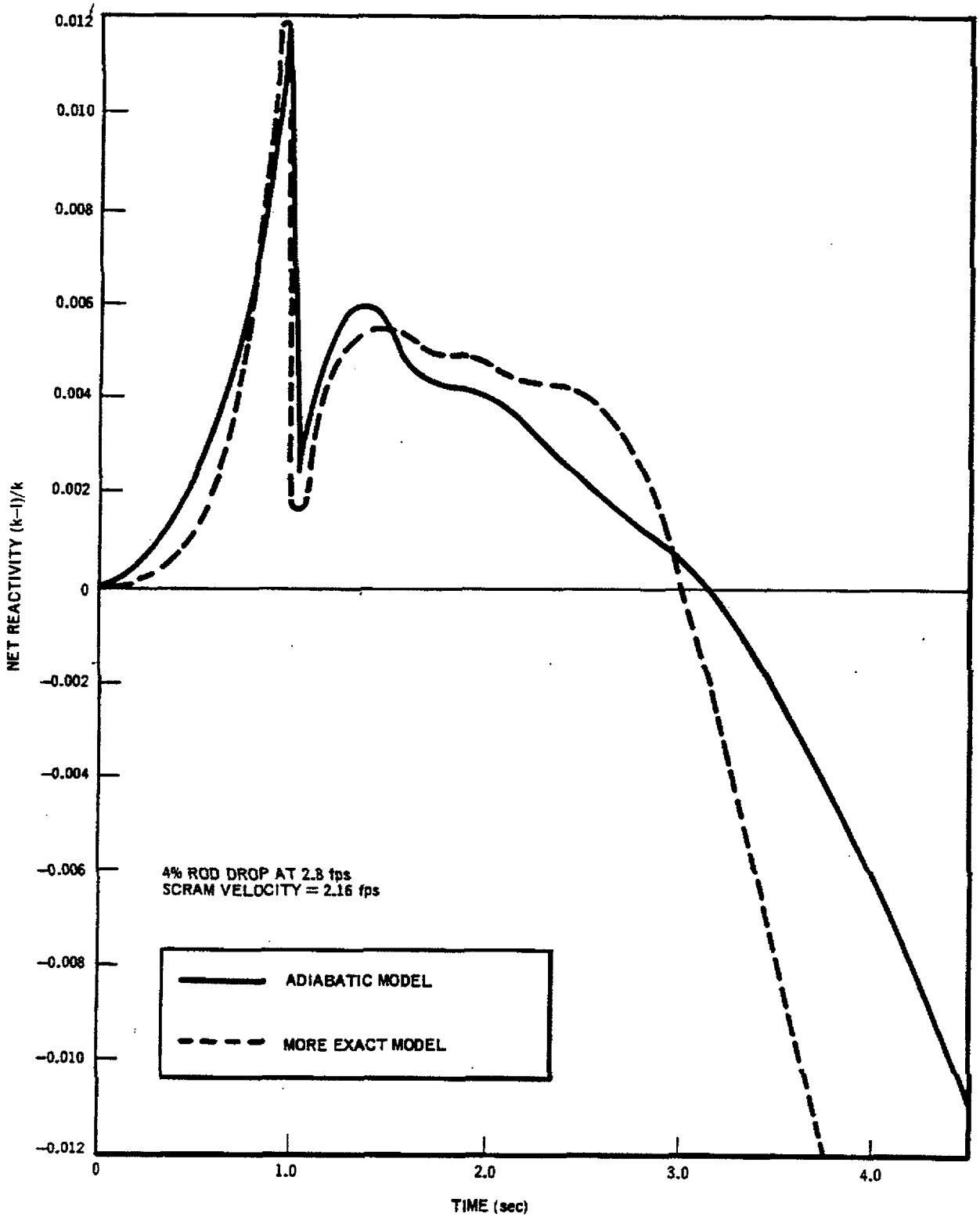

Figure 5-6 Net Reactivity vs Time (4% Rod Drop at 2.8 fps; Scram Velocity at 2.16 fps)

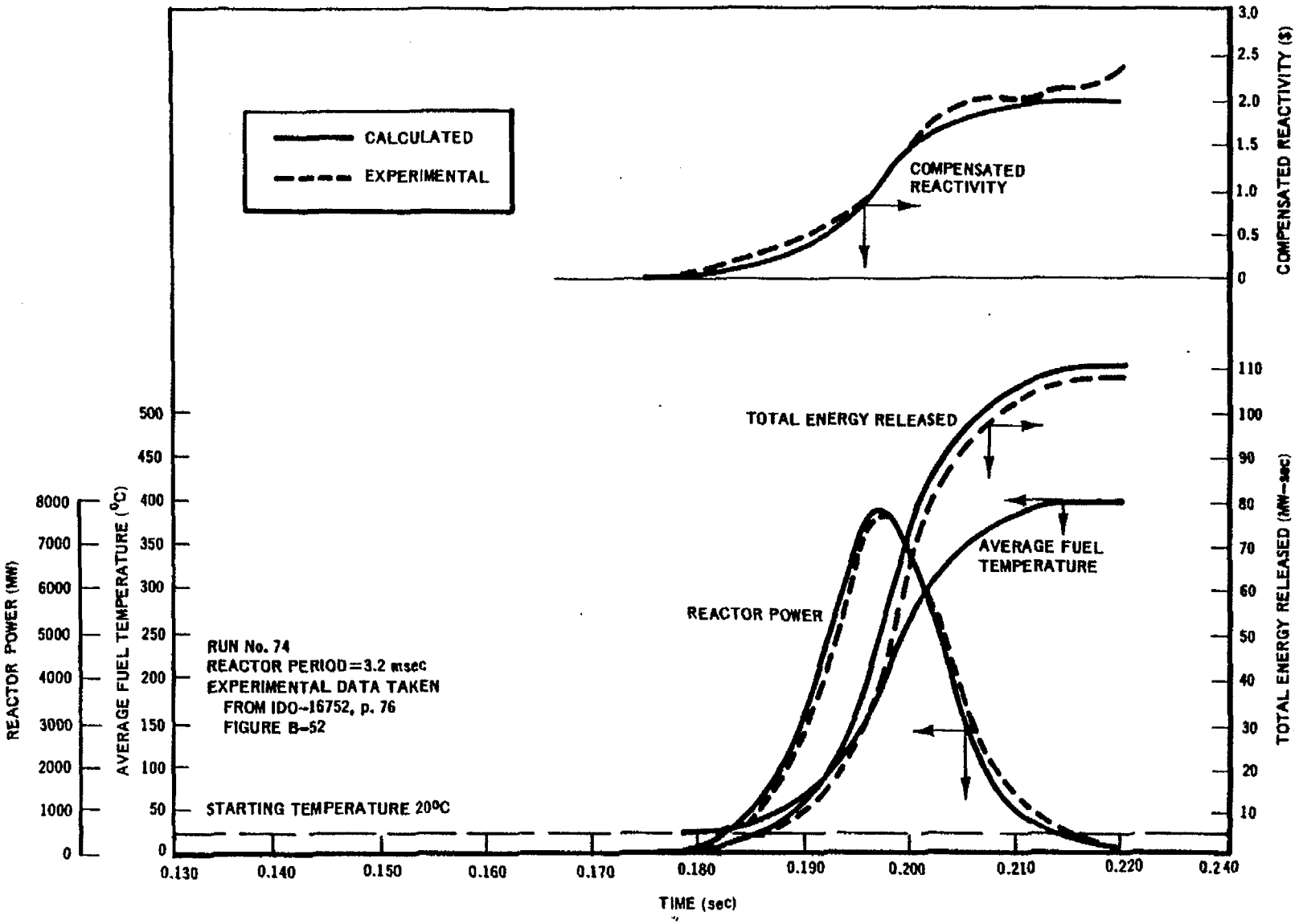

Figure 5-7 Experimental and Calculated Power, Energy, Average Fuel Temperature and Compensated Reactivity as Functions of Time

6. DEVELOPMENT OF EXPERIMENTAL INPUT DATA

6.1 Specific Heat of UO_2

Recent experiments on the physical properties of UO_2[32,33] have shown the specific heat of UO_2 to be highly nonlinear, especially when the fuel temperature approaches the incipient melting point. Figures 6-1 and 6-2 show these experimental results. In the range of 25 to 902°C, data which were obtained by Moore and Kelly[35] are applied, and between 900 and 2842°C the data of Hein and Flagella[32] were used. In addition, the melting point of 2842°C and the heat of fusion of 67.4 cal/gm was also taken from Hein and Flagella. Above the melting range, data from Hein and Flagella, Leibowitz, et.al.[33] and Chasanov[34] were used for the heat capaicty of the fuel.

Referring to Figure 6-1, it is seen that the incipient melting point and fully molten state for UO_2 occur at 269.4 and 336.8 cal/gm, respectively. It should be noted that in previous documents concerning rod drop accidents these values were quoted as 220 and 280 cal/gm.

6.2 Velocity Limiter Test Data

As discussed previously, the rod drop accident was analyzed parametrically, and one of the variables studied was the rod drop velocity. The extremes for this variable were based on the design limit drop velocity of 5 fps and the 99.9% confidence limit value which was determined from experimental testing of nine production blades. The details of the test procedures, test data, and the test results are presented in Appendix A. It will be sufficient to state here that the measured rod drop velocities referenced to in the results pertain to 2.36 fps and 2.79 fps rod drop velocities at the cold and hot-startup conditions, respectively.

6.3 Scram Insertion Test Data

In addition to parameterizing the control blade drop velocity, the scram insertion rate was also varied. The maximum scram insertion times used in this study were the tech spec values, and the minimum insertion times employed were experimentally measured values. The experimental average insertion times measured from the de-energization of the scram solenoid valves to the 90% insertion points were 1.6 and 2.6 sec for the cold and hot startup conditions, respectively.

Since tech spec scram times must be employed when doing safeguards analyses, no attempt will be made to justify the measured scram insertion times. The reason for including the measured scram times in this study was merely to demonstrate both the rod drop accident results under expected or realistic conditions and also the sensitivity of the accident to scram insertion rates.

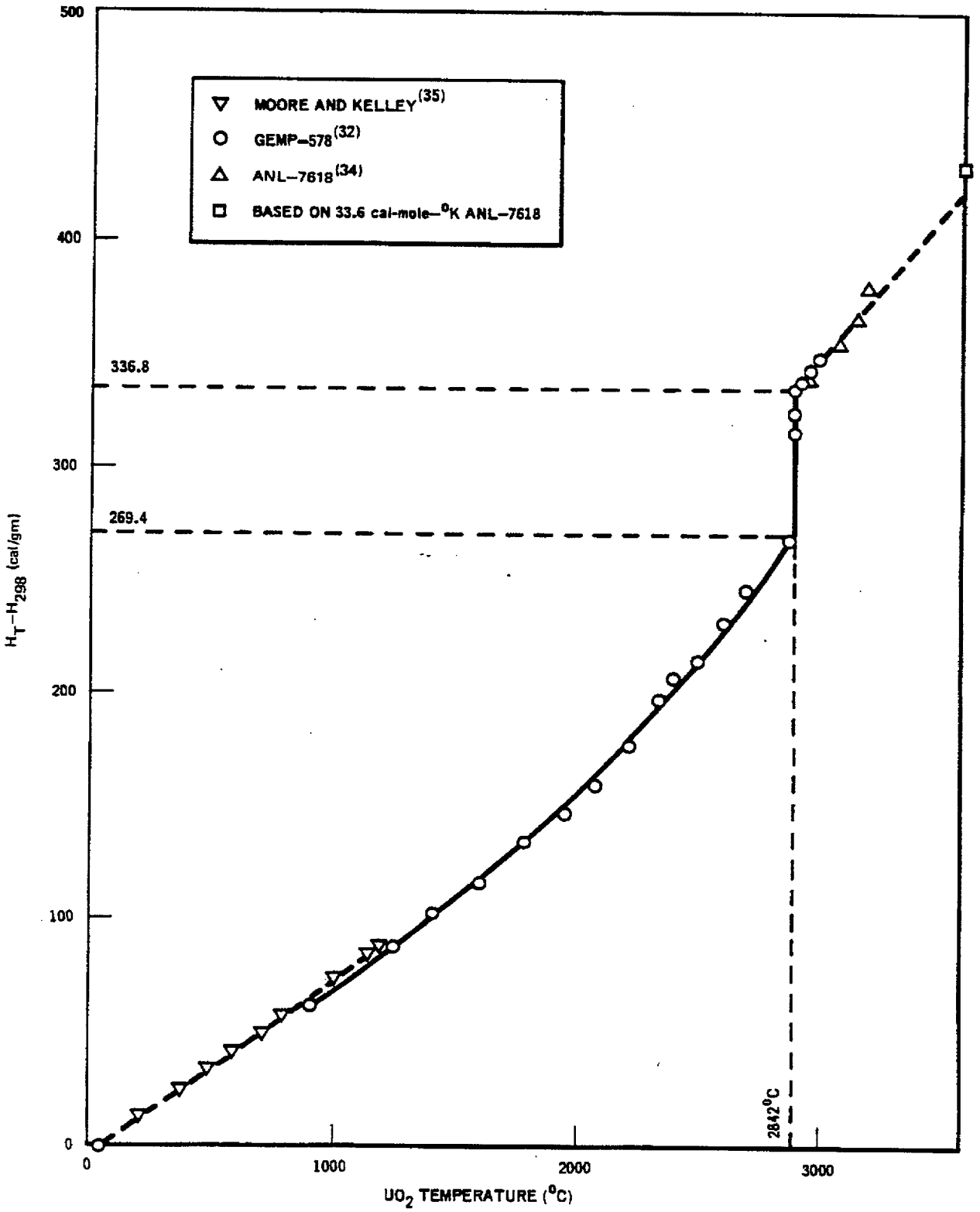

Figure 6-1 UO_2 Enthalpy as a Function of Fuel Temperature

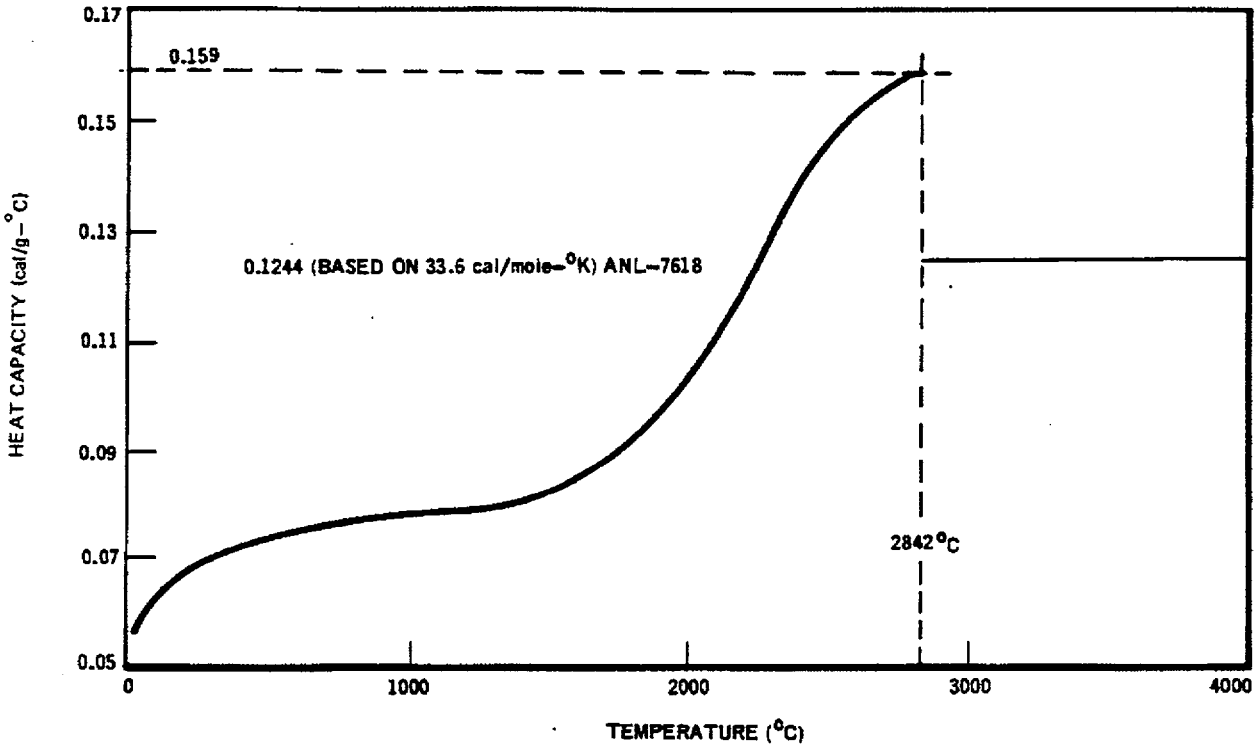

Figure 6-2 UO_2 Heat Capacity as a Function of Temperature

7. DEVELOPMENT OF ANALYTICAL INPUT DATA

7.1 Generation of Nuclear Constant

The nuclear constants, i.e., cross sections, average neutron speed, delayed neutron fractions are calculated using the standard lattice design techniques as described in the PSAR's and FSAR's and will not be discussed here in detail. It should be sufficient to state that the fuel bundle calculations are done using XY geometry with the fuel pins, in-channel moderator, channel, gap water, curtains, and control blade being discretely represented.

7.2 Delayed Neutron Fraction and Decay Constants

The basic delayed neutron fraction and decay constant data for the heavy metal isotopes was obtained from Keepin.[36] Since the material properties of the reactor vary spatially, the delayed neutron fraction will vary from region to region in the reactor core. For this reason, the effective delayed neutron fraction which is used in the point model kinetics equations must be spatially weighted.

The effective delayed neutron fraction used in the point model kinetics is calculated by using the methods outlined by Henry.[37] Using this approach and assuming that all neutrons (including the delayed neutrons) are born into the fast energy group, the expression for the effective delayed neutron fraction for precursor group i is as follows:

$$\bar{\beta}_i = \frac{\int_v \left[\sum_j \beta_i^j \sum_g \phi_{1,g}^* \nu \Sigma_{f_g}^j \phi_g \right] dV}{\int_v \left[\sum_j \sum_g \phi_{1,g}^* \nu \Sigma_{f_g}^j \phi_g \right] dV}$$

j = heavy metal isotope

g = prompt neutron energy group

In like manner, the average decay constant for the ith precursor group is calculated from the following relationship:

$$\bar{\lambda}_i = \frac{\int_v \left[\sum_j \beta_i^j \sum_g \phi_{1,g}^* \nu \Sigma_{f_g}^j \phi_g \right] dV}{\int_v \left[\sum_j \frac{\beta_i^j}{\lambda_i^j} \sum_g \phi_{1,g}^* \nu \Sigma_{f_g}^j \phi_g \right] dV}$$

The validity of this approach is borne out by the fact that the comparison between the adiabatic model and finite-differenced space-time kinetics was in very good agreement, as discussed previously in subsection 5.1.

7.3 Accident Reactivity Shape Function

As described previously in Section 4, the net reactivity for the adiabatic excursion model is calculated by summation of the accident, Doppler, and scram reactivities. Since spatial effects are very important in calculating these reactivity effects, multi-dimensional analyses must be performed.

The reactor geometries which are used for analyzing the rod drop excursions in the startup range and in the low power range are shown in Figures 7-1 and 7-2, respectively. In the startup range, material properties and nuclear properties change due to increasing temperatures. In addition, as the rod worth changes, the radius of Region 2 and the amount of control in Region 3 must vary to maintain a critical reactor with the center control rod fully inserted. Therefore, the geometry of the problem will vary with both the control rod worth and the reactor operating state.

In the power range the material properties of the system and nuclear properties change due to the in-channel void distribution. Also, the outer radius of Region 3 will vary with core power and rod worth. The void distribution and initial criticality state were calculated by doing a three- dimensional coupled nuclear-thermal-hydraulics calculation. These results were then reduced to RZ geometry by conserving volumes. In the power range the control rod worth is defined to be the excess reactivity which results due to the instantaneous withdrawal of a control rod; therefore, there is no heat loss or addition, and the void distribution remains fixed at its initial value.

As stated previously, the spatial effects on the control rod reactivity shape function for a specific rod worth are included by doing the analyses in RZ geometry as shown in Figure 7-1 and 7-2 at the desired initial reactor operating state. This is accomplished by doing a series of steady-state calculations with the center control rod in various axial positions, and the control rod worth is defined to be the eigenvalue difference relative to the initial eigenvalue.

Results of these analyses performed for the cold- and hot-startup reactor operating states are shown in Figure 7-3 and 7-4, respectively. In addition, the reactivity shape function for the maximum rod worth at hot standby is shown in Figure 7-5. Comparison of these results clearly demonstrates the importance of the spatial effects of rod worth and operating conditions on the control rod reactivity shape function.

7.4 Scram Reactivity Shape Function

7.4.1 Method of Calculation

7.4.1.1 Startup Range

In the startup range the scram shape function can be conservatively calculated by doing a series of one-dimensional steady-state calculations in the axial direction. Since there are no radial or axial void distributions to consider, the motion of the scram rods can be represented in slab geometry by the rods being inserted as a bank. It will be demonstrated below that this approach yields a conservative answer.

The calculation of the scram shape function was performed using a one-dimensional axial steady-state diffusion theory computer program with the cross-section represented by three neutron energy groups. The reactor was represented as a slab with 30 cm of reflector at each end. Since the control rods normally selected are fully withdrawn and uniform moderator conditions exist axially during startup, the reactor core can be represented with homogenized cross sections for the proper reactor state. This reactor system is then brought critical by varying the thermal absorption cross section.

The scram reactivity shape function is then calculated by adding fully controlled cross sections starting at the bottom of the reactor and progressing upward in incremental steps until the reactor is fully controlled. The difference in the steady-state eigenvalues between the initial state and with the control rods banked in various axial positions is defined to be the scram reactivity as a function of rod bank position. The results of these calculations for the cold and hot startup reactor states are shown in Figure 7-6.

7.4.1.2 Operating Power Range

The calculation of the scram function in the power range is more complex since the moderator density is nonuniform due to the formation of in-channel voids which vary both axially and radially. In order to account for the effects of this void distribution on the scram reactivity, the scram function in the power range is calculated using RZ diffusion theory for the geometry depicted by Figure 7-2. As was the case in the startup range, the scram reactivity is defined to be the difference between steady-state eigenvalues with the rods banked in various axial positions. It was also assumed that the void and Doppler reactivity distributions remained constant at their initial steady-state conditions during control rod insertion.

The void distribution and initial criticality state were calculated by using a three-dimensional coupled nuclear-thermal-hydraulics calculation. These results were then reduced to RZ geometry by conserving volumes. The scram reactivity function used for analyzing the rod drop accident inititated at 10% of rated power is shown in Figure 7-7. This function was calculated using the method described above.

7.4.2 Verification of Analytical Approach

To verify the accuracy of representing simultaneous control rod movement by summing the accident rod drop effect with the effect of scram bank insertion, where each is independently determined from steady-state fundamental mode calculations, this steady-state sum was compared with the total control rod effect obtained from a transient calculation with coincident rod motion. The transient calculation (previously described in subsection 5.1.3) was performed for accident rod worth values of 1, 2.5 and 4% relative to the critical $k_{eff} = 1.0$.

Figures 7-8 through 7-10 illustrate that the total delta-k due to control rods obtained by summing the separate effects of accident rod drop plus scram bank insertion, determined from steady-state fundamental mode calculations, is usually conservative when compared with total control delta-k resulting from simultaneous rod movement in a finite-differenced transient model. Total control delta-k determined by the transient model exceeds the steady-state sum only by a small amount over a short time period.

7.5 Neutron Generation Time

Since the material properties are spatially varying in the reactor, the nuclear constants and average neutron speeds will also vary spatially. As was the case for the delayed neutron fraction, the method which is used for calculating the neutron generation time used in the kinetics equations is based on previous work performed by Henry.[37]

The equation used to calculate the generation time, Λ, is as follows:

$$\Lambda = \frac{\int_{core} \sum_{g} \frac{\phi_g^* \phi_g}{v_g} \, dV}{\int_{core} \sum_{g} \phi_1^* \nu \Sigma_{f_g} \phi_g \, dV}$$

g ≡ prompt neutron energy group

The validity of this approach is borne out by the fact that the comparison between the adiabatic model and finite differenced space-time kinetics was in very good agreement as discussed previously in subsection 5.1.

7.6 Control Rod Worth

7.6.1 Control Rod Withdrawal Sequences

To understand the definition of an in-sequence, out-of-sequence, and maximum worth control rod, the control rod withdrawal sequences must be completely understood. For this reason a description of the control rod withdrawal sequences will precede the discussion of control rod reactivity worths.

To clarify this discussion it will be best to divide the control rod withdrawal sequences into two steps. The first range of withdrawals to be discussed will cover the fully inserted to the 50% density or checkerboard control configurations. For simplification this will be referred to as the startup range. The second step will cover control rod withdrawals from the checkerboard through the power range control configurations. This will be referred to as the power range. Although the examples shown here are, in part, for a 560 bundle reactor core, it should be kept in mind that this discussion is generic in nature and applies for all reactor sizes.

7.6.1.1 Control Rod Withdrawal Sequences in Startup Range

The selection of the control rod withdrawal sequences to the 50% control rod density point is relatively straight forward and is outlined in the following set of instructions:

RWM SEQUENCE A

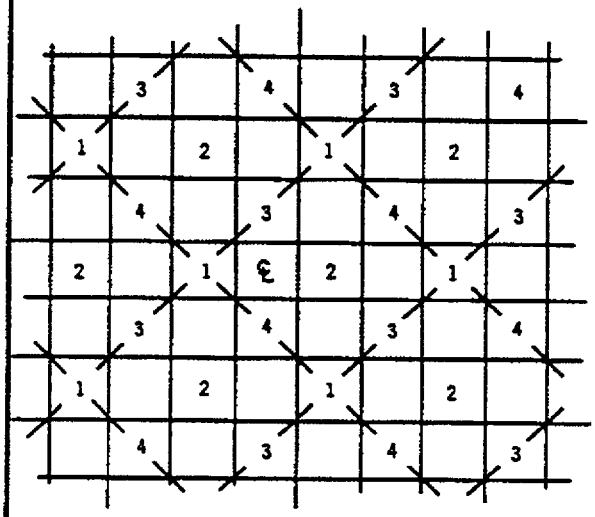

1. SEQUENCE A IS DEFINED AS THE SEQUENCE WHICH DOES NOT HAVE THE CENTER CONTROL ROD (℄) WITHDRAWN AT 50% CONTROL ROD DENSITY.
2. THE RODS WITHDRAWN AT 50% CONTROL ROD DENSITY ARE SHOWN BY THE NUMBERED LOCATIONS IN THE FIGURE. THE NUMBERS INDICATE THE GROUP NUMBER WITHIN SEQUENCE A.
3. THE LOCATION OF CONTROL RODS WITHIN A GROUP ARE DEFINED BY THE INTERSECTION OF DIAGONAL LINES OF A NINE ROD DIAMOND ARRAY. THIS IS ILLUSTRATED IN THE FIGURE FOR GROUP 1.
4. ALL THE RODS IN A GROUP MUST BE WITHDRAWN BEFORE PROCEEDING TO THE NEXT GROUP.
5. THE ORDER IN WHICH GROUPS ARE WITHDRAWN IS RESTRICTED BUT NOT TO JUST 1,2,3,4. ANY GROUP NUMBER MAY BE SELECTED AS THE FIRST GROUP OF CONTROL RODS TO BE WITHDRAWN. THE SECOND GROUP TO BE WITHDRAWN IS THE CRITICAL SELECTION. IT MUST NOT BE DIAGONALLY ADJACENT TO FIRST GROUP. THE REMAINING TWO GROUPS MAY BE WITHDRAWN IN EITHER ORDER.

RWM SEQUENCE B

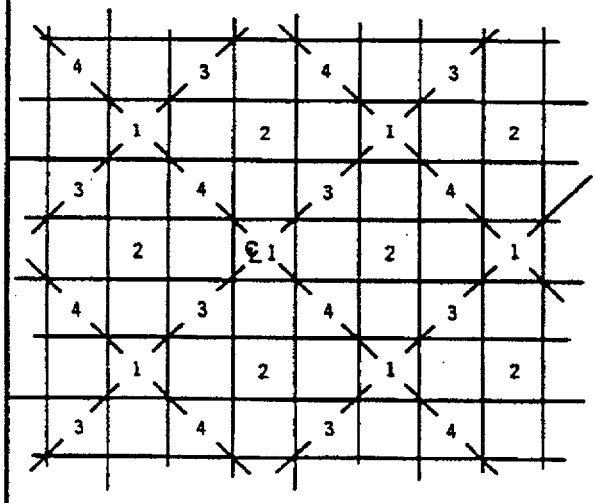

1. SEQUENCE B IS DEFINED AS THE SEQUENCE WHICH DOES HAVE THE CENTER CONTROL ROD (℄) WITHDRAWN AT 50% CONTROL ROD DENSITY.
2. THE RODS WITHDRAWN AT 50% CONTROL ROD DENSITY ARE SHOWN BY THE NUMBERED LOCATIONS IN THE FIGURE. THE NUMBERS INDICATE THE GROUP NUMBER WITHIN SEQUENCE B.
3. THE LOCATION OF CONTROL RODS WITHIN A GROUP ARE DEFINED BY THE INTERSECTION OF DIAGONAL LINES OF A NINE ROD DIAMOND ARRAY. THIS IS ILLUSTRATED IN THE FIGURE FOR GROUP 1.
4. ALL THE RODS IN A GROUP MUST BE WITHDRAWN BEFORE PROCEEDING TO THE NEXT GROUP.
5. THE ORDER IN WHICH GROUPS ARE WITHDRAWN IS RESTRICTED BUT NOT TO JUST 1,2,3,4. ANY GROUP NUMBER MAY BE SELECTED AS THE FIRST GROUP OF CONTROL RODS TO BE WITHDRAWN. THE SECOND GROUP TO BE WITHDRAWN IS THE IMPORTANT SELECTION. IT MUST NOT BE DIAGONALLY ADJACENT TO FIRST GROUP. THE REMAINING TWO GROUPS MAY BE WITHDRAWN IN EITHER ORDER.

Using the above set of instructions, the rod withdrawal sequences to 50% control density for sequence B have been developed and are shown in Figure 7-11. As has been stated in the instructions, these groups may be selected in any order, e.g., groups 3 and 4 have been interchanged in Figure 7-11.

Once a control rod has been selected for withdrawal in the startup range, it is withdrawn from its fully inserted to fully withdrawn position. Also, the order in which the control rods are selected and withdrawn in any one rod worth minimizer (RWM) group is not restricted. If any control rod selected for withdrawal is inoperable during this period, it may be valved out of service in its fully inserted position without adversely affecting the reactivity worths of the remaining control rods to be withdrawn.

(a) Maximum In- and Out-of-Sequence Control Rod Worth Patterns

Referring to Figure 7-11, it becomes obvious that any control rod which is not scheduled for withdrawal is an out-of-sequence control rod; however, it is not obvious which *single* operator error would produce the maximum out-of-sequence control rod worth. After extensive studies, it has been determined that the maximum in-sequence and out-of-sequence control rod worths occur at very selective points in the sequence, as shown in Figures 7-12 and 7-13, assuming an infinite lattice array.

Referring to these figures shows that the maximum in-sequence rod worth will always occur when the first rod for a RWM group is withdrawn. Therefore, upon completion of withdrawing RWM groups 1, 2, or 3, the next in-sequence rod withdrawn, e.g., the first rod of groups 2, 3, or 4, respectively will result in the maximum in-sequence rod worth. All other in-sequence rods withdrawn will be of lower worth.

In like manner it was determined that the maximum out-of-sequence rod worth with a single operator error will occur under the following set of circumstances:

(1) the withdrawal of all control rods in a RWM group has been completed;
(2) a single rod from the next scheduled RWM group has been selected and fully withdrawn; and
(3) at this point the operator makes a single error by selecting and withdrawing the out-of-sequence control rod adjacent to the in-sequence rod which had previously been selected and withdrawn in step 2. This out-of-sequence rod is of maximum worth.

Any sequence of events other than those stated above, involving a *single* operator error, will always result in a lower out-of-sequence control rod worth.

Although the above discussion was based on an infinite lattice array, the same argument and results will apply to interior control rods of a large BWR. Due to neutron leakage effects on the core edges, edge control rods will have lower reactivity worths.

(b) Maximum Control Rod Worth Geometry

If multiple errors are made by the operator, it is possible to establish control rod configurations which result in high rod worths. These maximum rod worths are calculated by using the geometry shown in Figure 7-1. In the startup range the maximum rod worth will occur for a critical reactor when the center control rod is inserted and Region 3 is fully controlled. This is commonly referred to as the black-white-black (BWB) control configuration. For these analyses the reactor is brought critical by varying the outer radius of the uncontrolled region.

Since the operator has been instructed to withdraw a checkerboard sequence, it is quite obvious that multiple operator errors would have to be made in establishing this geometry. Furthermore, it is highly unlikely that an operator would unwittingly withdraw such a pattern.

7.6.1.2 Control Rod Withdrawal Sequences in the Power Range

Once the checkerboard control rod configuration has been reached, the definitions which were previously applied for in-sequence and out-of-sequence rods in the startup range no longer exist, since (as seen by Figure 7-11) all interior control rods will have approximately the same reactivity worth. The worth of each of these interior control rods when fully withdrawn will be approximately 2.0% $\Delta k/k$ in the hot startup state; however, the amount of reactivity which can be added due to a dropping control rod is restricted since only partial withdrawal of all of the remaining control rods in bank occurs. This is also a requirement to minimize the gross peaking in the reactor once significant power levels have been achieved.

If the control rods are withdrawn in a normal sequence, by definition all tech spec requirements must be maintained. However, in the discussion which follows it is assumed that no tech specs are controlling in order to develop control configurations which result in maximum possible rod worths due to multiple operator errors. It is clear that the control configurations which yield the maximum rod worths are extremely abnormal and could not be achieved if tech specs are adhered to.

Since there are many control rods in a BWR and each control rod has 24 axial notch positions, clearly there are many degrees of freedom in developing withdrawal sequences in the power range which are acceptable from the standpoint of power distribution and tech spec limits. As can be appreciated, this makes it rather difficult to define the worst single operator error. However, given a specific withdrawal sequence, the worst single operator error which results in the maximum rod worth can be defined.

A typical control rod withdrawal sequence for a 560 bundle reactor is shown by Figure 7-14. If the withdrawal sequence in Figure 7-14 is strictly adhered to, reactivity additions from a dropping control rod will be minimized since the rod can drop no further than the partially withdrawn rod drive. Furthermore, the uniformly distributed control configuration will contribute to minimizing the effect of a rod drop. In addition, the scram reactivity response will be improved since the partially withdrawn rods will be inserted into the high flux region upon initiation of scram.

(a) Maximum Control Rod Worth Pattern With a Single Operator Error

Due to the complexity of the rod withdrawal sequences in the power range, it would be very difficult on a generic basis to define the worst single operator error. However, given a specific withdrawal sequence, e.g., Figure 7-14, the worst single operator error at various points in the sequence can be evaluated.

In the power range the worst single operator error will be defined to be the selection and full withdrawal of the maximum worth control rod. This could result in two ways that potentially high reactivity additions can occur if the specific control rods involved are decoupled and stuck fully inserted. The first and most obvious way is the high worth rod itself. The second situation would arise if an adjacent drive which had previously been withdrawn in the sequence had a blade stuck in the fully inserted position.

As an example, assume that at some point in the sequence Rod 12-17 of Figure 7-14 is the maximum worth rod, and the operator makes an error and fully withdraws this rod. If this rod or either Rods 10-17, 14-17, 12-15, or 12-19 were decoupled and the blade stuck in the full insert position, these rods would be the highest worth rods in the reactor at that point in the sequence.

(b) Maximum Control Rod Worth Pattern With Multiple Operator Errors

If safe operation procedures and tech specs are completely disregarded and multiple operator errors are evaluated, potentially high rod worths could be developed in the power range. In the startup range it was found that the BWB geometry yielded the highest rod worth; however, due to the formation of voids in the uncontrolled region, the BWB pattern no longer results in the maximum rod worth.

From studies it was determined that maximum rod worths would occur in the power range for reactors with neutronically decoupled uncontrolled regions. Furthermore, the BWBW pattern depicted by Figure 7-2 resulted in the maximum rod worth.

7.6.2 Control Rod Worth Calculations

7.6.2.1 Control Rod Worth in Startup Range

In the startup range the maximum in-sequence and out-of-sequence control rod worths are determined by doing full core XY diffusion theory calculations with three neutron energy groups. The control configurations for the in-sequence and out-of-sequence rod worth calculations are shown in Figures 7-11, 7-12, and 7-13. Each uncontrolled and controlled fuel bundle is represented by appropriate homogenized cross sections which have been generated by using standard lattice design techniques.

The control rod worth is defined to be the eigenvalue difference calculated with the rod fully inserted and fully withdrawn. The maximum in-sequence and out-of-sequence control rod worths in the startup range for a typical BWR are shown by Figure 7-15. These curves represent the maximum envelope of all the rods without (lower left curve) and with (middle left curve) a single operator error.

The upper curve on the left-hand side of Figure 7-15 represents the maximum rod worth in the startup range assuming multiple withdrawal errors. These rod worths were calculated using RZ diffusion theory for the BWB geometry shown by Figure 7-1.

7.6.2.2 Control Rod Worths in the Power Range

In the power range the rod worth calculations are affected by the formation of steam voids in the moderator; therefore, multidimensional calculations which properly account for the void distribution must be performed. When void formation is present, the control rod worth is defined as the excess reactivity that occurs due to the instantaneous withdrawal of a control rod; therefore, no heat transfer or heat addition occurs and the void distribution remains constant at its initial value.

The maximum rod worth at power was calculated with RZ diffusion theory using the geometry shown in Figure 7-2. The initial void distribution is obtained from a three-dimensional coupled nuclear-thermal-hydraulic calculation. The results of this analysis are shown by the upper right-hand curve of Figure 7-15.

Since the normal withdrawal sequence in the power range includes partially withdrawn rods, the maximum rod worth with a single operator error must be calculated in three dimensions. Therefore, three-dimensional coupled nuclear-thermal-hydraulic calculations were performed to develop the lower right-hand curve of Figure 7-15.

7.7 Doppler Reactivity Feedback Model

The Doppler reactivity decrement is derived directly from the lattice calculations which are performed to generate the nuclear constants. The lattice methods currently being employed in the fast and resonance neutron energy regions are based on the method of Adler, Hinman and Nordheim[38] with the inclusion of the intermediate resonance approximation. This provides an adequate calculation of both the spatial and energy self-shielding for the resonance absorbers that explicitly includes temperature, moderator density, and geometry effects. A fine group B-1 slowing down calculation of the fast and epithermal neutron spectrum provides the proper weighting of the resonance absorption to yield effective resonance integrals or cross sections that accurately represent the BWR environment.

The Doppler decrement is determined by doing the lattice calculations at several fuel temperatures holding all other input parameters constant. This results in a change in the neutron multiplication factor which is solely due to a change

in the fuel temperature, which is the Doppler effect. From these analyses it has been determined that the Doppler defect, Δk_{Dop}, can be represented very accurately by the following expression:

$$\Delta k_{Dop} = CDOP\left(\sqrt{T_2} - \sqrt{T_1}\right)$$

Therefore, the Doppler reactivity decrement increases proportionally with the square root of fuel temperature, T, and CDOP is the constant of proportionality.

Since the Doppler effect is due mainly to resonance absorption, it is a good approximation to assume that only the second group or epithermal absorption will be perturbed by a change in fuel temperature. Therefore, in the excursion model it is assumed that the Doppler reactivity feedback occurs in the second group absorption cross-section only.

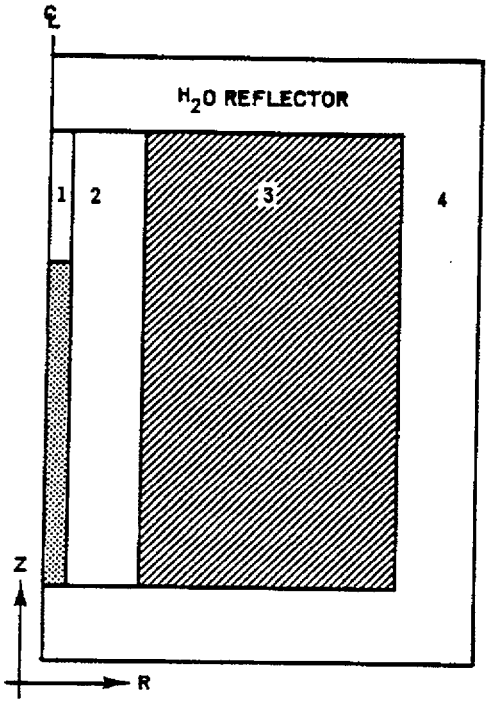

REGION	DESCRIPTION
1	THE RADIUS IS EQUIVALENT TO THAT OF AN EQUIVALENT CRUCIFORM CONTROL ROD.
2	UNCONTROLLED FUEL. THE RADIUS OF THIS REGION IS DETERMINED BY THE ROD WORTH.
3	PARTIALLY CONTROLLED FUEL. THE MATERIAL PROPERTIES IN THIS REGION ARE UNCONTROLLED WITH Σ_p REPRESENTING EITHER CONTROLLED OR EXPOSED CROSS SECTIONS. Σ_p IS DEPENDENT ON THE CONTROL ROD WORTH.
4	30 cm H_2O REFLECTOR.

Figure 7-1 Reactor Geometry for Analyzing Rod Drop Accident

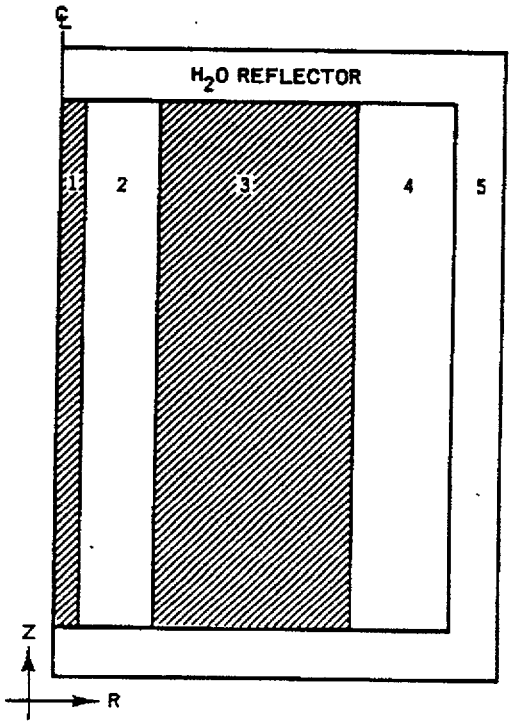

REGION	DESCRIPTION
1	CONTROLLED FUEL. THE RADIUS IS EQUIVALENT TO THAT OF A CRUCIFORM CONTROL ROD.
2	UNCONTROLLED FUEL. THE RADIUS OF THIS REGION IS SELECTED TO CONSERVE THE VOLUME OF THE 3–DIMENSIONAL CALCULATION.
3	CONTROLLED FUEL. THE RADIUS OF THIS REGION IS SELECTED TO CONSERVE THE VOLUME OF THE 3–DIMENSIONAL CALCULATION. IN THE 3–DIMENSIONAL CALCULATION, THE VOLUME OF THIS REGION IS ADJUSTED TO BRING THE REACTOR CRITICAL AT THE DESIRED POWER LEVEL.
4	UNCONTROLLED FUEL. THIS REGION REPRESENTS THE EQUIVALENT CORE RADIUS.
5	30 cm OF H_2O REFLECTOR.

Figure 7-2 Reactor Geometry for Analyzing Rod Drop Accident in Power Range

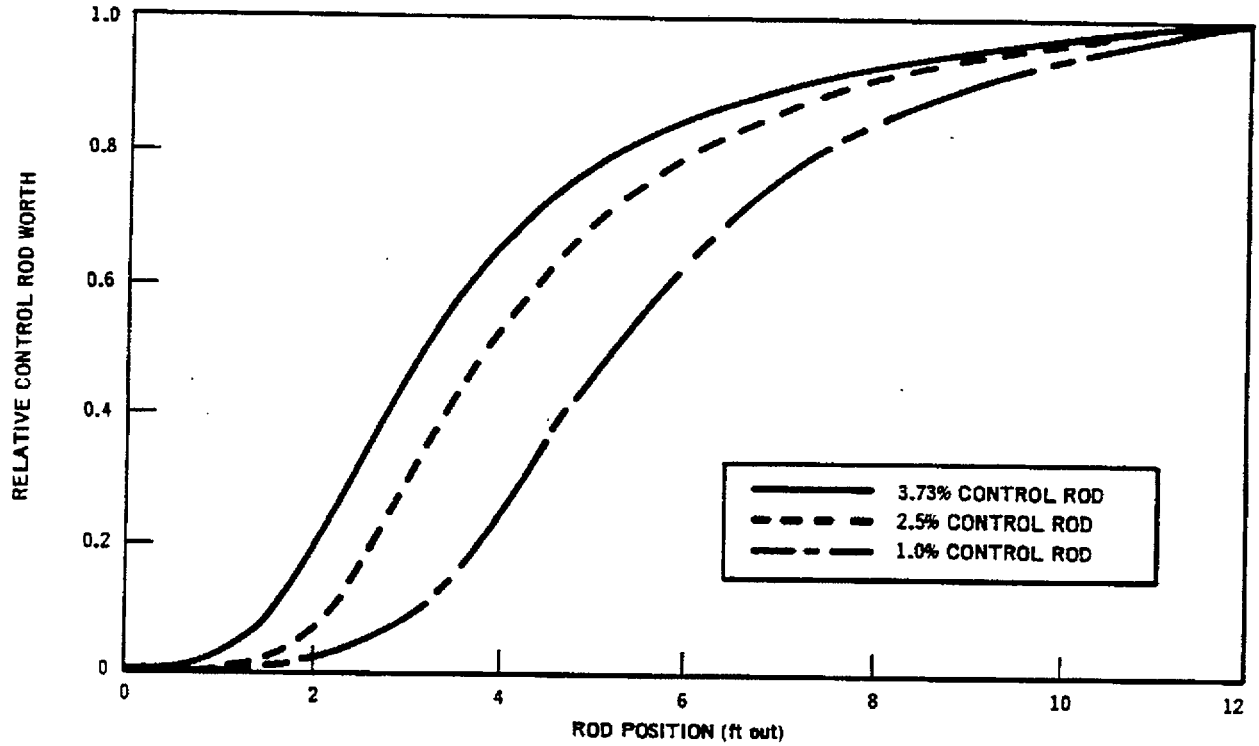

Figure 7-3 Relative Control Rod Worth for Rod Drop Excursion at 20°C

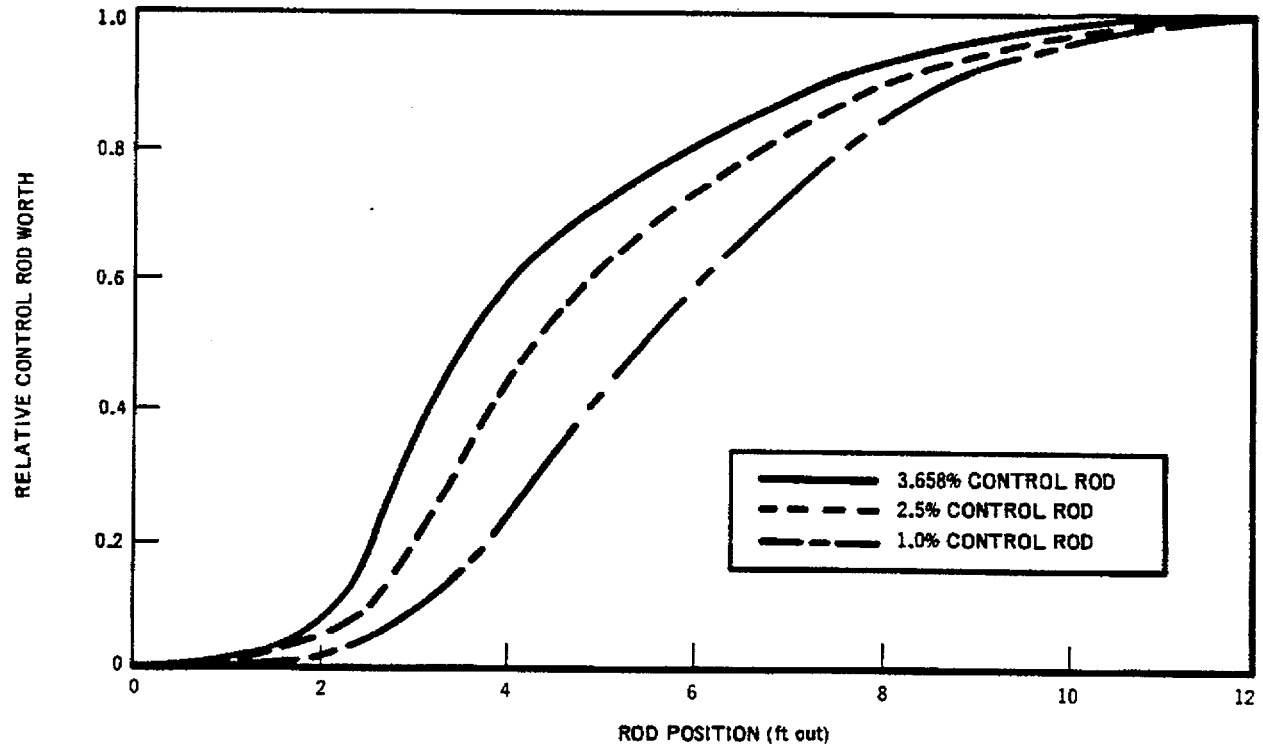

Figure 7-4 Relative Control Rod Worth for Rod Drop Excursion at 286°C

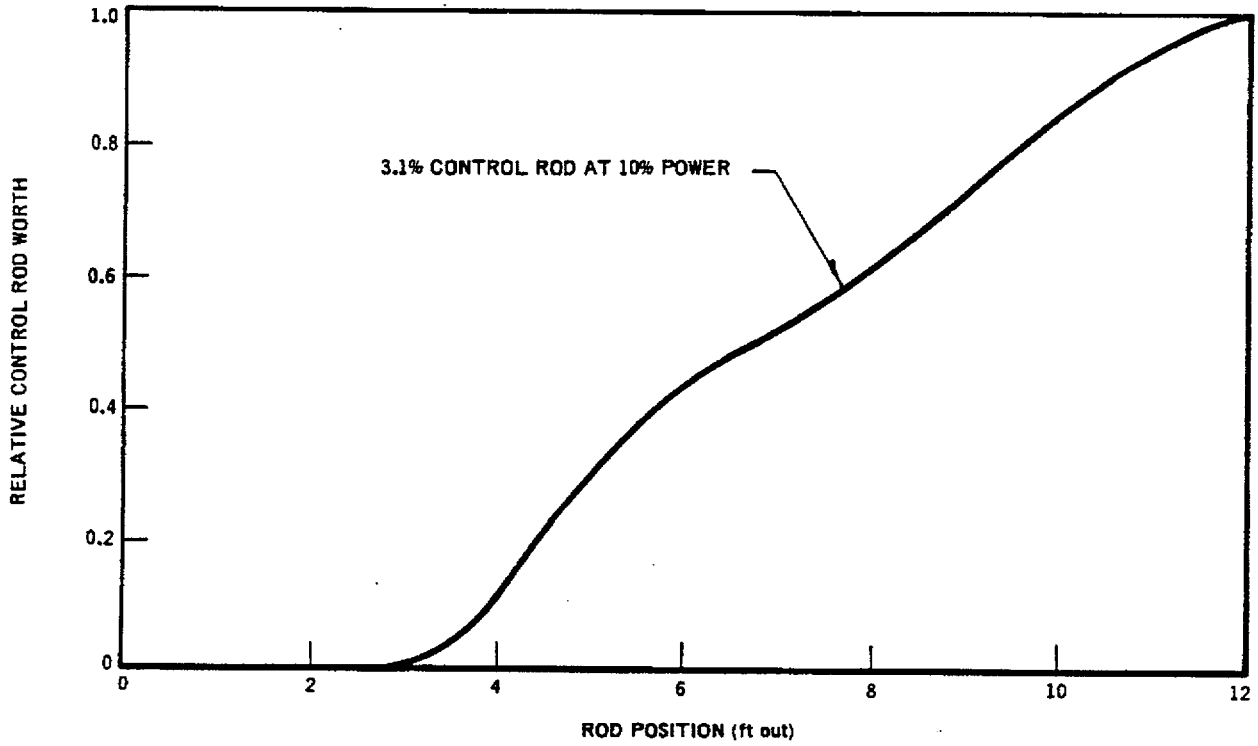

Figure 7-5 Relative Control Rod Worth for Rod Drop Excursion Initiating in Power Range

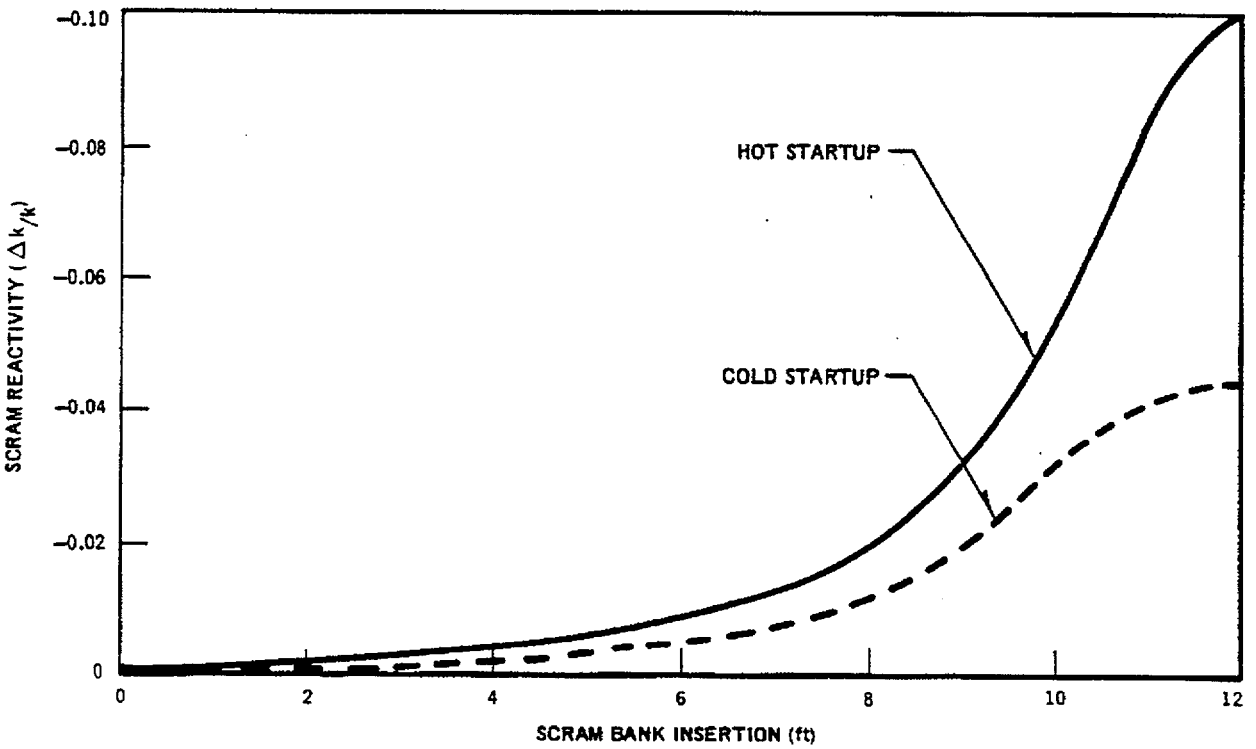

Figure 7-6 Scram Reactivity Shape Function for Cold and Hot Startup Reactor States

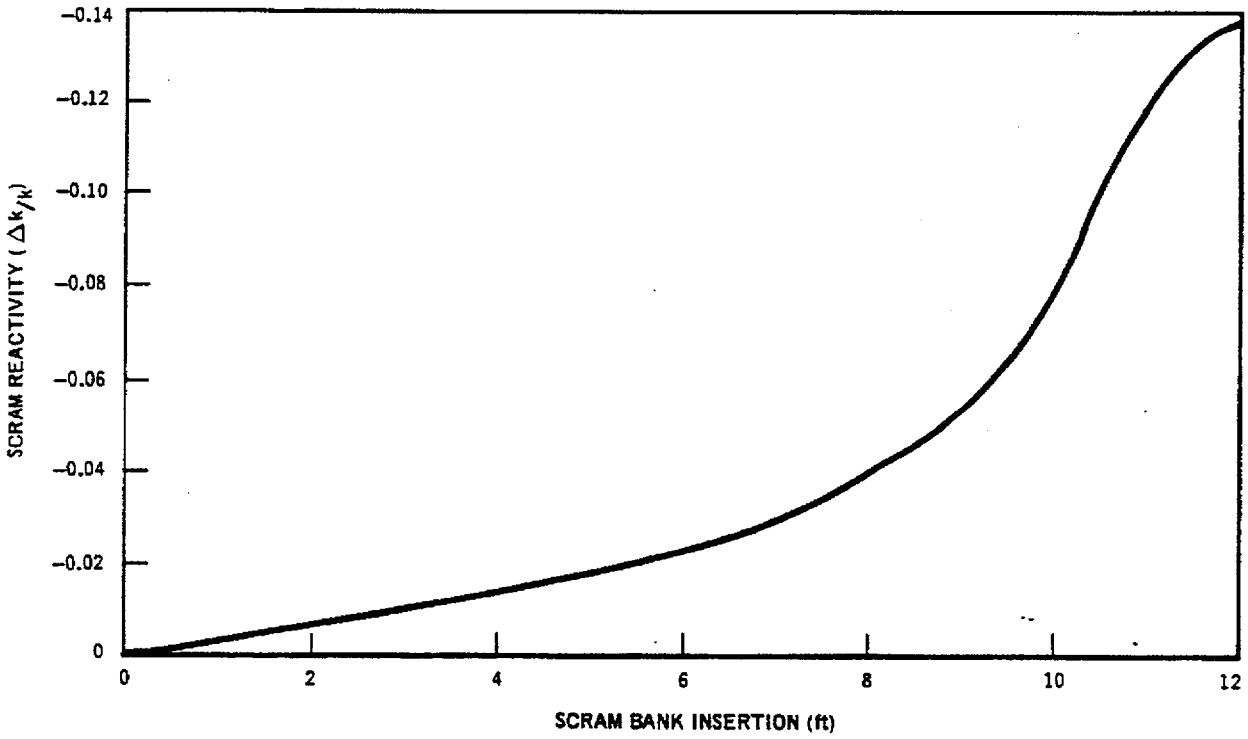

Figure 7-7 Scram Reactivity Function for 10% Power

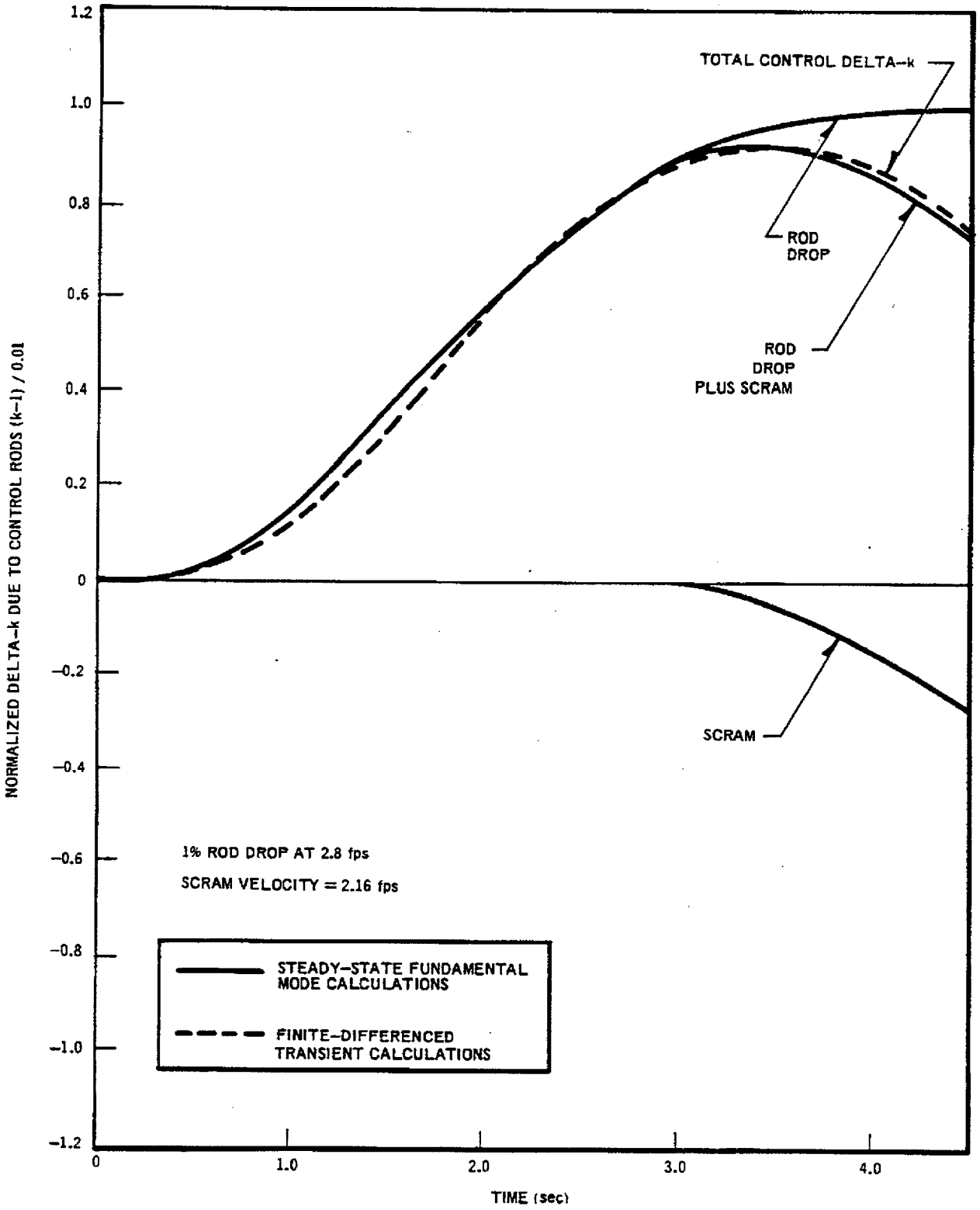

Figure 7-8 Delta-k Due to Control Rods vs Time Normalized so that Rod Worth is 1.0 (1% Rod Drop at 2.8 fps; Scram Velocity at 2.16 fps)

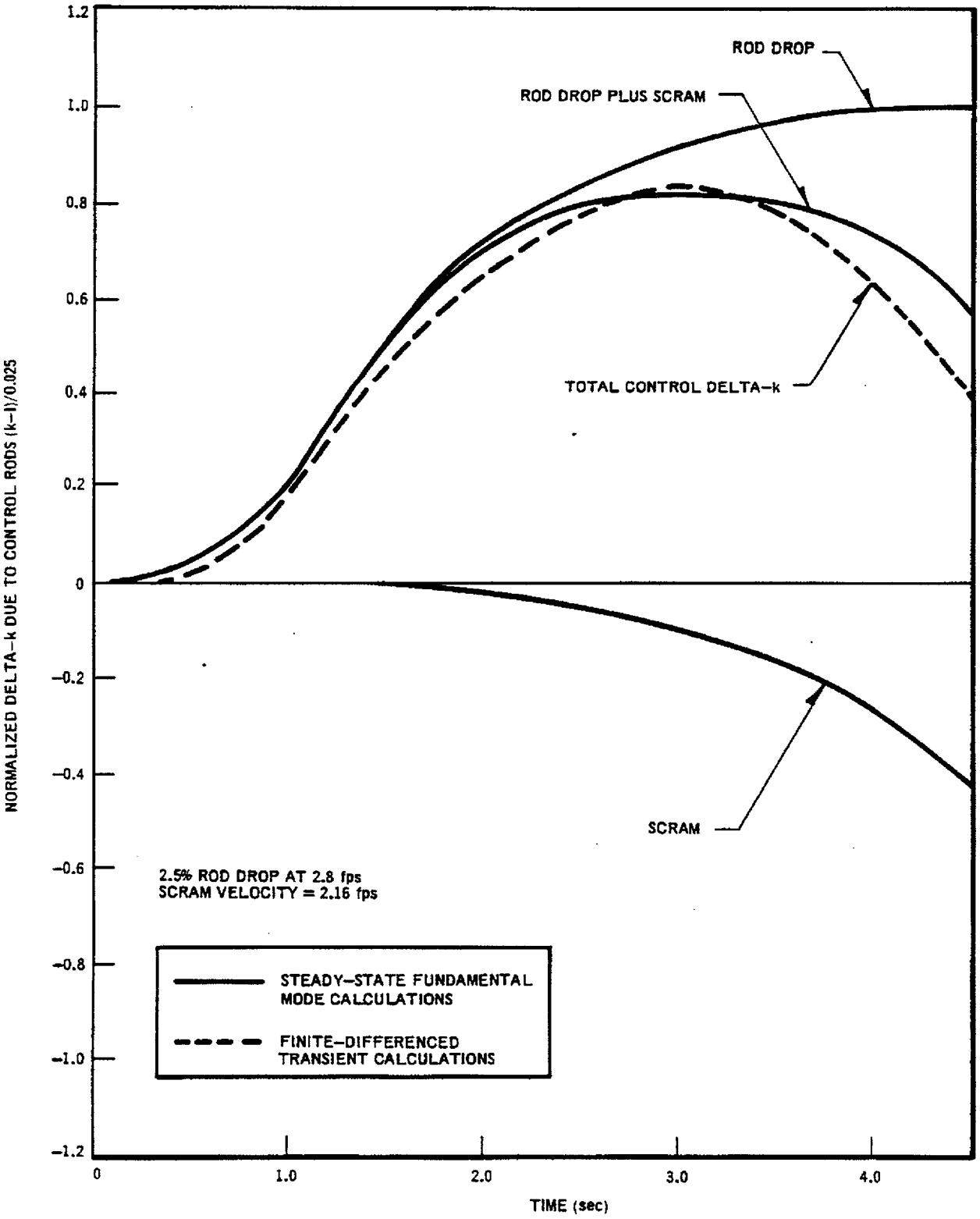

Figure 7-9 Delta-k Due to Control Rods vs Time Normalized so that Rod Worth is 1.0 (2.5% Rod Drop at 2.8 fps; Scram Velocity at 2.16 fps)

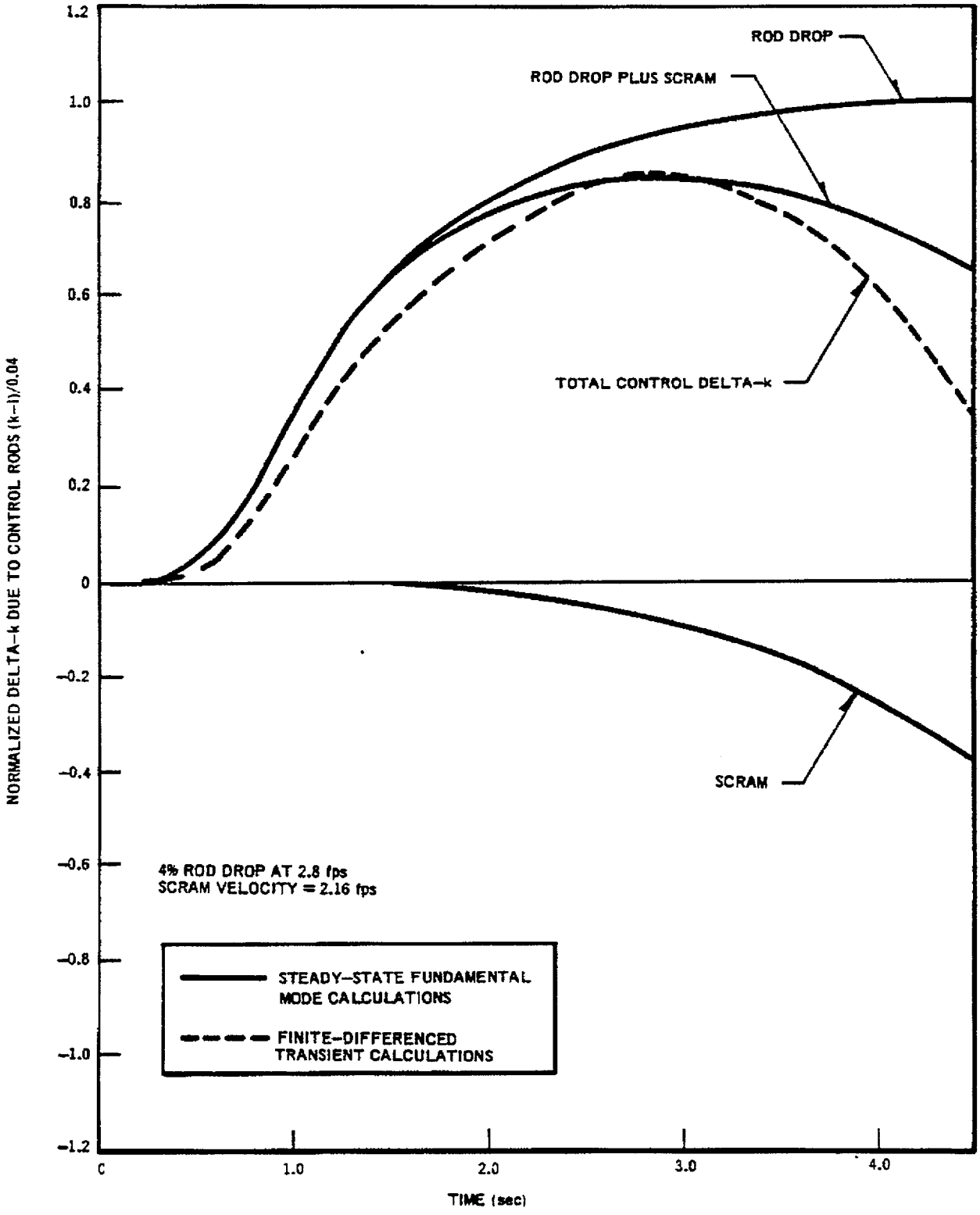

Figure 7-10 Delta-k Due to Control Rods vs Time Normalized so that Rod Worth is 1.0 (4% Rod Drop at 2.8 fps; Scram Velocity at 2.16 fps)

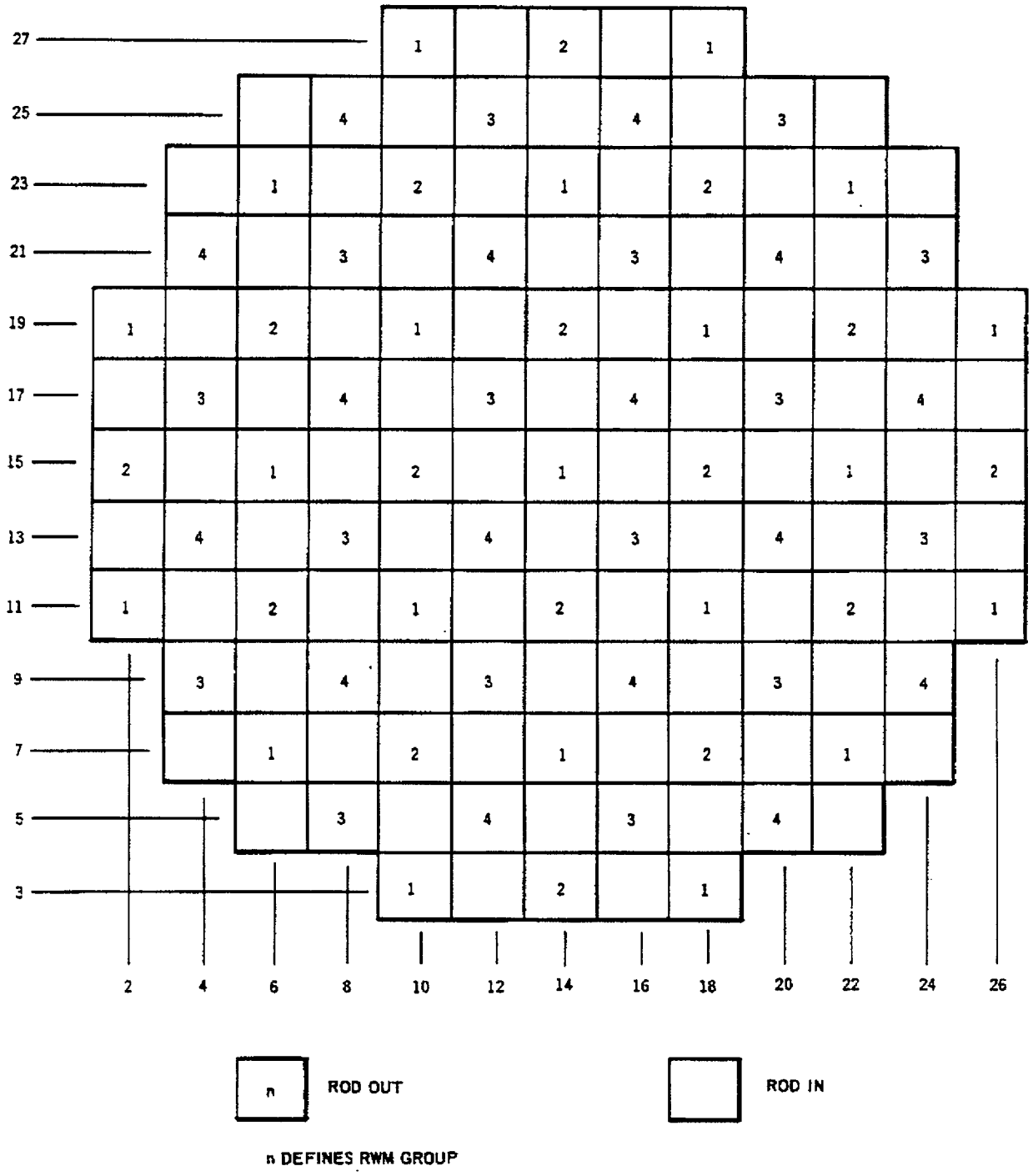

Figure 7-11 Control Rod Withdrawal and Rod Worth Minimizer Sequence to 50% Control Density

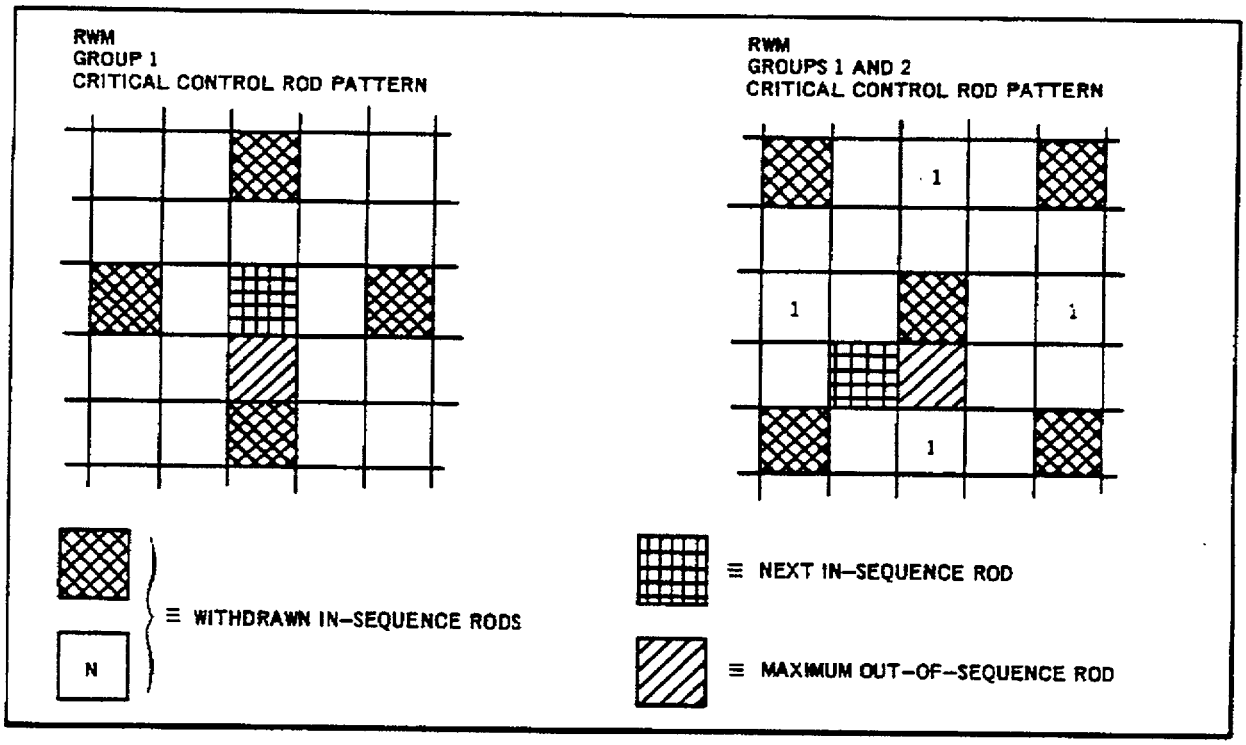

Figure 7-12 Maximum In-Sequence and Out-of-Sequence Rod Patterns for Control Rod Worths

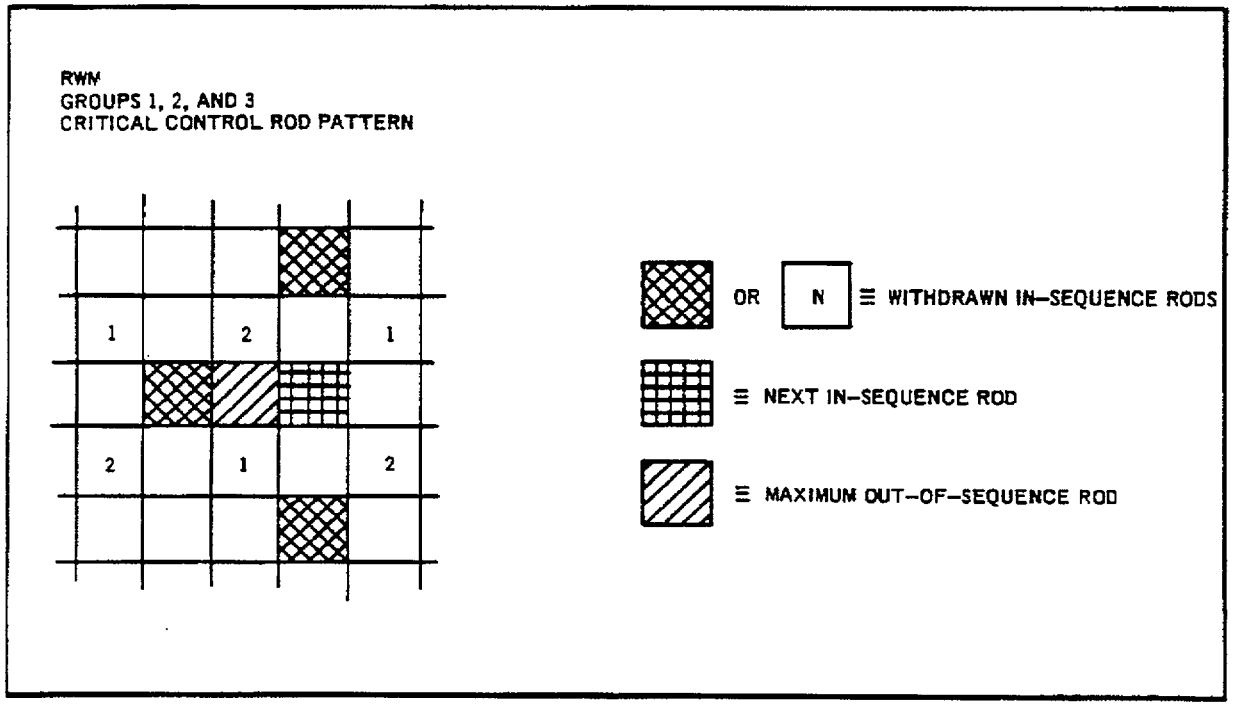

Figure 7-13 Maximum In-Sequence and Out-of-Sequence Rod Patterns for Control Rod Worths

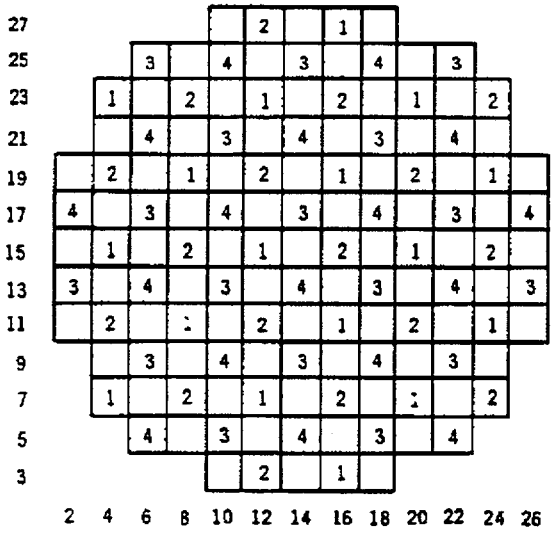

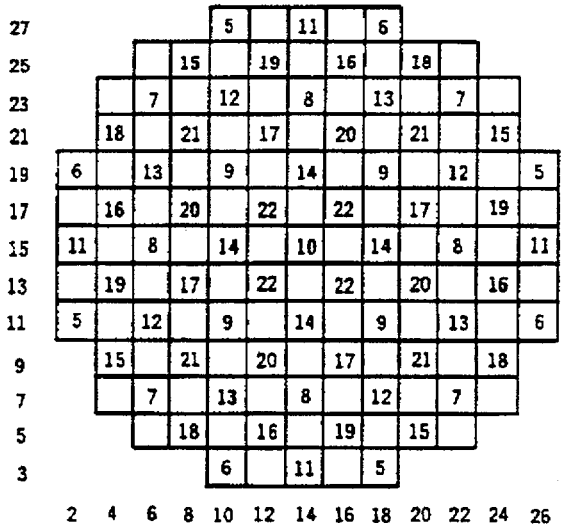

1. COMPLETE WITHDRAWALS INDICATED IN EACH COLUMN BEFORE GOING TO THE NEXT COLUMN.
2. WITHDRAW GROUP 1 THROUGH 4 RODS INDIVIDUALLY FROM 0 TO 48.
3. WITHDRAW RODS IN OTHER GROUPS BY BANKS.
4. FOR ROD INSERTIONS REVERSE THE SEQUENCE.

RWM GROUP	WITHDRAWAL SEQUENCE															
1	48															
2	48															
3	48															
4	48															
5	12	24	36	48												
6	12	24	36	48												
7	8	16	24	32	40	48										
8	8	16	24	32	40	48										
9	8	16	24	32	40	48										
10	8	16	24	32	40	48										
11		12	24	36	48											
12		8	16	24	32	40	48									
13		8	16	24	32	40	48									
14		8	16	24	32	40	48									
15			8	16	24	32	40	48								
16			4	8	12	16	20	24	28	32	36	40	44	48		
17			4	8	12	16	20	24	28	32	36	40	44	48		
18				8	16	24	32	40	48							
19				4	8	12	16	20	24	28	32	36	40	44	48	
20				4	8	12	16	20	24	28	32	36	40	44	48	
21					4	8	12	16	20	24	28	32	36	40	44	48
22					4	8	12	16	20	24	28	32	36	40	44	48

Figure 7-14 Typical Control Rod Withdrawal Sequence for a 560 Bundle Reactor

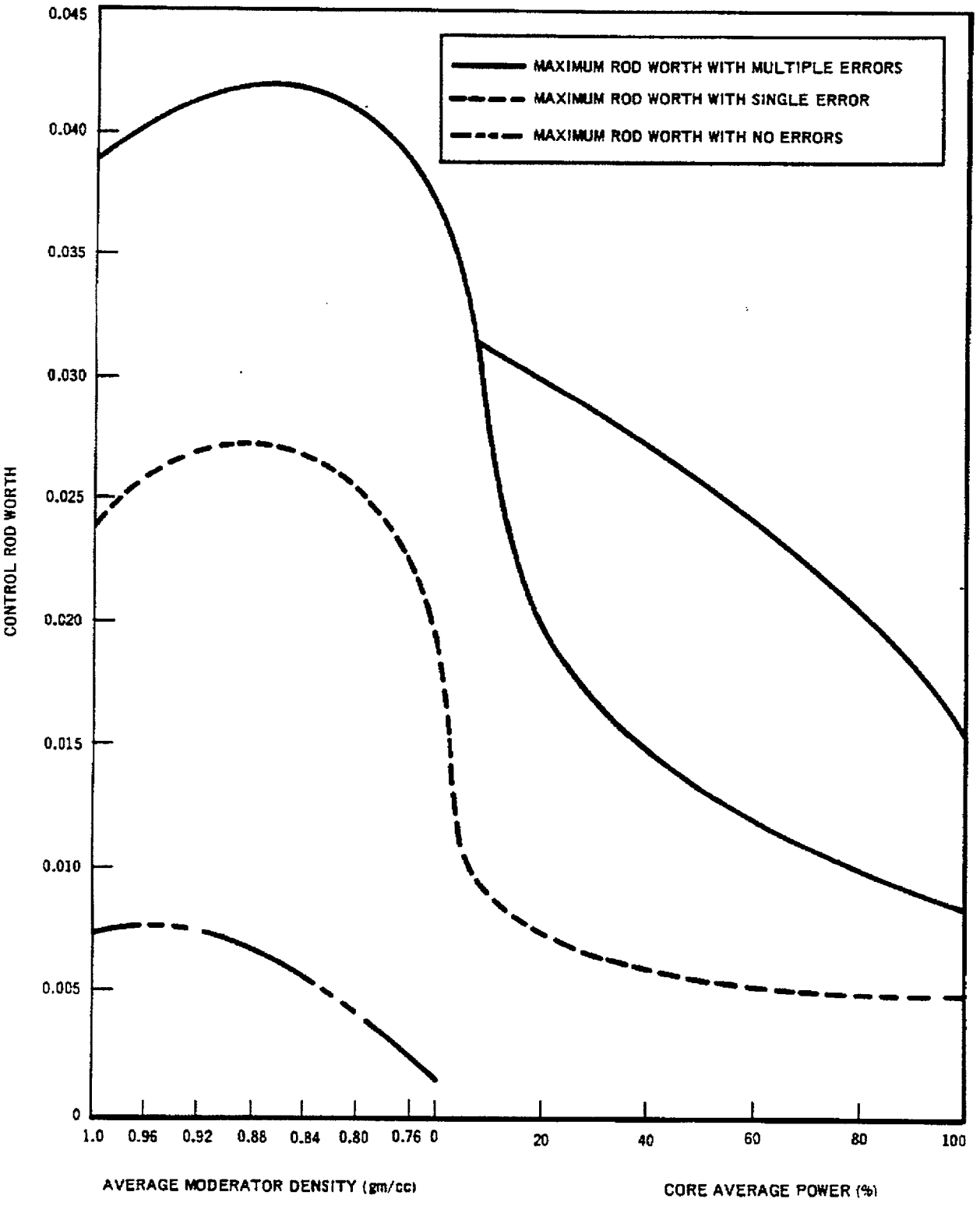

Figure 7-15 Maximum Control Rod Worth at Various Normal and Abnormal Operating States

REFERENCES

1. Brammer, H.A., et. al., *Nuclear Excursion Technology*, September 1965, Revised August, 1967 (APED-5528).

2. Wood, J.E., *Analysis Methods of Hypothetical Super-Prompt Critical Reactivity Transients in Large Power Reactors*, APED-5448, April, 1968.

3. Boyden, J.E., et. al., *Summary Memorandum on Excursion Analysis Uncertainties*, Dresden Nuclear Power Station Unit 3 Plant Design and Analysis Report Amendment No. 3, May 23, 1966.

4. Grund, J.E., et. al., *Subassembly Test Program Outline for FY 1969 and FY 1970*, IN-1313, August 1969 (IDO-17277).

5. Lussie, W.G., *The Response of Mixed Oxide Fuel Rods to Power Bursts*, April 1970 (IN-ITR-114).

6. Lussie, W.G., *The Response of UO_2 Fuel Rods to Power Bursts: Detailed Tests on 5/16-Inch OD, Pellet Fuel, Zircaloy-Clad Rods*, January 1970 (IN-ITR-112).

7. McClure, J.A. and Siefken, L.J., *Transient Irradiation of 1/4-Inch OD Stainless Steel Clad Oxide Fuel Rods to 570 cal/g UO_2* , October 1968 (IDO-ITR-100).

8. Stephan, L.A. and Olsen, C.S., *Transient Irradiation of 0.466-Inch OD Stainless Steel Clad Oxide Fuel Rods to 300 cal/g UO_2*, November, 1968 (IDO-ITR-101).

9. Martinson, Z.R. and Johnson, R.L., *Transient Irradiation of 1/4-Inch OD Zircaloy-2 Clad Oxide Fuel Rods to 590 cal/g UO_2*, November, 1968 (IDO-ITR-102).

10. Miller, R.W. and Lussie, W.G., *The Response of UO_2 Fuel Rods to Power Bursts; 5/16-Inch OD, Pellet and Powder Fuel, Zircaloy Clad*, January, 1969 (IDO-ITR-103).

11. Miller, R.W. and Lussie, W.G., *The Response of UO_2 Fuel Rods to Power Bursts; 9/16-Inch OD, Pellet and Powder Fuel, Zircaloy Clad*, April, 1969 (IDO-ITR-104).

12. Stephen, L.A., *The Response of Waterlogged UO_2 Fuel Rods to Power Bursts*, April, 1969 (IDO-ITR-105).

13. Lussie, W.G. and Miller, R.W., *The Response of UO_2 Fuel Rods to Power Bursts; Detailed Tests on 5/16-Inch OD, Powder Fuel, Zircaloy Clad Rods*, June, 1969 (IDO-ITR-106).

14. Martinson, Z.R., *Behavior of 5-Inch Long, 1/4-Inch OD, Zircaloy-2 Clad Oxide Fuel Rods Subjected to High Energy Power Bursts*, July, 1969 (IN-ITR-107).

15. Olsen, C.S., *Measurements of the Reaction of UO_2 with Water for Transient Energy Depositions to 550 cal/g UO_2*, November, 1969 (IN-ITR-103).

16. Siefken, L.J., *The Effects of Axial Length on the Response of Zircaloy Clad, UO_2 Fuel Rods to Power Bursts*, January, 1970 (IN-ITR-109).

17. Stephan, L.A., *The Effects of Cladding Material and Heat Treatment on the Response of Waterlogged UO_2 Fuel Rods to Power Bursts*, January, 1970 (IN-ITR-111).

18. Miller, R.W., *The Effects of Burnup on Fuel Failure I. Power Burst Tests on Low Burnup UO_2 Fuel Rods*, July, 1970 (IN-ITR-113).

19. Lussie, W.G. and Miller, R.W., *Carbon Impurity in UO_2 and Its Effect on Cladding Swelling During Power Bursts*, July, 1970 (IN-ITR-115).

20. Siefken, L.J., *The Response of Fuel Rod Clusters to Power Bursts*, May, 1970 (IN-ITR-116).

21. Lussie, W.G., *The Response of Heterogeneous Mixed-Oxide Fuel Rods to Power Bursts*, September, 1970 (IN-ITR-117).

22. McCordell, R.K., et. al., *Reactivity Accident Test Results and Analysis for the SPERT-III E-Core. . . A Small, Oxide-Fueled, Pressurized-Water Reactor*, March, 1969, p. 77 (IDO-17281).

23. Ergen, W.K., "Self-Limiting Power Excursions in Large Reactors," *Trans. American Nucl. Soc., 8*, 1, p. 221 (June, 1965).

24. Gyorey, G.L. and Keck, Carolyn A., "A Time-Integrated Model for Reactor Excursion Calculations," *Trans. American Nuc. Soc., 8*, 2, pp. 498-499 (November, 1965).

25. West, D.L., et. al., "Use of the Adiabatic Approximation in Prompt-Critical, Large Core Reactor Excursion Analyses," *Trans. American Nuc. Soc., 8*, 2, pp. 497-498 (November, 1965).

26. Hageman, L.A., *The Chebyshev Polynomial Method of Iteration*, WAPD-TM-537 (January, 1967).

27. Wachspress, E.L., *Iterative Solution of Elliptic Systems*, Prentice-Hall, Englewood Cliffs, N.J., pp. 26-27 (1966).

28. Woolley, J.A., "Reduction of Few-Group Diffusion Theory to One Equivalent Group," *Trans. American Nucl. Soc., 14*, 2, pp. 671-672, (October, 1971).

29. Cadwell, W.R., et. al., *WIGLE-A Program for the Solution of the Two-Group Space-Time Diffusion Equations in Slab Geometry*, WAPD-TM-416 (1964).

30. Grund, J.F., *Experimental Results of Potentially Destructive Reactivity Additions to an Oxide Core*, December, 1964 (IDO-17028).

31. Scott, R., Jr., Wasserman, A.A., and Schmitt, R.C., *Transient Tests of the SPERT-I Low-Enriched UO_2 Core*, Data Summary Report, September, 1963, (IDO-16752).

32. Hein, R.A., Flagell, P.N., *Enthalpy Measurements of UO_2 and Tungsten to 3260°K*, February 16, 1968 (GEMP-578).

33. Leibowitz, L., Mishler, L.W., and Chasanov, M.G., "Enthalpy of Solid Uranium Dioxide from 2500°K to its Melting Point," *Journal of Nuclear Materials, 29*, P. 356-358, (1969).

34. Chasanov, M.G., "Materials Behavior and Energy Transfer: High-Temperature Physical Properties," *Argonne National Laboratories: Reactor Development Progress Report*, September, 1969 (ANL-7618).

35. Moore, G.E., and Kelley, K.K., "High Temperature Heat Contents of Uranium, Uranium Dioxide and Uranium Trioxide," *Jour. Am. Chem. Soc., 69*, p. 2105, (1947).

36. Keepin, G.R., *Physics of Nuclear Kinetics*, Addison-Wesley, Reading Mass., 1965.

37. Henry, A.F., "The Application of Reactor Kinetics to the Analysis of Experiments," *Nucl. Sci. and Engr; 3*, 52-70 1958.

38. Adder, F.T., G.W. Hinman, and L.W. Nordheim, *The Quantitative Evaluation of Resonance Integrals*, Paper No. P/1988. Proceedings of the Second United International Conference on the Peaceful Uses of Atomic Energy, vol. 16, pp. 155-171, United Nations, Geneva, 1958.

ACKNOWLEDGMENTS

The work reported here represents the efforts of many people in General Electric as reported in internal documents and memoranda. Particular acknowledgment is due to Ivan Stuart, John Power, and Rich Ranellone for their contributions to the section on description of the rod drop accident.

APPENDIX

VELOCITY LIMITER TESTS

A.1 INTRODUCTION

Boiling water reactors designed by the General Electric Company incorporate control rod velocity limiters as an additional engineering safeguard. The basic concept of the velocity limiter requires that a device be integrally attached to the lower end of a control rod to restrict its free-fall velocity through the reactor water without causing excessive retarding of its upward motion during scram.

The function of the control rod velocity limiter is to reduce the consequences of a high-worth control rod dropping out of a reactor core. The probability of a rod drop occurrence is small because it requires simultaneous multiple malfunctions of equipment and erroneous operation to produce a significant rod dropout accident. This sequence of events involves establishing a high-worth control rod pattern, mechanical failure of the drive line coupling, the control rod being held in the core and not withdrawing with the control rod drive, withdrawal of the detached control rod drive mechanism and subsequent release of the control rod. The velocity limiter was developed as a safeguard to limit the velocity of the assumed rod dropout (hence, reactivity insertion rate) to a value which would limit the rate of a resulting nuclear excursion.

This appendix presents the results obtained from the testing of a representative sample of nine production velocity limiters (complete control rods) in a representative sample of nine production guide tubes and a "worst case" condition. Also included in this appendix are the results of the statistical analysis of the data.

A.2 CONCLUSIONS

The test results show a mean rod velocity at 1030 psig of 2.72 ft/sec. The worst case condition results were extrapolated (because of physical test limitations) to give a maximum rod velocity of 3.11 ft/sec at 1030 psig. 3.11 ft/sec is considered to be the absolute maximum velocity that could be achieved at normal operating conditions due to the physical variables reflected in this test program.

A.3 TEST PROCEDURE

A.3.1 Pretest

Nine production control rods and guide tubes were selected from the last production run at San Jose. These were considered as representative of all control rods and all guide tubes.

In addition, a worst case control rod was constructed by maximizing tolerance conditions. The gap allowed between the velocity limiter and guide tube was maximized and the roller center was moved in to maximize the off-center possibilities. An epoxy compound was molded onto the bottom surface of the upper cone to maximize cone thickness and minimize nozzle gap and the sharp edge was rounded to over .005 R. All these modifications were judged as having notable effect on performance based on previous testing.

The velocity limiter drop test equipment, as shown on Figure A-13, was installed in the control rod drive system for the 30" vessel, shown schematically as Figure A-14. A special uncoupling rod was installed in the drive to keep the CRD coupling from locking. The system was instrumented to obtain vessel pressure and control rod position versus time during the actual drop.

A.3.2 Testing

The test setup for the first cold drop is shown on Figures A-2 and A-3. Figure A-4 shows the vessel head with the spool that the probe and drywell fit through during all other testing. A typical control rod is shown on Figures A-5 and A-6 and a typical guide tube is shown on Figure A-7. The worst case is shown on Figures A-8 and A-9 and the modified worst case is shown on Figure A-10. Figure A-11 shows a typical Sanborn trace where velocities are obtained by knowing chart speed and distance between probe switches.

The drops were accomplished by first positioning the CRD at the top of the stroke. The control rod latching mechanism (Figure A-15) was then actuated and observed to be properly latched. The CRD was withdrawn to its lowest position and the latching mechanism was vented, releasing the control rod. Utilizing a Sanborn oscillographic recorder operating at a chart speed of 100 min/sec, the control rod position versus time was recorded. The vessel head was then secured and ten drop cycles were recorded.

The vessel pressure was increased to 500 psig and five velocity limiter drop cycles were conducted and recorded. Vessel pressure was increased to 1030 psig and ten velocity limiter drop cycles were run. The vessel was allowed to cool to ambient atmospheric conditons and the velocity limiter and guide tube were removed and inspected for test wear and/or damage.

A different control rod and guide tube was installed in the test facility, and the test was repeated as above except the head was installed before any testing was performed. All nine control rods and guide tubes were tested in this manner, as was the modified worst case. The worst case was tested cold only.

A.4 DISCUSSION

A.4.1 Types of Blades Tested

During the course of testing, three different configurations of blades were tested. The first group tested was nine production blades from the last San Jose production run. These blades were dropped in the test facility yielding a total of 1848 data points.

In order to generate a condition of maximum clearances and features which are known to contribute to higher rod velocities, a "worst case" rod was fabricated. The ID of a guide tube was measured and the gap between it and the velocity limiter was maximized by machining the velocity limiter OD to 9.220 inches. The roller center was moved in to 4.530 R to maximize the off-center possibilities. An epoxy compound was molded to the bottom surface of the upper cone to maximize cone thickness at 0.50 inch and minimize nozzle gap at 0.88 inch. The sharp edge (0.0 to 0.005 R) was rounded to over 0.005 R. This blade was dropped at ambient temperature only because it was determined that the epoxy used could not withstand elevated temperatures. Eighty data points were realized as a result of the cold drops.

A "modified worst case" was then prepared by removing the epoxy. In this condition the guide tube to velocity limiter clearance was maintained at maximum, as was the off center possibilities. The sharp edge on the cone was still rounded to over 0.005 R. With this modified worst case, a series of drops were made at ambient, 500 psi and 1030 psi for a total yield of 208 data points.

A.4.2 Velocity Measurement

A special position indicator was used to measure control rod velocity. A series of reed switches are attached to an aluminum rod and are actuated magnetically. The actuation device is a round magnet attached to the control rod while the reed switches are held stationary. When the control blade is dropped, the magnet passes the reed switches generating a series of on-off pulses recorded on a Sanborn oscillographic recorder. From the pulses on the Sanborn, the time to travel a given distance can be determined. The distance between reed switches was measured by slowly passing the magnet by each reed switch, carefully noting the point of actuation and de-actuation. To compensate for thermal expansion, this procedure was done at 60°F and 500°F. Any errors due to velocity measurement calibration were considered to be minimized due to the method of data reduction, i.e., the data were averaged.

A.4.3 Data Analysis

The data were analyzed primarily using statistical methods to determine the maximum velocity* that could possibly be expected even if all pertinent variables went the wrong way. The values of velocity expected under normal conditions were also determined from the data analysis.

Determination of the mean value of each appropriate test group was the first step in the data analysis. The results are tabulated below:

	Vessel Pressure	Mean Velocity	No. of Data Points
Production Samples	22 psi	2.305	768
	500 psi	2.607	360
	1030 psi	2.720	720
Worst Case	22 psi	2.624	80
Modified Worst Case	22 psi	2.483	80
	500 psi	2.753	40
	1030 psi	2.936	80

In comparing these means, we see the data are ordered as would be expected. The velocities at low pressure for a set of conditions is lower than the velocities at higher pressures. For example, the mean velocity of the production samples at 22 psi is 2.305 ft/sec while at 500 psi, it is 2.607 ft/sec and at 1030 psi it is 2.720 ft/sec. This same pattern is seen in the results of the modified worst case.

The worst case (with the epoxy) would be expected to yield to similar pattern if it could have been tested at elevated temperatures. With this in mind, the curve shown in Figure A-1 was generated. This shows an extrapolated mean value of about 3.04 ft/sec which would be the maximum *mean* that could be expected based on this experiment. There is no no reason to expect any hardware to have worse tolerance conditions than those generated in the worst case sample. Consequently, rod drop velocity exceeding the extrapolated mean as a result of hardware variations is not considered to be a possibility.

If we assume that a series of worst-case rods was tested in the same manner as the production samples and the distribution of rod drop velocities was the same, then we have the basis for establishing a statistical limit for worst case rod velocity. Applying the difference for the 99.9% confidence limit derived from the production samples we come up with a velocity of 3.04 + .07 = 3.11 ft/sec at 1030 psi. This maximum has a 99.9% confidence limit associated with it with respect to the 3.04 ft/sec mean.

Further, if we compare the 3.04 ft/sec worse case velocity with the mean from the production samples of 2.72 (σ = .0391), the 3.04 ft/sec is approximately 8.2 standard deviations from the mean of the assumed random sample. If the statistical analysis of the production samples reflects the effect on velocity of hardware and other variables, then the probability of a worst case of 3.04 ft/sec occurring is extremely small. Further, if such a rod does occur, there is a 99.9% confidence that its velocity cannot exceed 3.11 ft/sec.

*It should be recognized that throughout this report the word velocity refers to average velocity between two points.

The data analysis summary for the nine blades is shown in the following table.

CONFIDENCE LIMITS TABLE

Confidence Limit	Velocity At 22 psi	500 psi	1030 psi
99.9%	2.360	2.710	2.790
99.5%	2.349	2.687	2.776
99.0%	2.343	2.677	2.769
97.5%	2.336	2.664	2.760
95	2.331	2.654	2.753
X	2.305	2.607	2.720
σ	0.0540	0.0574	0.0391

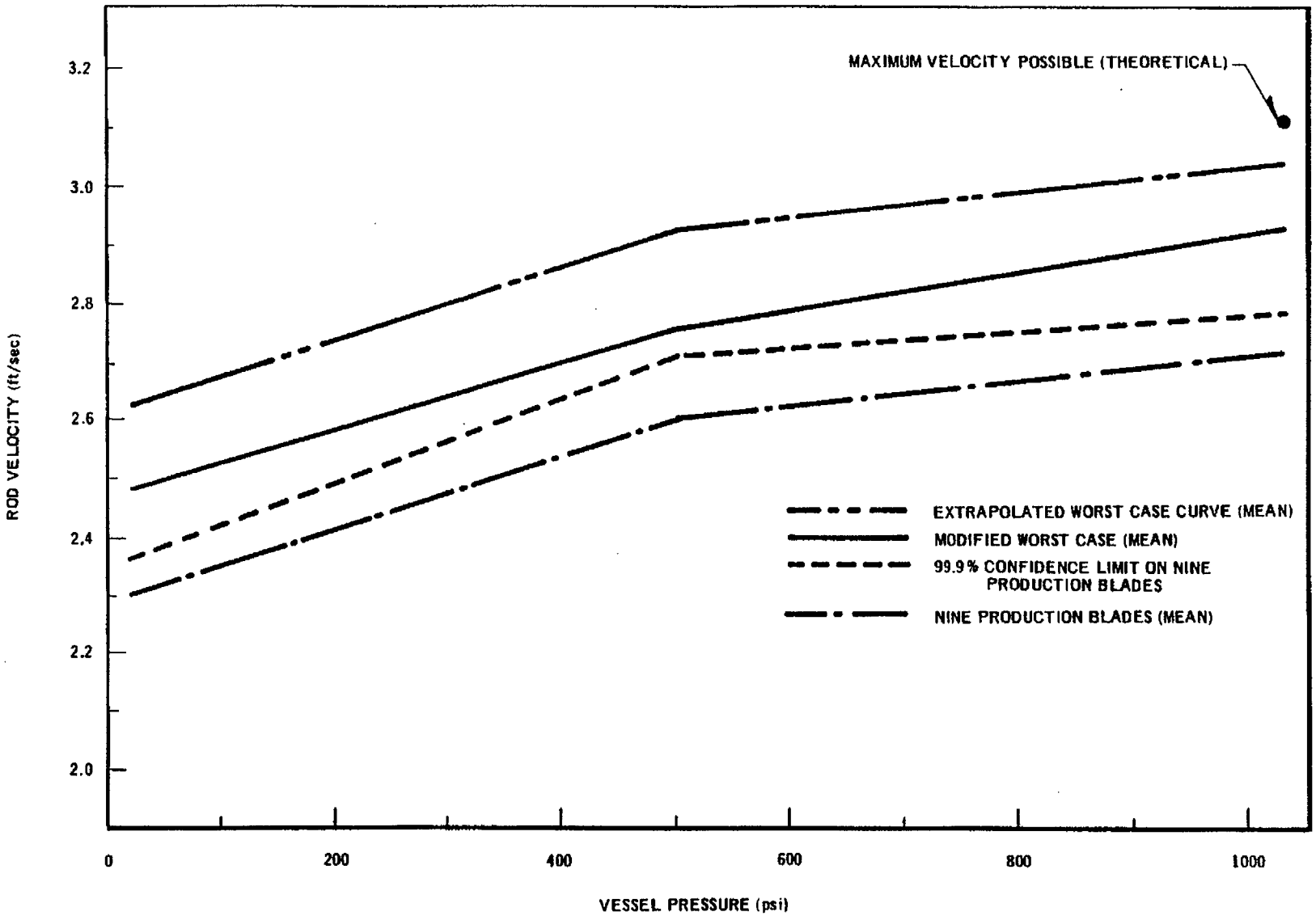

Figure A-1 Velocity Curves

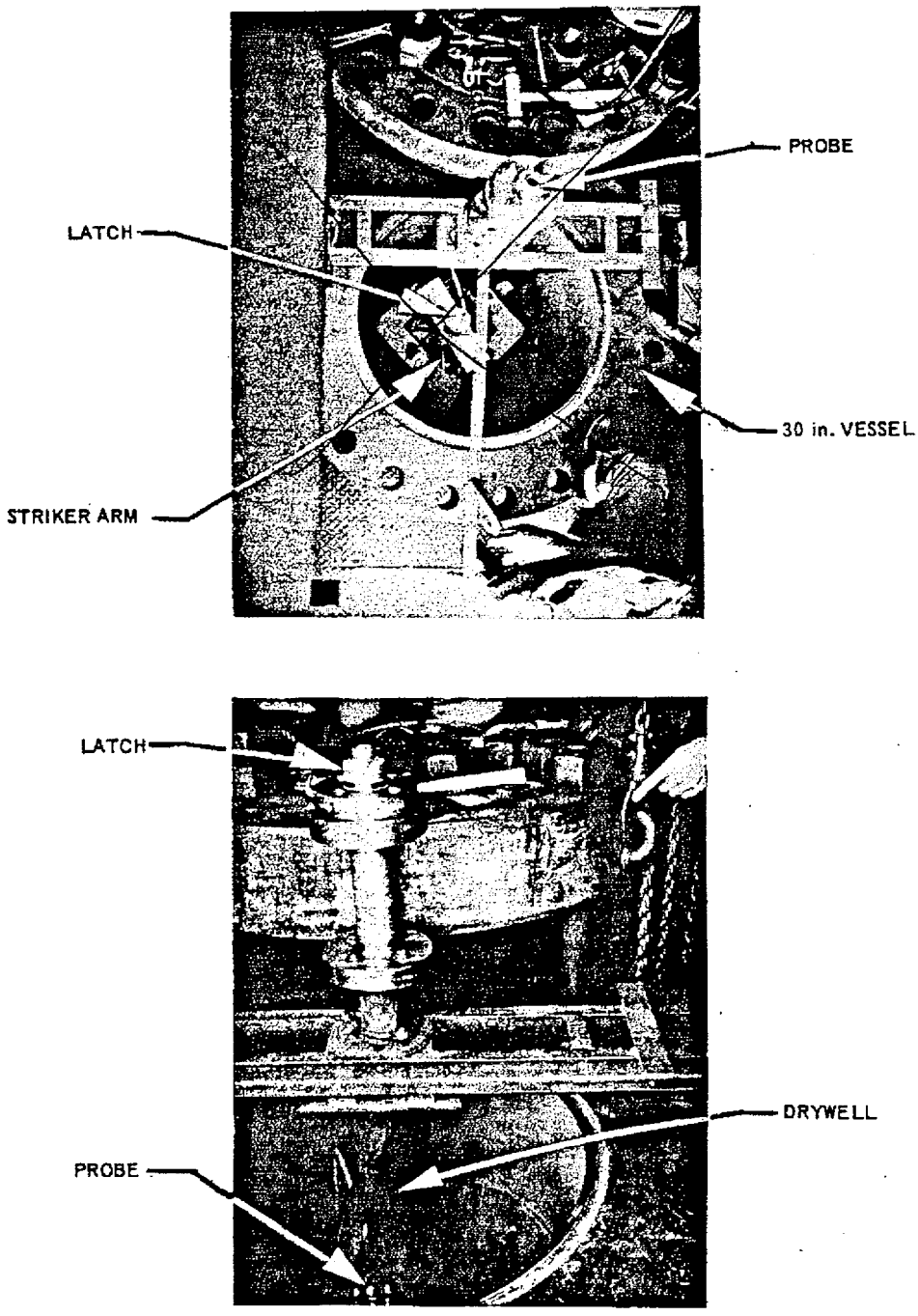

Figure A-2 Latch and Position Prove Assembly

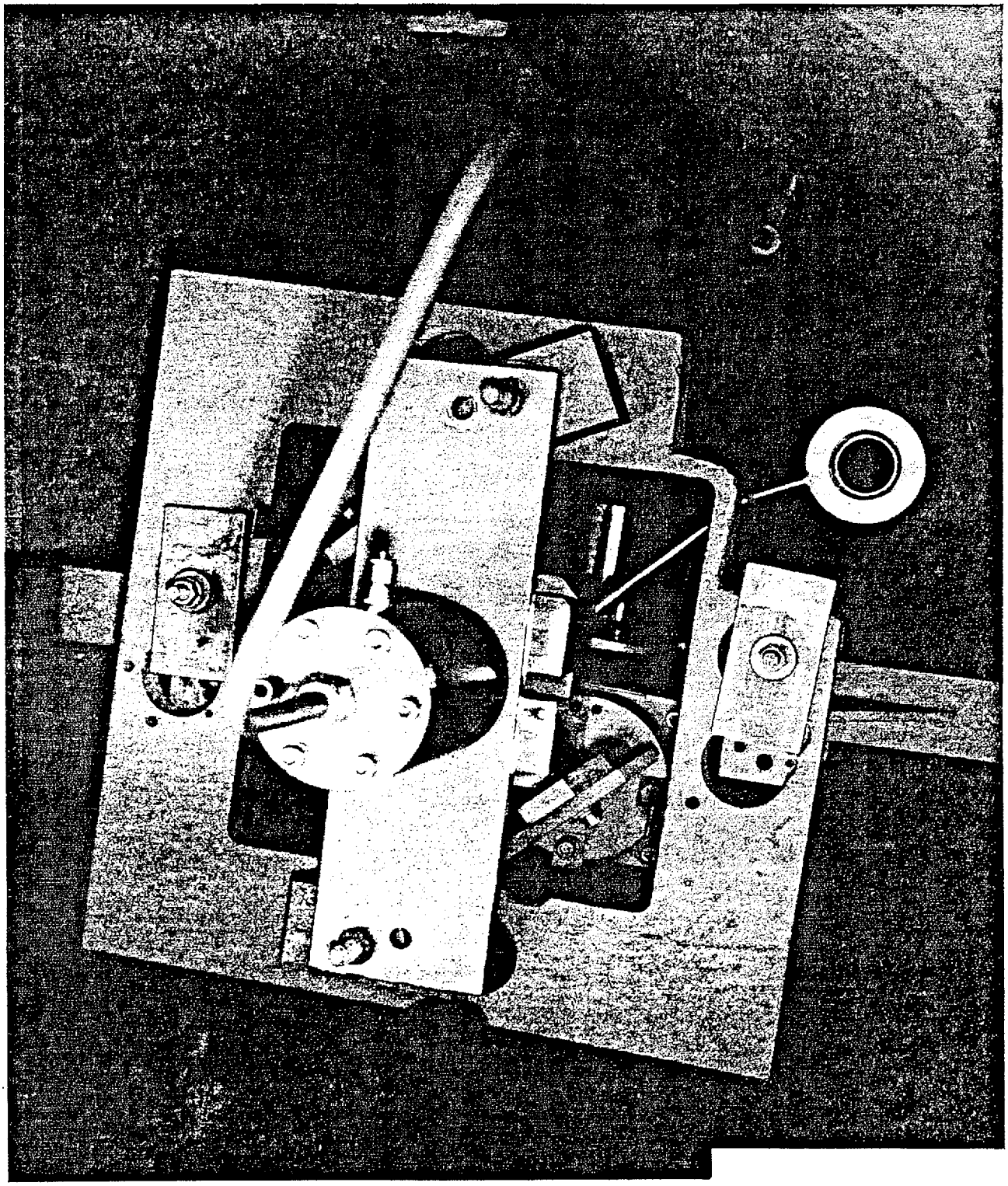

Figure A-3 Velocity Limiter Drop Test of Ten Production Blades

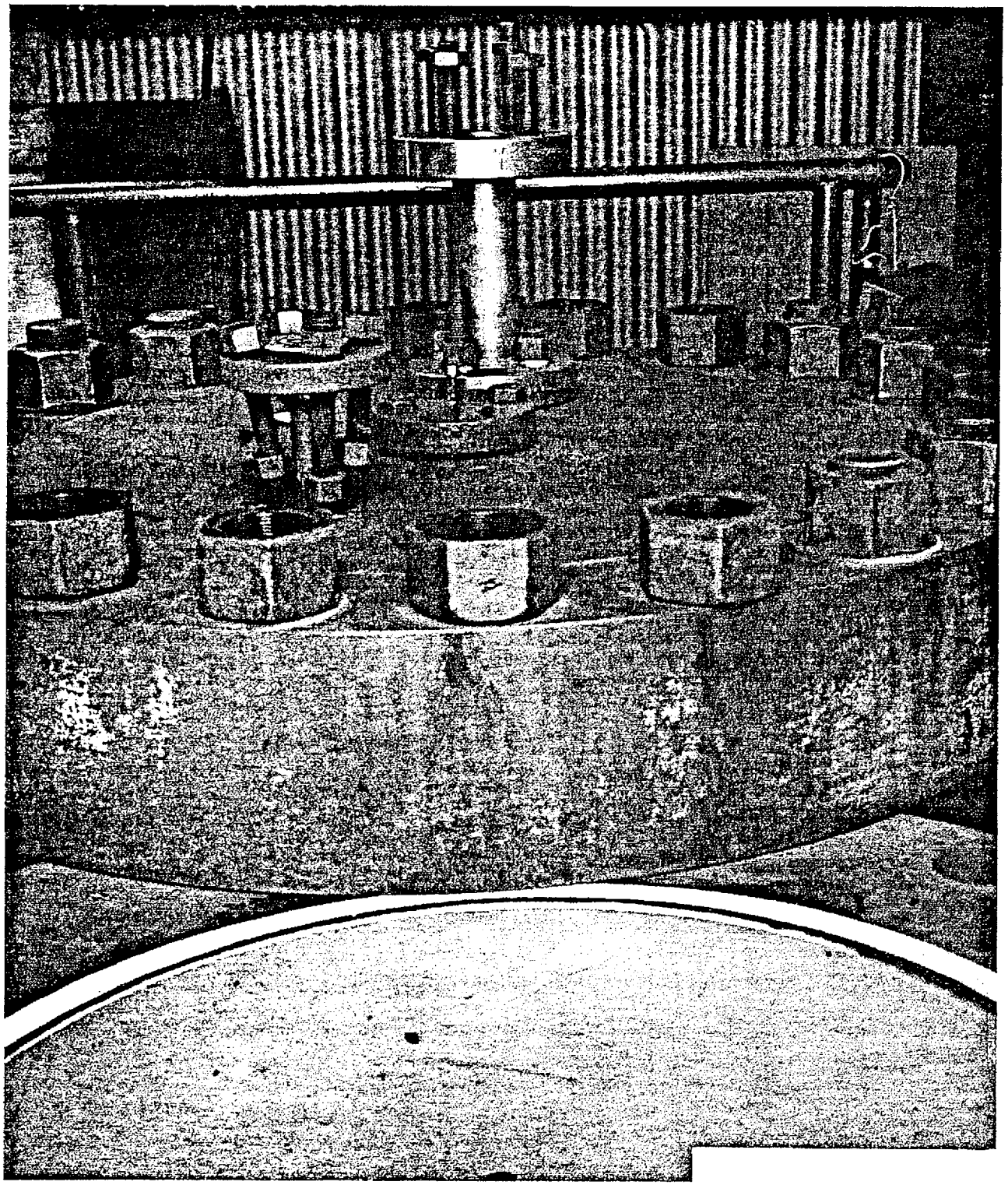

Figure A-4 Velocity Limiter Drop Test of Ten Production Blades

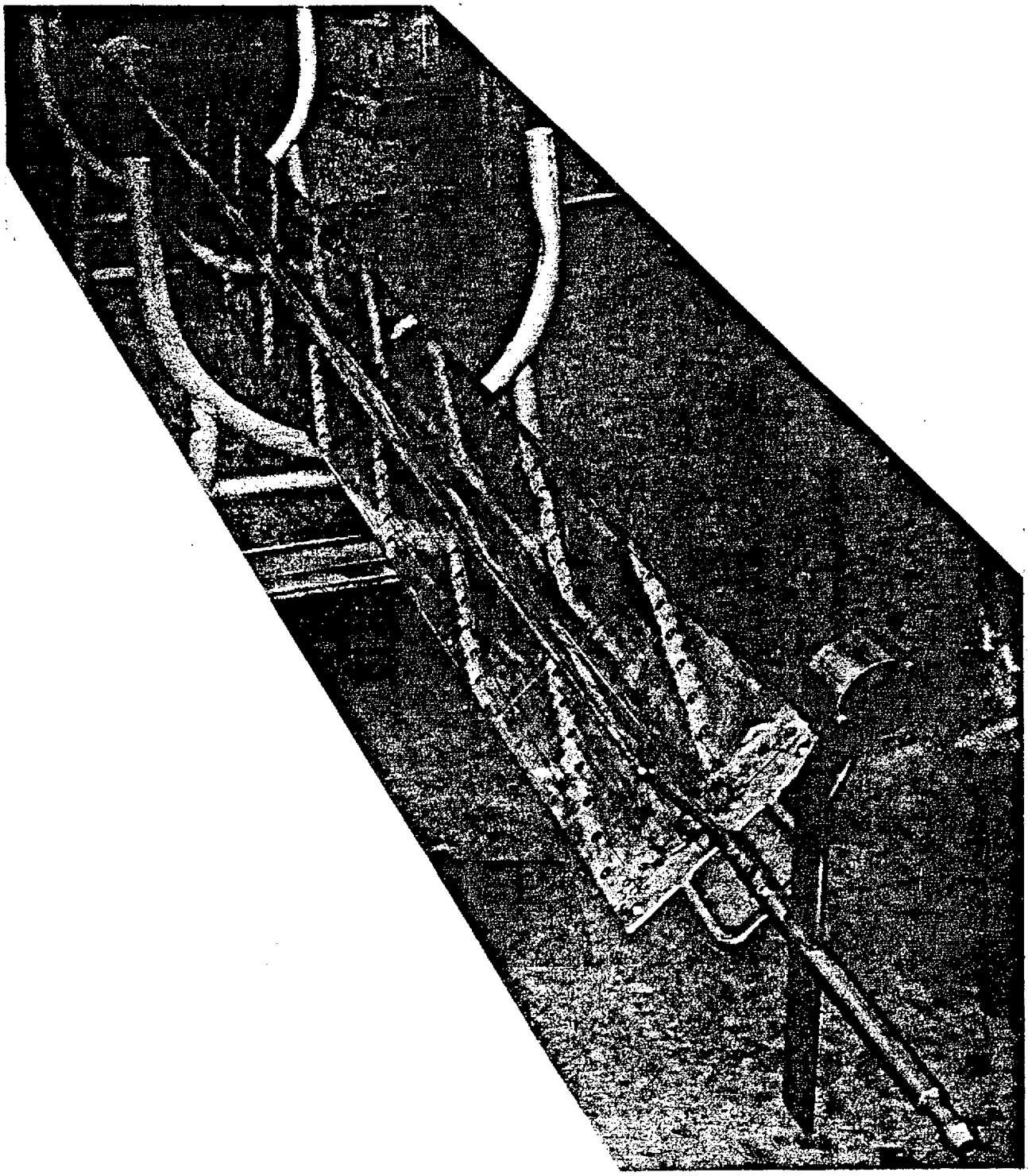

Figure A-5 Typical Control Rod with Drop Test Mechanism Attached

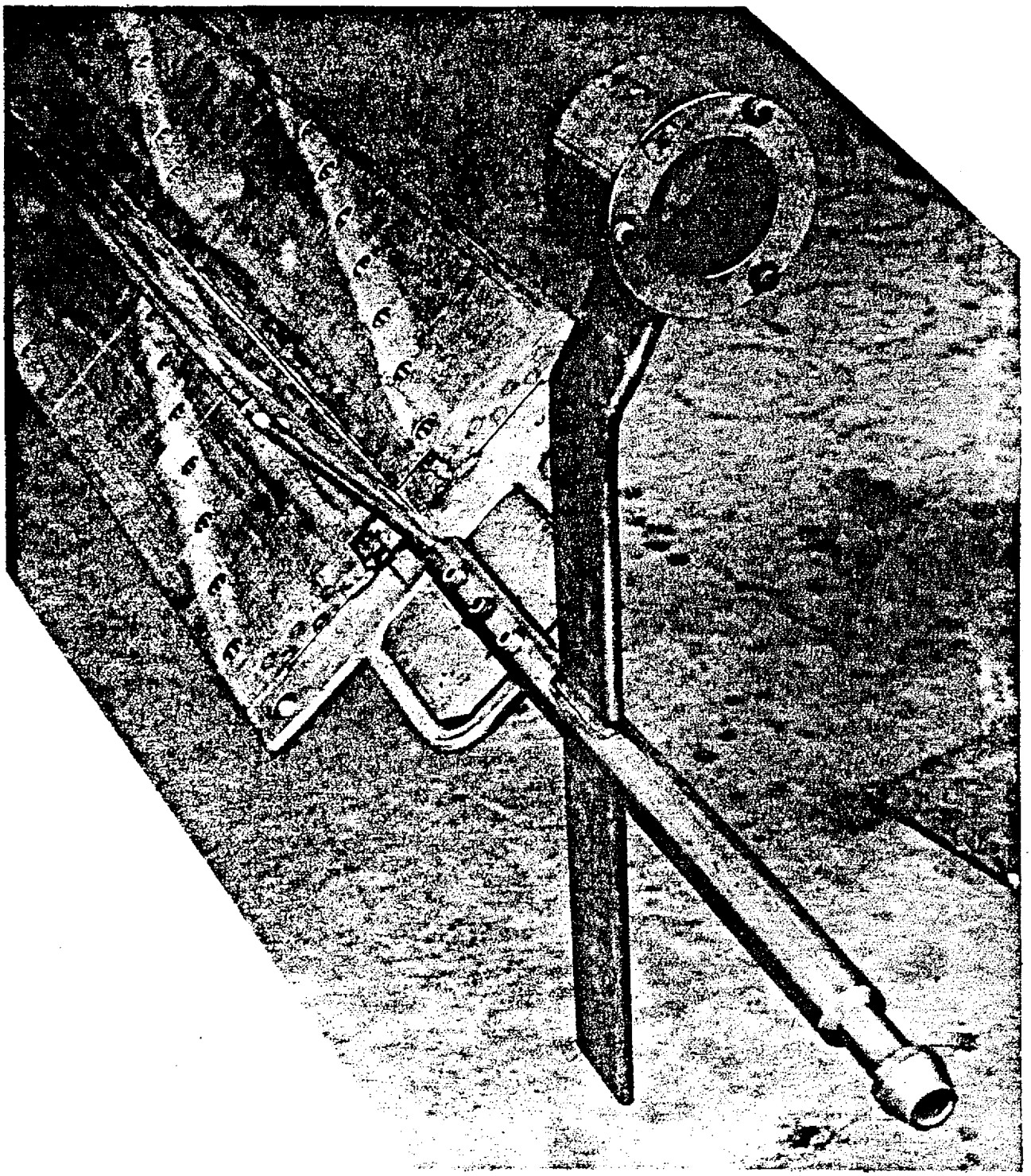

Figure A-6 Control Rod Closeup Showing Drop Test Mechanism

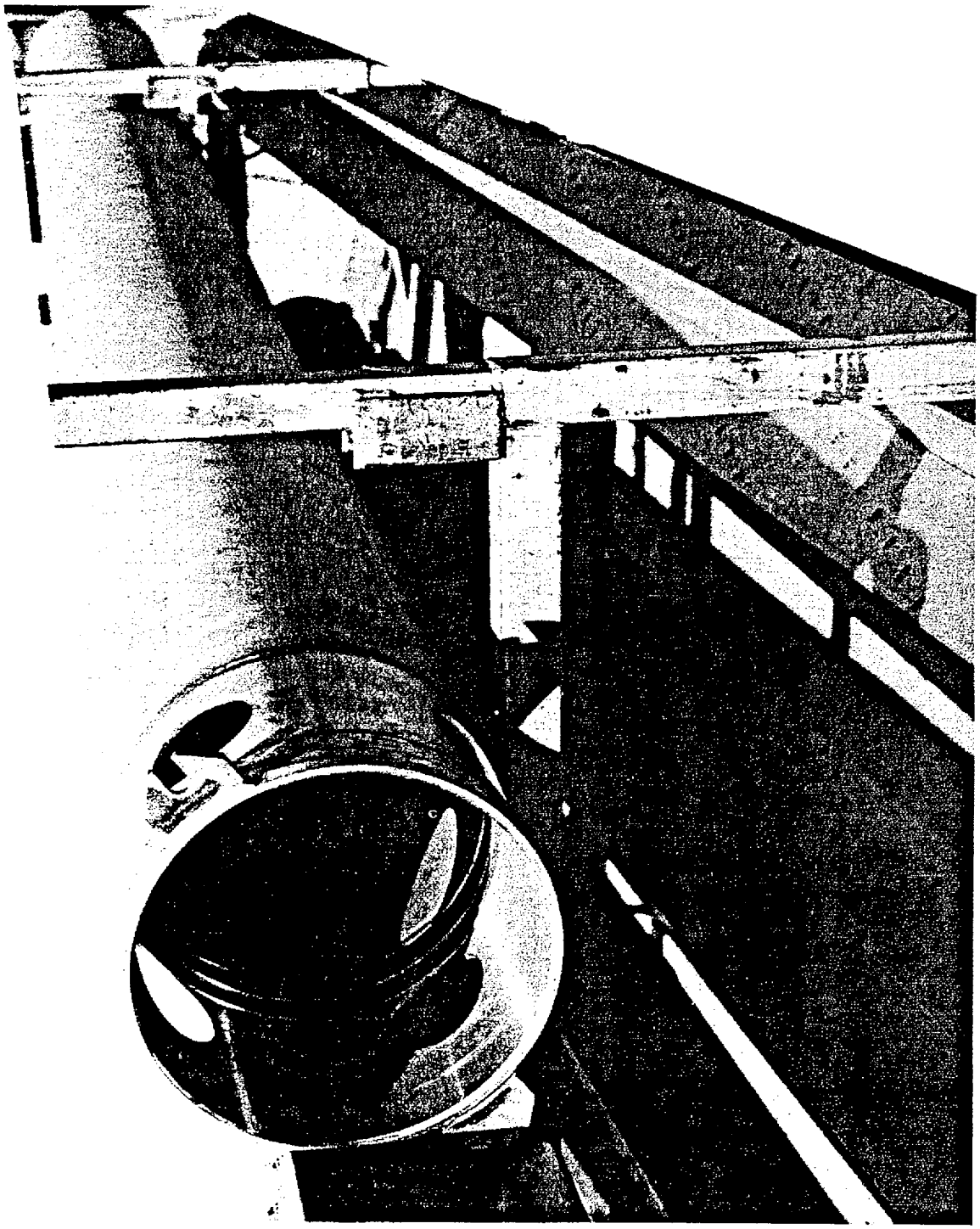

Figure A-7 Typical Control Rod Guide Tube

Figure A-8 Worst Case Control Rod

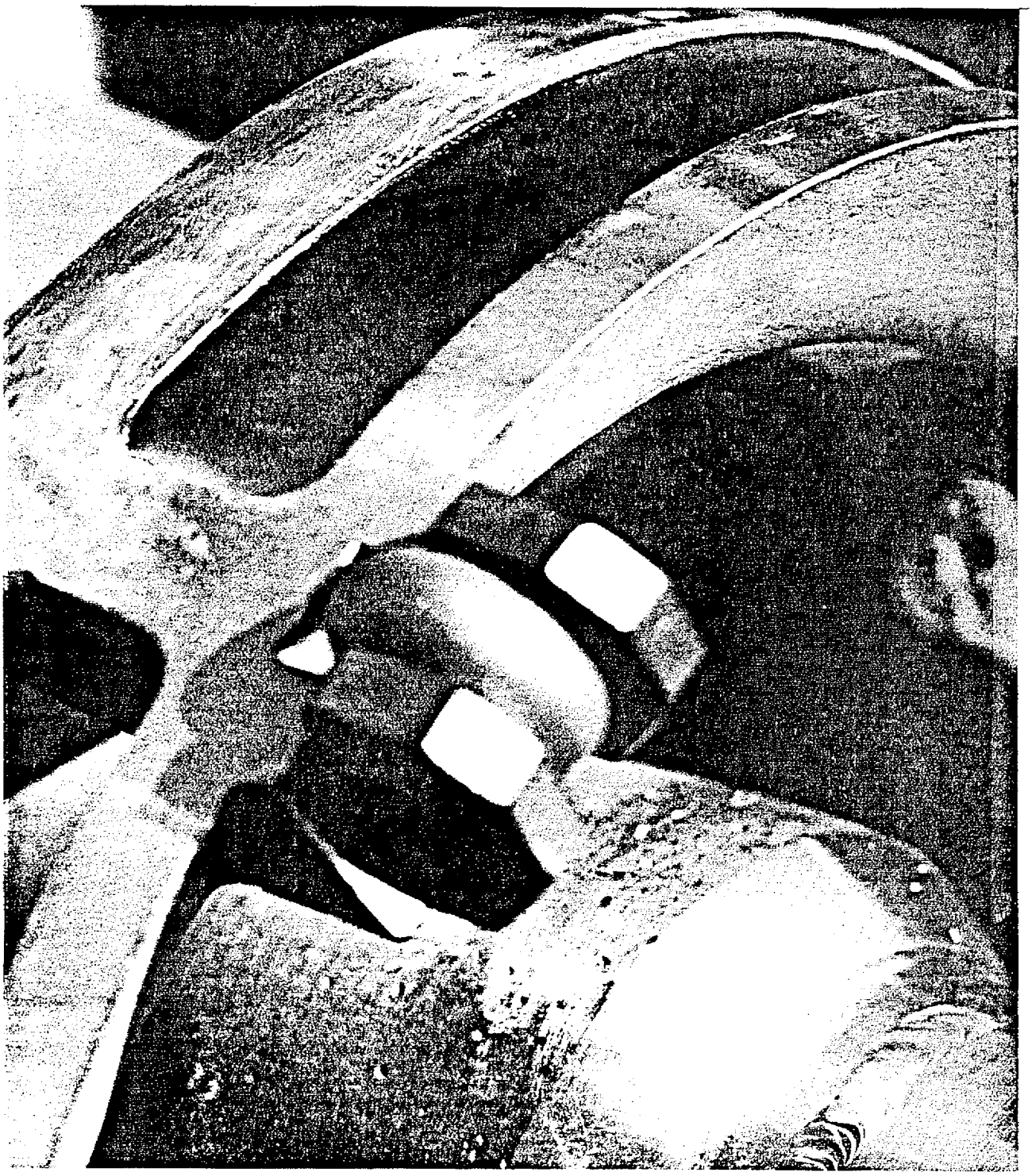

Figure A-9 Worst Case Control Rod Closeup

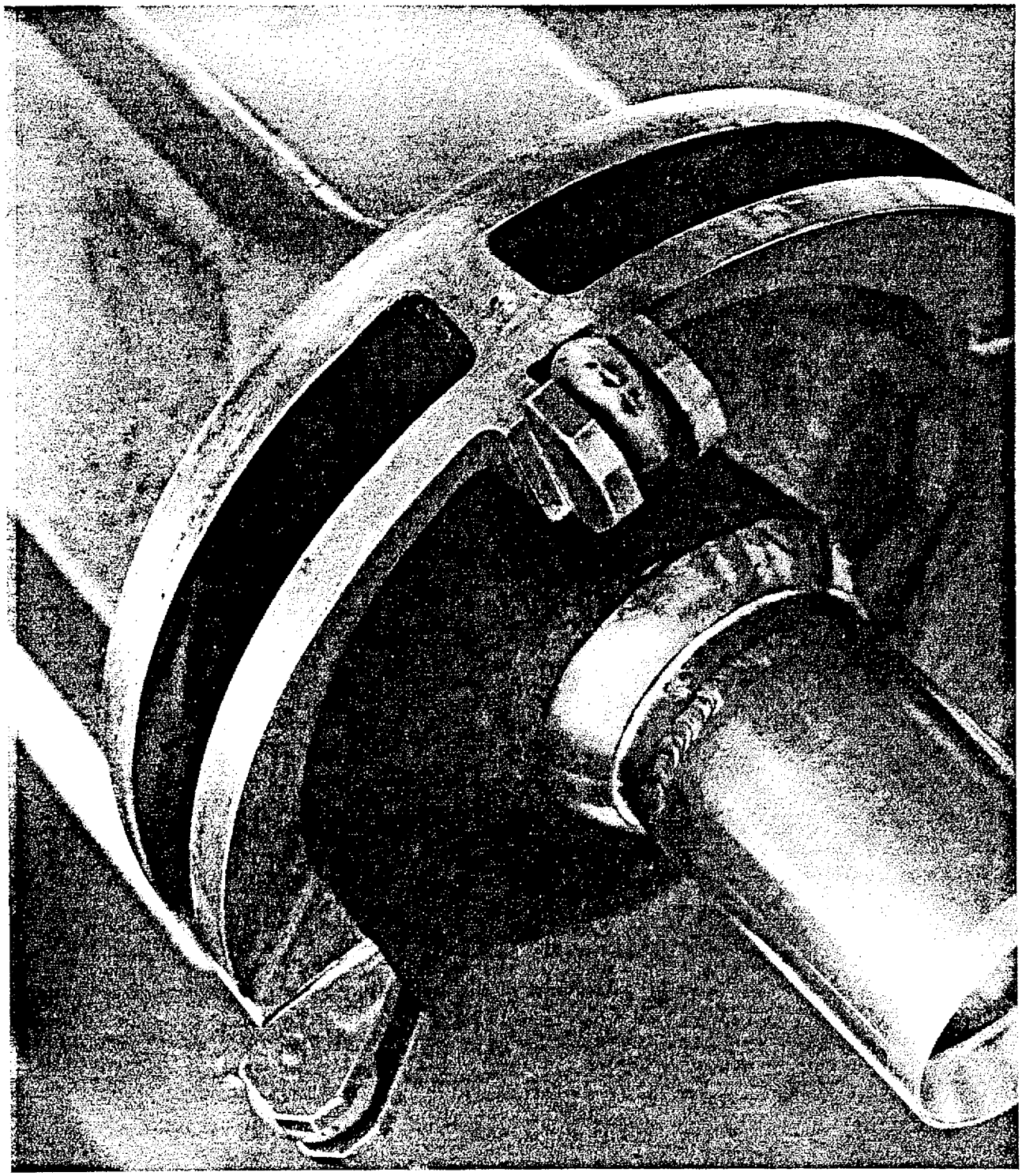

Figure A-10 Modified Worst Case

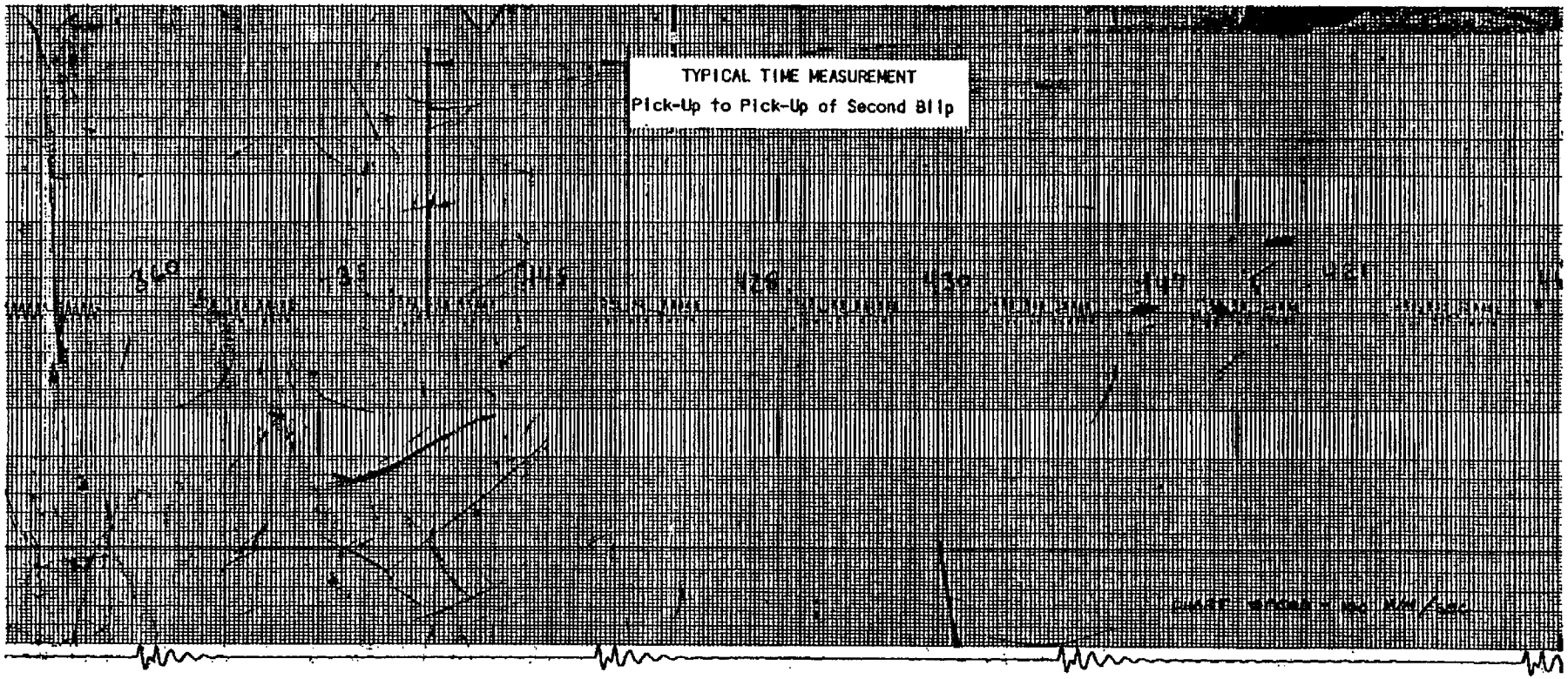

Figure A-11 Typical Sanborn Trace of a Rod Drop

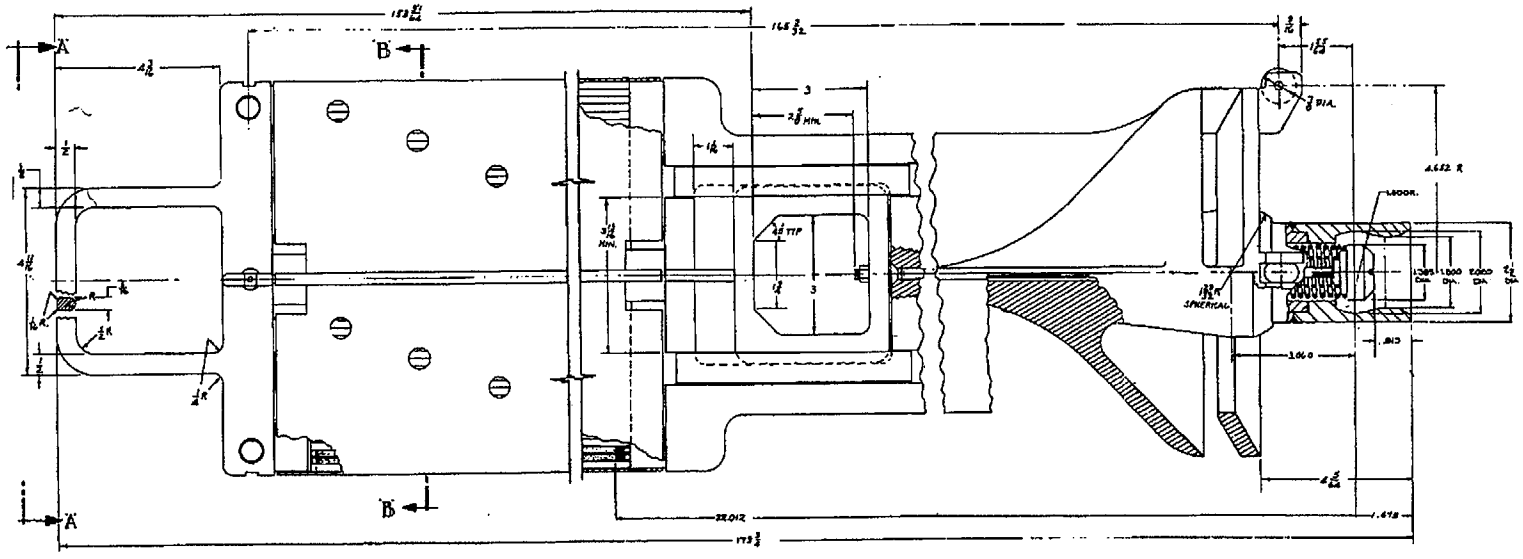

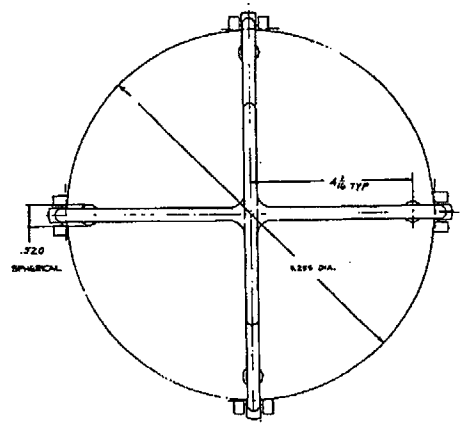

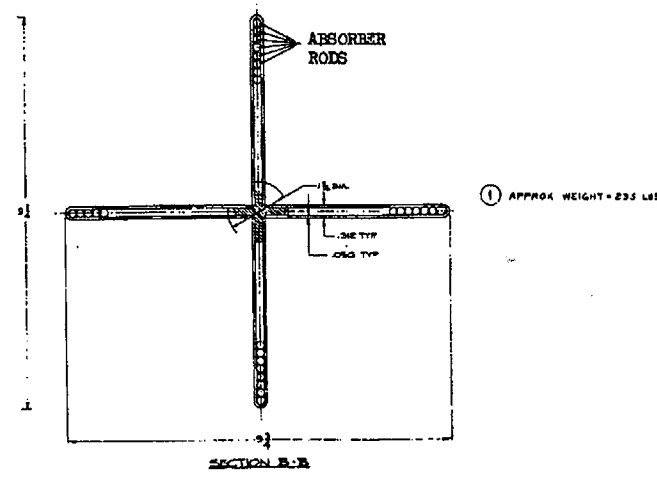

Figure A-12 Control Rod – Outline Drawing

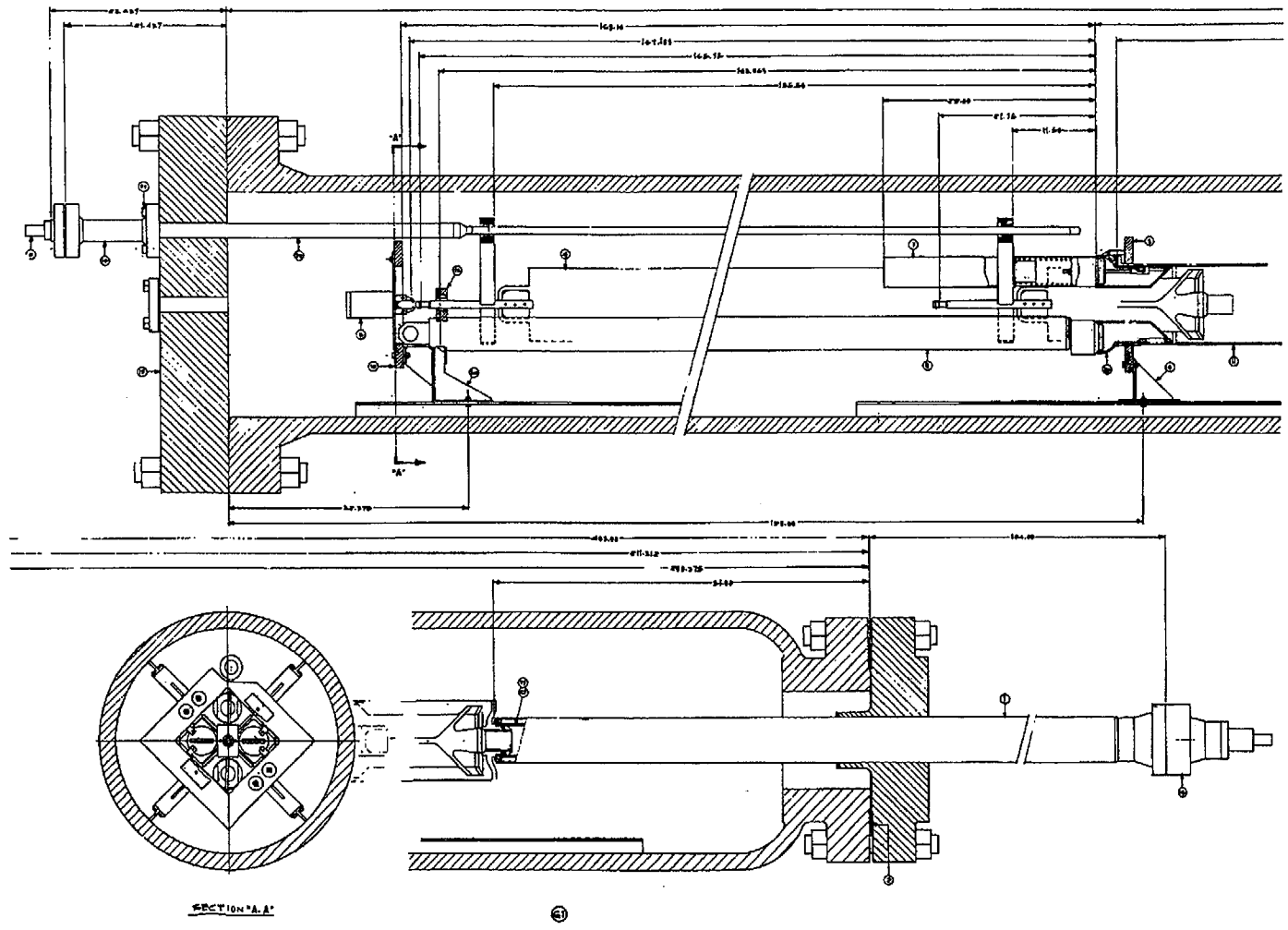

Figure A-13 Test Facility – Assembly Drawing

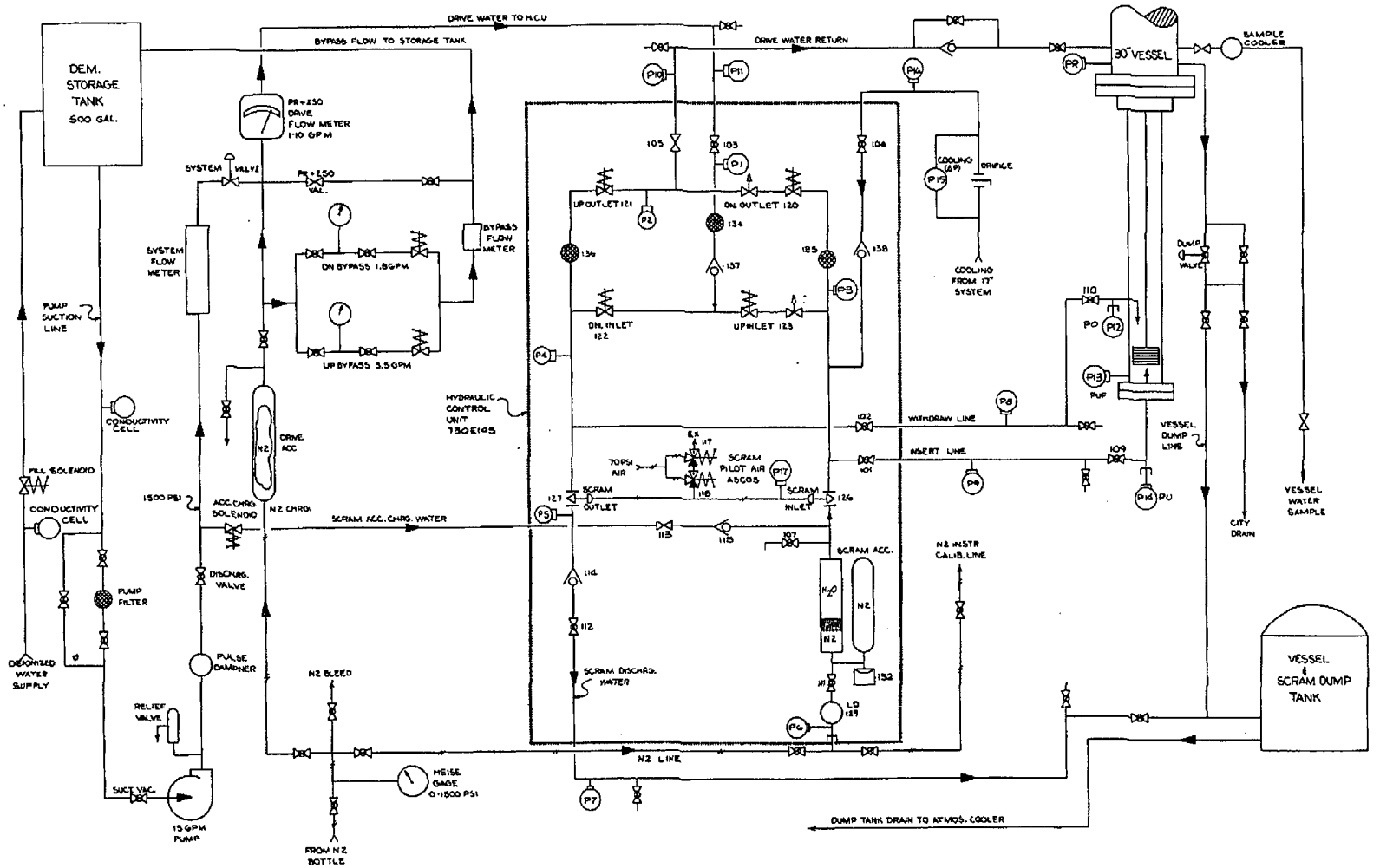

Figure A-14 Control Rod Drive System for 30-Inch Vessel

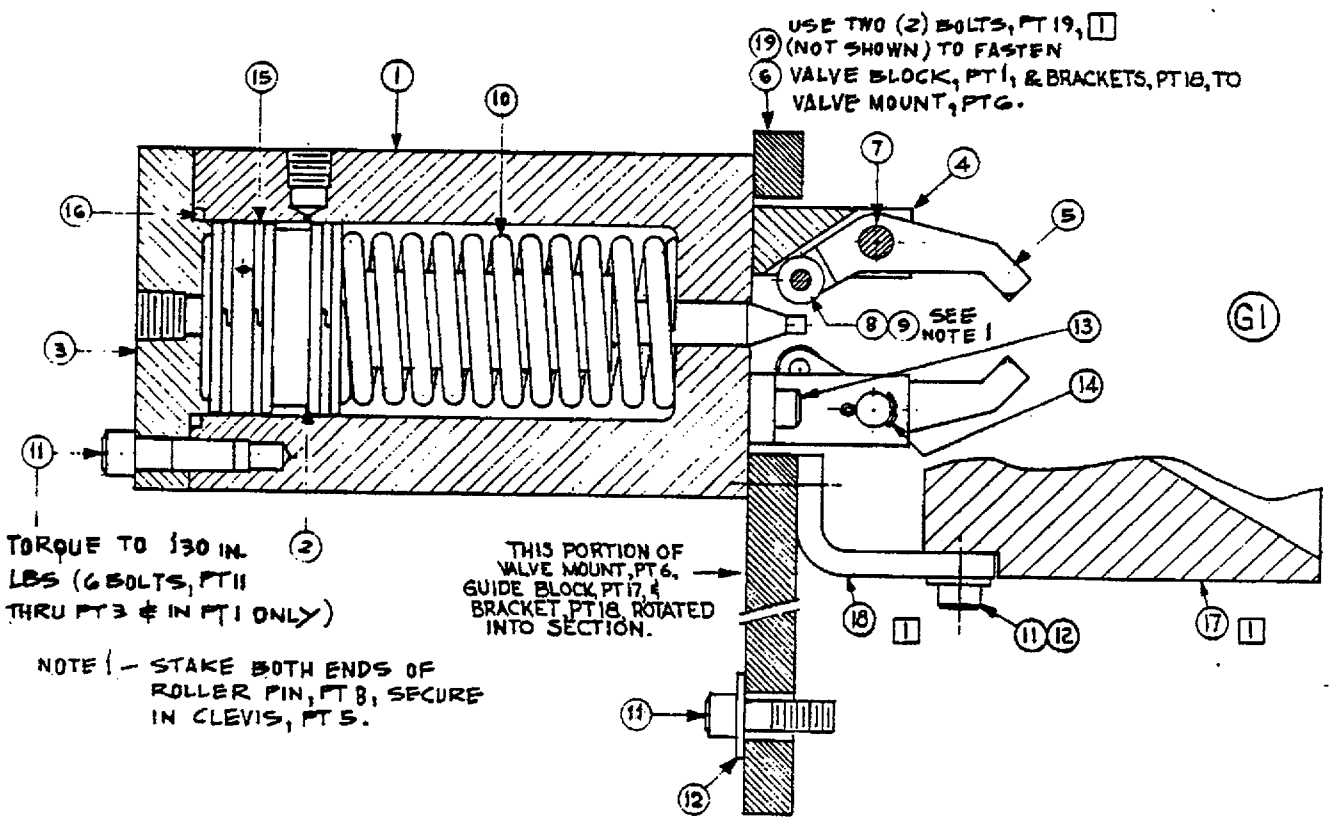

Figure A-15 Latch Valve – Assembly Drawing

NUCLEAR ENERGY DIVISION • GENERAL ELECTRIC COMPANY
SAN JOSE, CALIFORNIA 95125

GENERAL ELECTRIC

TECHNICAL INFORMATION SERIES

TITLE PAGE

AUTHOR	SUBJECT	NO. 72NED18
C.J. Poane, R.C. Stirn, and J.A. Woolley	ROD DROP ACCIDENT ANALYSIS	DATE March 1972
TITLE ROD DROP ANALYSIS FOR LARGE BOILING WATER REACTORS		GE CLASS 1 GOVT. CLASS
REPRODUCIBLE COPY FILED AT TECHNICAL PUBLICATIONS, R&UO, SAN JOSE, CALIFORNIA		NO. PAGES 78

SUMMARY

This report describes the current methods used by the Atomic Power Equipment Department of the General Electric Company for the analysis of super-prompt critical nuclear excursions in large water-moderated reactors. The technical analysis tools used in studying hypothetical nuclear transients are described herein, without considering the probability of such an occurrence.

The rod drop accident has been reanalyzed generically using the improved methods, and the results of these analyses are presented. In addition, detailed sensitivity studies have been performed to evaluate the effects of initial reactor conditions, control rod worth, rod drop velocity, and scram insertion rate on the resultant peak fuel enthalpy.

By cutting out this rectangle and folding on the center line, the above information can be fitted into a standard card file.

For list of contents – drawings, photos, etc. and for distribution see next page (FN–610–2)

JOB NUMBER 466-U9177

INFORMATION PREPARED FOR U.S. AEC

TESTS MADE BY APED

COUNTERSIGNED A.P. Bray SECTION Applications Engineering

BUILDING AND ROOM NO. K LOCATION San Jose